Mechanical stress induced electrical emissions in cement based materials

A thesis submitted for the degree of Doctor of Philosophy

by

Antonios Kyriazopoulos

School of Engineering & Design, Brunel University-United Kingdom

July 2009

Table of Contents

Acknowledgements

I would like to express my deepest gratitude and respect to Mr. Chris Brown, my supervisor, who encouraged me to do the present research work against all problems arising from the distance between the places that we live and work. I would also like to thank him for his interest about the progress of the project and willingness to correct the manuscripts and discuss the results.

I am grateful to my respectable supervisor Dr. Cimon Anastasiadis who, managed to help me finish the present study. In the friendliest yet strict and inspiring way, he guided me with his positive criticism and careful corrections to the present point.

I would like to thank Prof. Dimos Triantis, my invaluable friend who introduced me to the "secrets" of the PSC and BSC techniques and with fruitful discussions helped me interpret some of the experimental results.

My gratitude is also due to Dr. Ilias Stavrakas for his positive advice and suggestions.

Finally, I express my thanks to my wife Fotini for her patience and continuous encouragement.

Abstract

This work deals with the underlying physical mechanisms and processes that dominate the fracture of cement based materials and their electrical properties. Electric current emissions were recorded when hardened cement pastes and cement mortars suffered mechanical loading in various modes.

Such electric current emissions are known as Pressure Stimulated Currents (PSC) when the applied loading is compressional while they are mentioned as Bending Stimulated Currents (BSC) when the material suffers bending loadings. The physical mechanism responsible for the PSC and BSC emissions can be interpreted in terms of the Moving Charged Dislocations model that correlates mechanical deformation and electric charge distortions in the sample bulk.

Laboratory experiments were designed based on the mechanical and physical properties of cement. To conduct the experiments all the background material concerning cement fracture mechanics, the microstructure of the hardened cement paste and the Interfacial Transition Zone of cement mortar were taken into consideration.

Additionally, the experience of the PSC technique when it was applied on marble samples was used to guide the experimental procedures and compare qualitatively and quantitatively the experimental results.

The relationship between the emitted PSC and the strain was established for the very first time for cement based materials in the present work. When the material was stressed within the range where stress and strain are linearly related a linear relation between PSC and stress rate ($d\sigma/dt$) was observed. Deviation from this linearity appeared when the applied stress was in the range where the applied stress and the yielded strain were not linearly related. Slightly before fracture, intense, non-linear PSC emissions were detected. The damage of the sample structure due to excessive loading in the plastic region significantly affected the recorded phenomena.

Bending tests proved that similar electric current emissions are detected when a sample beam suffers 3 Point Bending Tests. The dependence of the emitted electric current on the way of fracture (i.e. compressional or tensional) was proved.

It was also shown that the magnitude of the emitted electric current is directly related to the magnitude of damage due to the external loading. Thus, as it was expected, the electric current emitted from the tensed zone is significantly greater than the corresponding emitted from the compressed zone.

List of Symbols and abbreviations

General abbreviations

PSC   Pressure Stimulated Currents

BSC   Bending Stimulated Currents

MCD   Moving Charged Dislocations

ITZ   Interfacial Transition Zone

3PBT   Three Point Bending Test

OPC   Ordinary Portland Cement

NDT   Non Destructive Tests

NDE   Non Destructive Estimation

AE   Acoustic Emissions

cbm   cement based materials

hcp   hardened cement paste

CM   cement mortar

CP   cement paste

SEM   Scanning Electron Microscopy

FPZ   Fracture Process Zone

w/c   water –cement ratio (% (mass fraction))

LSRT   Low stress rate technique

ASST   Abrupt step-stress technique

Cement compounds and Hydrates

C-S-H   Calcium-silicate-hydrate

C3S $3CaO.SiO_2$

C3A $3\ CaO.Al_2O_3$

C2S $2CaO.SiO_2$

C4AF $4CaO.Al_2O_3.Fe_2O_3$

Symbols

δx Distance a dislocation moves due to mechanical loading

D   Factor depending on the bulk structure of the material

I   Electric current

Γ	Factor depending on the physical and electrical parameters of the material
ε	Strain
σ	Stress
σ_y	Yield stress
$\hat{\sigma}$	Relative compressional stress
E_0	modulus of elasticity
$\dfrac{d\varepsilon}{dt}$	Strain rate

1. Introduction

1.1 Generalities

Cement as unprocessed mortar, and without several of its initial properties, can be found deep in the past.

There is a reasonable assessment that the connecting material for the processed stones in the Egyptian pyramids was a mortar type material, with similar properties (regarding stone connection and adhesion) to cement. In addition, it is certain that the Romans used mortar of volcanic origin (due to the volcano of Vesuvius) and the term puzzolana derives from these hydraulic mortars.

John Smeaton, in 1756, discovered cement as the primary connecting mortar after reacting with water, while Joseph Aspdin in 1824 defined the principles for introducing cement in industrial use; the Portland cement name is due to the colour of the cement mortar, which was the same with that of the rocky beaches of Portland.

The use of cement has been continuously increasing during its 120-year presence in numerous constructions. The main reason is that cement is the basic component of reinforced concrete, with which various constructions are built: buildings, bridges, aqueducts, dams, roads, etc. The current era is characterized by the development of heavy and technologically evolved machinery, along with the great advance of applied Chemistry for cement; these two contribute indirectly to the evolution of cement based materials (cbm), such as reinforced concrete, cement mortars and other derivative products (lightweight concretes, etc), to which they provide flexibility, a larger degree of automation and a smaller need for labour, parameters which are important for the competitive aspect of cement.

Along the development of cement through time, during the past few years, the technology has been developed regarding the production of various additives to cement that improved certain of its properties (delay in water evaporation, acceleration, or deceleration of solidification, etc).

In addition, there has been a significant development in the theoretical simulation and calculation of space frame constructions from cbm (rheological models, fracture mechanics, etc), along with the development of various methods for examining the static strength and durability of the cbm and for the restoration of inefficiencies in cases of static micro damage of the cbm constructions (due to earthquake, overload, subsidence, or any other reasons causing large deformations or discontinuities in the construction. The reason

for the above is that in case of a cbm failure due to the above mechanical reasons, there are serious social and financial repercussions to the society.

This fact renders the examination of the cbm more important regarding engineering, and in particular regarding their static adequacy.

Consequently, the methods examining the microstructure of the constructions made of cement based materials during their dynamic loading phase and during their status when they are subjected to various kinds of loads, result in conclusions about the deformation of these constructions which are very important. Within this framework, various methods have been developed of both destructive and non destructive tests for the cbm constructions.

1.2 Aims

This work aims at the study of weak electric current emissions detected during the application of mechanical stress on cement based materials. In the past such emissions have been detected on marble samples and potential underlying theoretical models have been proposed to explain the physics that dominate this phenomenon. Moreover, it was investigated, if it is plausible for these electric current emissions to be used as indices of the damage caused in the structure of a brittle geomaterial when external mechanical stress was applied. Until the beginning of this work, such laboratory experiments had been conducted only on marble samples and the electric emissions have been rendered under the term Pressure Stimulated Currents (PSC) while their existence is attributed to the Moving Charged Dislocations (MCD) model. In order to examine if the MCD is the dominant physical mechanism, cement products that favour also the electrokinetic and the piezoelectric effects are used in this work to investigate if they exhibit similar behaviour to that of marble samples. Comparative experiments were conducted on cbm and marble samples in order to investigate probable qualitative and quantitative differences on the experimental results. Discussion is made on these experiments. An observation of the emitted electric current when a marble sample repetitively suffers mechanical stress is evaluated here for the cement based materials.

1.3 Objectives

The dominant underlying physical mechanism of the PSC emissions from cement based materials will be revealed. The experimental results will be compared to those of marble samples. Novel experimental techniques like PSC emissions during bending tests and the

influence of the strain rate on the PSC emissions will be presented. To achieve that, cement product samples were subjected to a series of controlled stress and strain variations during which the emitted PSC was measured. After completing this work the possibility of using the PSC methodology as a Non Destructive Testing protocol will be investigated. The purpose of the current thesis: is to contribute, by providing information regarding the static condition of a cbm construction; through the new method, presented for the first time that we regard the weak electric current emissions henceforth mentioned as Pressure Stimulated Currents (PSC) and that relation with the mechanical parameters of the cbm test samples.

1.4 Literature Survey

Laboratory experiments in order to investigate the conditions and the mechanisms under which various materials emit electric current when they are subjected to mechanical stress have been designed by scientists when they were studying earthquake prediction processes. Scientists after field observations measuring changes in natural quantities like the resistance of rocks, the intensity of the geomagnetic field, considered some of them as potential indicators of pre-seismic behavior. However results remained unsatisfactory and attention turned to the phenomena of the electric and electromagnetic fields (1980). Observations led to the conclusion that electric currents could provide information regarding the mechanical status of geomaterials and how that status could be conceived through electric current emissions. Moreover, the study of the earthquake precursory phenomena further than the field measurements was also moved to laboratory environment in order to build physical models to explain electric current emissions due to mechanical stress. In attempting to observe and measure such phenomena in the laboratory it is important that the only difference should be in scaling. Consequently, the existence of transient electric signals, (precursor of failure), of a laboratory fracture, should demonstrate a potential mechanism for the full scale event.

Laboratory fracture tests have been conducted using various kinds of materials "dry" or "saturated" in order to clarify the mechanism of the electric phenomena, (Ogawa et al., 1985; Nitsan, 1977; Cress et al., 1987; Brady and Rowell, 1986; Yamada et al., 1989; Hadjicontis and Mavromatou, 1994, 1995; Enomoto and Hashimoto, 1990; Freund, 2000; O'Keefe and Thiel, 1995; Takeuchi and Nagahama, 2001).

Contact or separation electrification is favoured by Ogawa et al. 1985; while Cress et al. 1987, also suggest that the ionization of the void space within the crack and the acceleration of unbound electrons may intensify charge production.

Acoustic, electromagnetic and electric signals exist, which are detected before and during the fracture of geomaterials. There is a clear similarity between the electric, electromagnetic and acoustic emissions. Acoustic Emissions methodologies have been proposed by J. Kaiser 1950, E. Landis and L. Baillon, 2002**.**

1.4.1 Models for electrical phenomena accompanying materials fracture

Theoretical models have been built and proposed to investigate the electric phenomena observed during brittle material fracture. A very important is the piezoelectric effect by Finkelstein et al., 1973, Yoshida et al., 1997, Nitsan, 1977. This model can be applied on materials that contain piezoelectric components. Another potential mechanism that explains electrification due to mechanical fracture is the electrokinetic effect proposed by Mizutani et al.,1976; Jouniaux and Pozzi,1995; Lockner et al., 1983. This model is applicable that enable fluid transportation in their bulk and are of significance size.

1.4.2 Experiments on electric currents produced during fracture

Since 1833, M Faraday has written: "Usual phenomena of electrification can be observed in the electric machines in the atmosphere and in the compaction or fission of crystals". A hundred years later, in 1933, A.W. Stepanov first observed electric phenomena in the plastic deformation of ionic materials.

The generation of electric currents was fin detected when studying rocks under stress and has long been observed in experiments. For instance, Whitworth, (1975) demonstrated such an effect in alkali halides. Microfracturing electrification*,* i.e. the appearance of electric current production and electromagnetic emissions of microcracks, has been presented by several authors: (Warwick et al., 1982; Cress et al., 1987; Ogawa et al., 1985; Enomoto and Hashimoto, 1990). Warwick et al., 1982, have measured electric current emissions from microcracks, associated with crack opening processes. Compatible values have been reported by Ogawa et al. 1985, while Enomoto and Hashimoto in 1990 also measured similar electric emissions from cracks. Another approach on the underlying physical mechanism that dominates the spontaneous

electric current emissions has been piezoelectricity which was proposed by Warwick et al. 1982, Nitsan, 1977.

There is a clear link between the mechanical process of microfracture and electric phenomena and this has stimulated further measurements to quantify further phenomena that occur as a result of the microfracture process. This includes investigation of acoustic emissions (AE) (Fiffolt et al., 1993; Mavromatou and Hadjicontis, 1994; Hadjicontis and Mavromatou, 1994; Hadjicontis and Mavromatou, 1996; Enomoto et al., 1994; Chen et al., 1994; Yoshida et al., 1994; Yoshida et al., 1997). These experiments were conducted under different conditions so that they may not all be directly comparable, while some may exhibit intrinsic inconsistencies attributable to the hardware. For instance, G. Nover of Bonn University (personal communication), indicated that in a series of unpublished experiments, he observed a strong dependence of low frequency electric and electromagnetic field based on the choice of electrodes. Although the experimental results should be considered with caution, it is clear that they indicate that AE with electromagnetic activity occurs in both piezoelectric and non-piezoelectric materials. In all cases the microfracturing and causes intense electric current prior to failure. It was common to detect electric current during mechanical loadings on dry rocks. Chen et al., 1994, for the first time used saturated rocks. In a very interesting experiment, Bella et al. 1994 observed simultaneous AE and electric activity in caves within non-piezoelectric limestone rocks suggesting that both AE and electric signals are local. Hence, they propose that pressure variations may induce frictional sliding between adjacent rock blocks, triggering relative displacement and charge separation. This mechanism is similar to the one proposed by Yoshida and co-workers (Yoshida et al. 1994; Yoshida et al. 1997). The important result of this field experiment is that simultaneous AE and electric signals may be observed in field conditions.

Electric signals are also observed simultaneously with crack propagation in non-piezoelectric materials, indicating the existence of additional electrification phenomena. This may be explained by lattice separation and bond breaking, ionization of void space, acceleration of free electrons and other charges and the motion of charged dislocations. The contribution of these effects cannot be determined; they act additively, subtractively or even competitively. The way these mechanisms interact depends on the material and its mechanical history, as well as on its mechanical state. Theoretical work on this effect is provided by Teisseyre, and Nagahama, 1999. Note

however that the motion of charged edge dislocations (MCD) is always present during brittle fracture. This will be examined herein regarding the cement based materials.

Edge dislocations may be formed by a half plane of atoms inserted into, or removed from the lattice. Around the dislocations the physical fields related with it are concentrated. Similar mechanisms are valid and active in ionic structures leading to electrically active dislocations. Ordinarily, a dislocation is expected to be electrically neutral but still to contain various charges of different polarities that are compensated. Such electric charges are around point defects (for cement based materials they are capillary pores, air voids and generally the Interfacial Transition Zone) which coincide with the regions of high stress concentration in cases of mechanical loadings (Whitworth, 1975). Sudden stress changes below a certain threshold do not produce dislocation motion with macroscopic plastic yielding, because of substantial stress barriers for an elementary dislocation displacement and the pinning of dislocations at various points due to elastic and coulombic interactions with other defects (Slifkin, 1993). There can, however, be a displacement of the free dislocation segments between the pinning points, which bow out until the force exerted on the dislocation is compensated for. Depending on the magnitude of the applied stress, the segments may bow out through a distance of many lattice space units. Although the dislocation segments can be highly mobile, the compensating charge cloud cannot. The mechanism of electric current emissions from disordered materials due the existence of dislocation or other defects has been considered only in the work of Hadjicontis and Mavromatou, 1994; 1996. In order to move closer to the kind of materials used for this thesis (i.e. cement based materials) the Slifkin (1993) theory must be generalized or slightly extended. The process of crack opening and propagating in a material like cement mortar due to externally applied mechanical loading following the previous assumptions will result in an extended dipole. Specifically the electric charges that are concentrated around a physical defect are influenced by the mechanical loading which causes a measurable dipole moment.

Here the second approach is considered to be the case of non-elastic deformation, when the stress exceeds a critical level and dislocations begin to multiply, break away from their pinning points and migrate through the lattice expanding to new loops between stronger pinning points. If an obstacle occurs, the moving dislocations will pile up against it, concentrating the stress and initiating a crack at the head of the pileup result in an extended electric dipole. Moving dislocations, since they act as stress

concentrators may cause additional electric effects. All these in the frame of mechanical view can be interconnected with the Griffith's theory for the crack modeling and surface energy. For instance they may propel dormant charge carriers, while bond breaking and separation effects take place in their shear stress plane. In another case, the piezoelectric polarization reduction due to the stress drop resulting from crack opening, releases bound charges (as in the experiment of Yoshida et al., 1997). Determining how these multiple mechanisms interact may be an important objective, but will not be considered here. It is assumed that the additional effects are integrated in the MCD / microfracturing process.

1.4.3. Electric current emissions from geomaterial samples under mechanical stress

A sequence of experimental recordings and analyses of electric signals emitted under temporally varying uniaxial compressional stress upon rock samples like marble and amphibolite have been conducted (Vallianatos et al., 2004; Anastasiadis et al., 2004; 2007b; Stavrakas et al., 2004; Triantis et al., 2007). The electric signals emitted during this process are known as Pressure Stimulated Currents (PSC). Fresh experimental results show that the emitted PSC during the application of mechanical stress has a deterministic form and can be used as a tool for detecting the upcoming event of fracture (Anastasiadis et al.,2004; 2007a,b; Kyriazis et al., 2007; Triantis et al., 2006a,b; Stavrakas et al., 2004;,2004;). Moreover, the form of the emitted PSC can be used to distinguish whether the sample has entered the permanent deformation ranges or it approaches fracture. It is also clear that the emitted PSC is directly related to the strain variation (Kyriazis et al., 2007). Through these experiments the MCD model was evaluated and its applicability on the electric current emissions from geomaterials was proved (Anastasiadis et al., 2004; Stavrakas et al., 2003; 2004; Triantis et al., 2006b).

Analogous phenomena have been recorded using the acoustic emission technique (AE) in coal-mines all over the world. The same holds for acoustic emissions measured in lab tests prior to the failure of rock specimens. The acoustic emission technique experiments are equally interesting in the study of the mechanical behaviour of materials (Lavrov, 2005; Yamada et al., 1989; Lockner 1993; Tatum, 2003; Hardy 1989).

Another approach is to model the microcrack as an active element (dipole, quadrapole) as by Guo et al., 1994 and study the power spectrum of the emitted electromagnetic

signal. An alternative model is to consider the microcracks to be capacitors (O' Keefe and Thiel, 1995) and analyze the RC circuit formed by this process using circuit theory. An overview and critical analysis is available, as Freund et al., (2000), which combines the best of each theory and concludes with their own model.

1.4.4 Electric current emissions from cement products subjected to mechanical stress

For cement product samples it has also been observed that stress development due to axial compressional load and bending moments induces electric signals as a result of mechanical strain (Sun et al., 2004, 2006; Wittmann, 1973). These electric signals are observed during the laboratory experiments on cement mortar samples. Such phenomena are developed and analyzed theoretically at a microscopic scale by laboratory experiments.

Wittman in his work published in 1973 applied a bending moment by external load on a bar of hardened cement paste. He detected a voltage between the compression and the tension zone. The measured a voltage which according to the author is attributed to the moisture content of the cement bar. He also reversed this process since he observed that when applying a voltage to a hardened cement bar he managed to bend the bar. This phenomenon was attributed to electro-osmosis.

Sun et al., 2004 in their work investigate electric emissions in mortar sample when this is subjected to compressive loading. The authors found that electrical emissions can be detected even at low stress levels, lower than 30% of the ultimate strength of the material. When applying loadings and unloadings on the cement mortar two electrical emissions of opposite signs were detected. Additionally, when the applied loading was increased the measured electrical emission was also increased. This behaviour was attributed to microcrack opening processes and to the fluid transportation in the sample bulk. The authors, in published works during 2004 and 2006 reported that a probable cause for electric current emissions due to externally applied stress is the piezoelectric effect. They also found that the emitted current is not linearly increasing with the applied stress. They attribute the piezoelectric effect to the transportation of mobile ions along with water in the hardened cement paste. Sequential loadings and unloadings show that the emitted electric current becomes progressively lower. Finally, when repeating Wittman's experiment and applying an external electric current on a cement paste beam

at the opposite surfaces they managed to bend the beam and attributed this phenomenon also to electro-osmosis.

1.5 The contribution of this work

For the first time in this work, it is attempted through various experimental techniques and various ways of the application of mechanical stress to show up Pressure Stimulated Currents (PSC) on cement mortar and paste samples. More specifically it is attempted:

- To show up electric emissions in cbm samples of clearly more distinct and bigger in magnitude compared to PSC recordings on geomaterials as marbles, amphibolites etc.
- To correlate PSC emissions with the strain rate on cbm samples.
- To conduct for the first time experiments on cbm samples, recording electric emissions during three point bending in beam type–samples. Detection of BSC both in the tensioned and compressed zone of the beam and correlation of electric signals with the applied load.
- One more objective of this thesis is to focus on the PSC emissions that take place during repetitive mechanical loadings and unloadings.
- An embodiment of the above tests in the Non Destructive testing methodology will also be attempted.

To confirm experimentally the relationship between PSC recordings and stress application on cement mortar and hardened cement paste (hcp) samples and compare them with the corresponding results of marble samples, several experimental methodologies are applied. Some of them have already been applied on marble and some of them are novel and are applied for the very first time on cement based materials.

2. Theoretical Background

2.1 Fundamentals of fracture

2.1.1 Introduction

The current thesis examines the electric current emissions detected during the mechanical stress of cbm samples. For this reason, it is important to define the natural mechanisms that take place during the application of mechanical loads in such materials. This will act as an important tool for the interpretation, correlation, and interaction of the mechanical with the electrical phenomena.

Cement, as the standard component for the production of important construction materials, such as cement mortar, concrete, etc, has a double faced construction character when used autonomously as hardened cement paste (hcp). One view defines it as a material with crystal properties, while another regards it as a gel type material. Therefore, an interpretation for the creation or development of micro/macro-cracking to the cement paste, and for its fractioning manner, is governed, up to a point, by the crystal breaking mechanism (in quasi brittle materials), and also by the standard theory of cracking development (Griffith), as evolved and specialized for cbm.

However, when the hardened cement paste is a part of a cbm, then the microcracking - cracking procedures are described by other mechanisms, whose main characteristic is the Interfacial Transition Zone, analytically described in section (2.2.7).

The above are very important, since the development of cracks in a cbm is directly linked to the emission of electrical currents in the samples examined in the present thesis.

Further below, certain fundamental principles of Fracture Mechanics and a small reference to lattice imperfections will be stated, governing the behaviour of cbm, which in combination with the reference made to the microstructure of these materials, will provide the necessary information for interpreting their deformations and development, through the cracking mechanism. In addition, a reference will be made to the mechanisms producing electrical current after mechanical stress and results from previous works geomaterials (marble) on will be presented. Specifically the combination of the above aids to understanding and interpreting the respective experimental results in the hardened cement paste and cement mortar samples, which are the research objects of the current thesis.

2.1.2 Fracture mechanics

A structure fails when it ceases serving the purpose for which it was built. The term fracture is linked to the term "fail"; a form of the former is fracture due to static loads. When this occurs to a brittle material, it is sudden and total. It starts with a crack, usually in a region of high concentration of stress. No sudden fracture occurs in ductile materials, but significant elastic and inelastic deformations have been reported. The fracture due to repeated loads comes as a consequence of the repeated loading of the structure and is known as fatigue. It is usually unpredictable: The quick development of the crack size causes the fracture of the material even with an additional load smaller than the fracture load (creep).

Fracture Mechanics was developed, initially for metals, polymers and ceramics, while in the past 40 years the research in the microcracking - cracking in concrete has been significantly developed. The effort is focused on researching the evolution of microcracking and its relation to the mechanical behaviour (stress – strain) mainly of concrete. In this area, significant observations were made in relation to the hcp microstructure and its interaction with fine and coarse aggregates. With the help of Fracture Mechanics, significant quantitative differences were found in regard to the evolution of microcracking in compression and tension tests on cbm. Moreover differences were also observed in the fracturing mechanism of the materials, i.e. hcp and cement mortar.

2.1.3 Brittle and quasi brittle materials failure theories

A) Internal Friction Theory: This is based on the assumption that the critical shearing tension τ_{max}, during which a material fails because of its yielding, is affected by the presence of internal shear forces. In addition, there is an assumption that the internal shear forces are affected by the average stress, σ_m, acting on the slip plane. As a result, the limit value of the shearing stess, τ_{max}, is affected by the forward stress, σ_m, and has a linear relation between:

$$\tau_{max} = \alpha \, \sigma_m + \beta \quad (2.1)$$

where α and β are constants depending on the mechanical properties of the material. From the above equation, it results that the critical shearing stress depends on the values of the main stresses.

The internal friction theory could be a special application of Mohr's failure theory, which applies to both ductile and brittle materials.

The internal friction theory applies for elastic and inelastic material behaviours, as well as for cases of failure with fracture, with fairly satisfactory results.

B) Theory for the propagation of cracks: Griffith's theory of fracture: In the case of a brittle material, and in particular of a cbm, a complication is presented, due to the local imperfections of the material, such as microscopic cracks and encapsulations (microscopic grains of foreign materials or water in the material). Griffith's theory on propagation of cracks, along with the aid of statistics and Scanning Electronic Microscopy (SEM), is applied in order to predict fracture, while there are newer methods about the propagation and development of cracks in concrete and other cement products (Moavenzadeh and Kuguel, 1969; Shah and McGarry, 1971; Midness et al., 1982; Shah et al., 1995).

Based on the intermolecular forces, it has been proven that the theoretical strength of materials is much larger than the actual strength. The term stress concentration applies here, which refers to the points of a material where cracks exist. Griffith's theory is based on the energy required for fracturing a material that contains an elliptic hole (simulation of a crack) under stress.

2.1.4 Cracking process

The basic parameter governing fracture mechanics in regard to brittle materials, and in particular cbm, is the development of the cracks procedures on the surface and in the bulk of the materials. This is of special concern for the current thesis, which is based on the adopted MCD model interpreting the production of electrical current emissions during the development of such deformations, included in the term "dislocations". This model has been successfully applied to various geomaterials (marble, etc); for this reason an analysis is performed concerning the deformation manner of the cbm, which are the materials of the current thesis.

On experimental level, the use of SEM has substantially contributed information related to the geometrical details concerning the evolution of cracks. The large majority of researchers in the field of cbm fracture agree that the basic procedure of the cracks develops in the region called "Interfacial Transition Zone" (ITZ), which, as stated in Section 2.3, is the weakest area in the bulk of composite materials as cement mortar. The evolution of cracks above one level leads the stress - strain curve to a non linear

behaviour, and, as it will be presented in the following experimental sections to the intense peaks of PSC emissions.

The cbm are created with a number of microcracks, a fact due to the procedure of drying shrinkage, as well as with a number of point defects, such as air voids; all these depend on the drying and curing process of the cbm, as well as on the sizes of the aggregates, the water/cement (w/c) ratio, the mixing process, etc. Obviously, most of the microcracks are located in the ITZ (Interfacial Transition Zone), which is activated during the stress procedure; however, there are some views that the cracks occur even more further from the ITZ area, e.g. at the location of air voids (Kotsovos, 1983). The Fracture Process Zone (FPZ) expresses the amount of microcracks preceding the main crack that are points of high stress concentration; a quantity of energy develops there which shall finally lead the material to failure. (Fig 2.1)
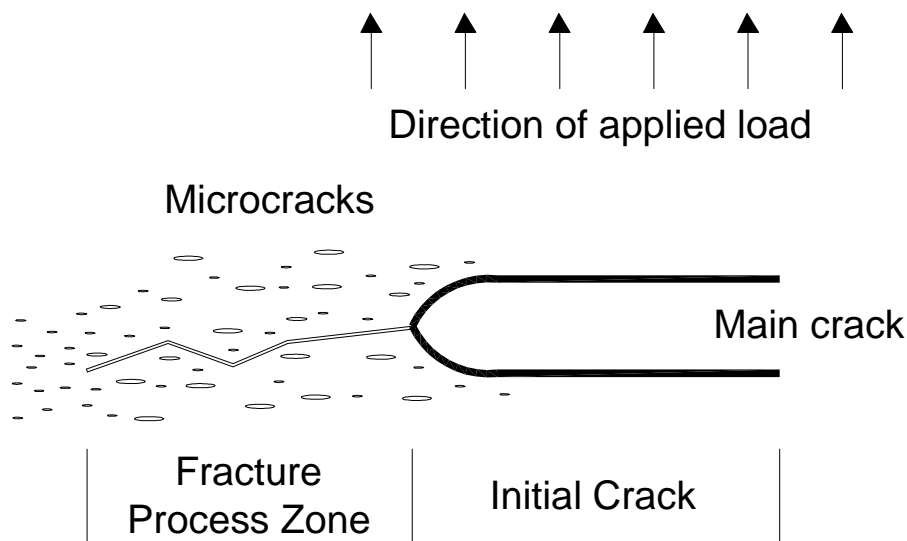
Fig. 2.1: *Fracture Process Zone in cement based materials (Shah et al. 1995)*

There is a difficulty in calculating the total energy in the area of the FPZ, but this is basically due to the heterogeneity of the material and to the amount and diversity of the toughening mechanisms developing during crack growth. Characteristic differences in the crack development manner are stated, such as crack branching that refers to the

parallel creation of a secondary crack along the main one, and crack bridging, which is due to the existence of two aggregates of different diameter in front of the path of the main crack and also crack face friction and crack deflection.   Shah et al. in 1995 suggested that crack face friction, which, as a geometrical development of the crack, renders the calculation of the energy in the FPZ area composite.

Microcracks

Main crack

(a) Microcracking

(b) Crack branching

Secondry Crack tip

Main crack

Aggregate

(c) Crack deflection

Main crack

Main crack

(e) Crack face friction

Aggregate

Main crack

(d) Crack bridging

Void

Main crack

(f) Crack tip blunting
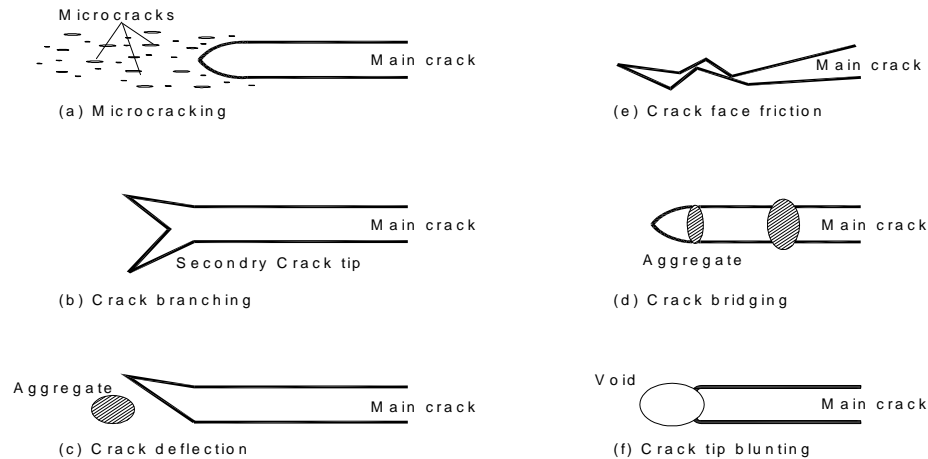
Fig. 2.2: Several crack process mechanisms of FPZ (Shah et al. 1995)

Various techniques have been suggested in order to interpret the evolution of FPZ and crack growth with indirect manners, such as the procedure of acoustic emissions (Sok and Baron, 1979) and the method of the strain gauges (Chuy, 1989); the latter studies the surface deformations but both methods produce results based on assumptions and conditions.   In addition, changes are observed in the crack growth from tensile or compression stresses, depending on the sample size.

The evolution of cracks and the simultaneous creation of the main crack follow a tortuous path, whose tortuous line is registered in the aggregate via the ITZ. Merchant et al., in 2001, suggested the idea that due to the particular development of the FPZ (crack bridging), the deviation from the straight path of the crack to a tortuous path, created for bypassing the different size aggregates, requires additional energy that is redistributed each time until the final fracture.

2.1.5 An approach to the fracture mechanism and its models.

The basic models used to simulate fracture mechanisms involve concrete; however, they can be applied with relative success to cement mortar. A basic assumption is that concrete involves three phases: one of coarse aggregates, one of ITZ and one of the connecting materials, which is hcp and sand. Therefore, concrete is integrated in cement mortar in one phase.

However, when cement mortar is examined separately, the coarse aggregates phase is replaced by the fine aggregates phase.

Linear elastic fracture mechanics (LEFM): Kaplan, 1961, paved the way for the capability to apply, with an experimental manner, the LEFM that defined in the post-Griffith model that the release of a critical percentage of stress - energy is a condition for the rapid development and propagation of cracks, and for the resulting fracture for a cbm material.

The application limitations for the method include the brittle fracture of cbm; the strength of cbm significantly depends on the loading rate and on the fact that tensile strength = 1/10 compressive strength.

Elasto-plastic fracture mechanics (EPFM): Nishioka et al. applied in 1972 this method in fibre reinforced concrete originally created to serve applications of plastic behavior in polymers.

An interesting application of this method is Crack Opening Displacement (COD) and its evolution to Crack Tip Opening Displacement (CTOD), which is a powerful tool for the non linear behaviour of deformations, hence for the development of the crack, with the aid of FPZ in cbm. Another parameter is Crack Mouth Opening Displacement (CMOD), which is used for calculating CTOD. An interesting assumption for a future project would be the connection of CTOD formula with the MCD model applied in the current thesis, in order to correlate the mechanical deformations in cbm with PSC emissions.

Quasi Brittle fracture Mechanics (QBFM): Due to the existence of the FPZ in the cbm that is of a relative large extent, contrary to other materials, a significant difference was noted in their fracture manner. The basic theory in this model is that the stress developed in a crack is limited by the precursor microcracks in the crack tip.

QBFM include the fictitious model suggested by Hilleborg in 1976, who introduced the stress-elongation curves in order to study the behaviour of the development of cracks in concrete.

2.1.6 Cement mortar in compression –stages of stress-strain

The stress-strain curve for the cement mortar samples can be divided in three stages (see Fig. 2.3). That is one stage less than the concrete (see Fig. 2.4). As can be seen in the two Figs the stage II of the cement mortar samples corresponds to stages 2 and 3 of the concrete stress strain curve. This is due to the smaller size of the aggregates in the cement mortar bulk that form a more homogeneous material than concrete. The latter fails with different mechanical behavior regarding the propagation and growth of cracks. The second stage of the cement mortar samples approaches linearity due to the smaller size of the aggregates that are distributed in the bulk and act in a more ordered way. The limiting stress for which fracture will not occur is about 70% of the ultimate for both compression and tension (Fig. 2.3 for mortar and 2.4 for concrete). The non-linear inelastic behaviour of the cement mortar that occurs in stage III can be attributed to the progress of internal microcraking distributed as can be seen in the Fig. 2.5, captions 3 and 4.
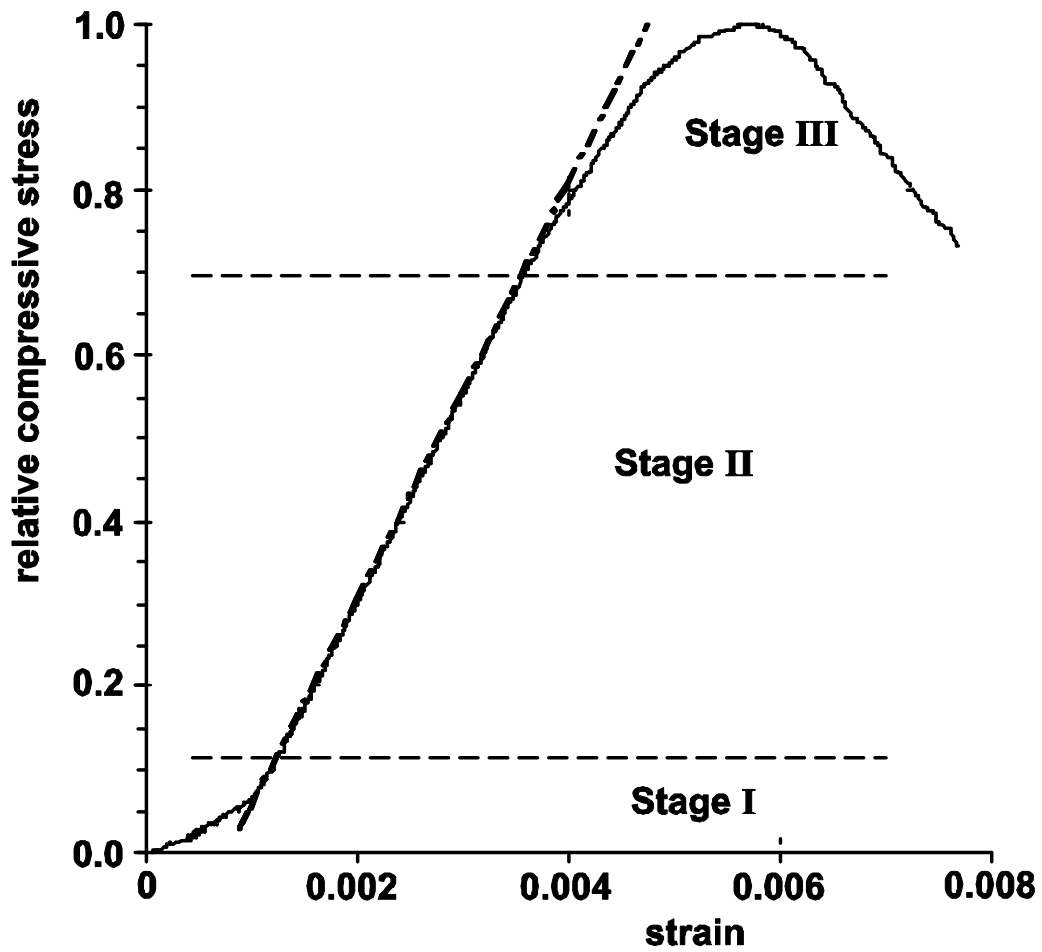
Fig. 2.3: *Normalized stress-strain diagram of used cement mortar sample*
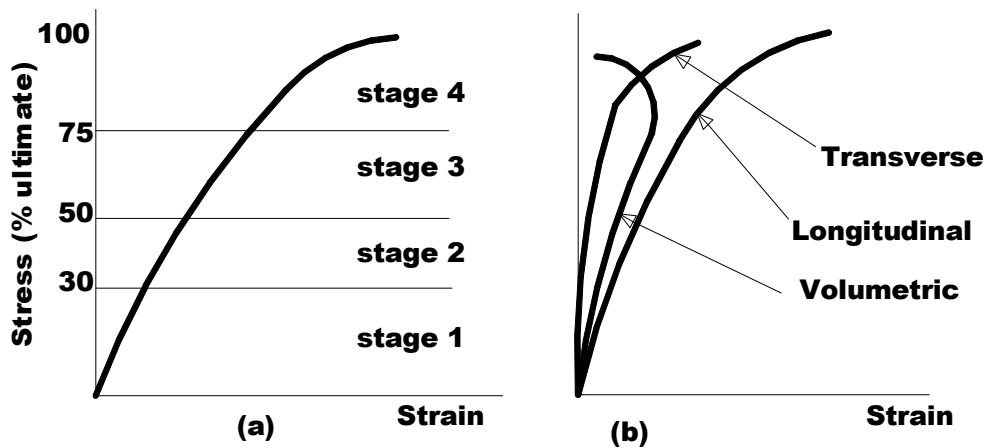
Fig 2.4: *Stress-strain behaviour of concrete under compressive loading: (a) from Glucklich (1965) (b) from Newman (1966).*
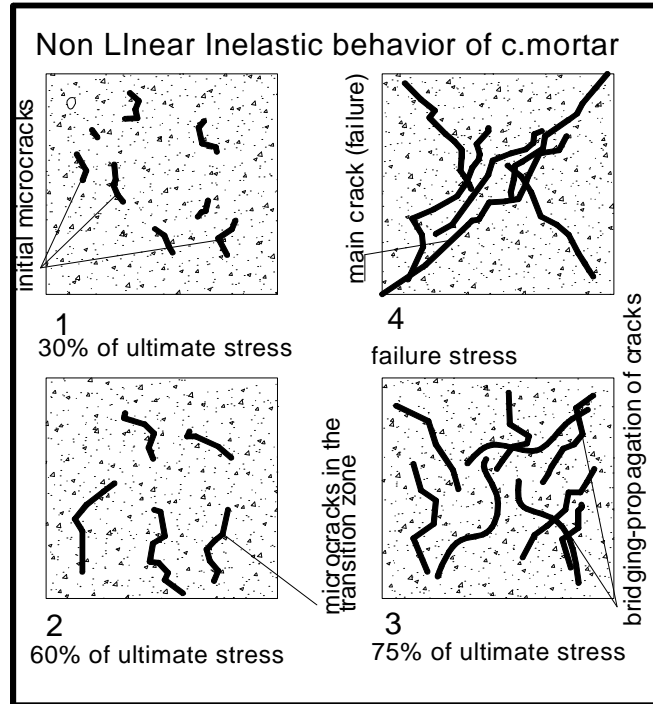
Fig 2.5: *Diagrammatic representation of cracking process of cement mortar cube (50/50/50mm) under uniaxial compress ional load*

2.1.7 A short reference to lattice imperfections

The complexity in the microstructure of the examined materials of the current thesis, which are basically hcp and cement mortar, as presented earlier in this chapter, requires a reference to be made to the crystal structure of the materials and to its characteristic imperfections. This is also suggested by the view that the hcp has a micro-crystal structure, and also by the fact that during the stress of these crystals with mechanical loads, the deformations to which they are subjected until fracture are involved with the emissions of electric currents. The other view regarding the behaviour of hcp as viscous-elastic and simulating it with a gel refers to the microstructure through the Van Der Waals model, and macroscopically in cbm constructions through the rheological models of Maxwell, Kelvin, as well as the time – variable rheological models.

2.1.8 Types of lattice imperfections

Point defects: This term refers to the deviations in the periodic and symmetric development of the entire crystal lattice extended in the area of the grid, at distances respective to the lattice constant. The deviations refer to the absence of the construction element from the position provided for by symmetry and frequency. One of the most basic imperfections is the one of Frenkel, where atoms from the crystal structure abandon their locations in order to be moved to inter-lattice locations. Another imperfection created when a foreign particle enters the crystal structure - a small similarity with hcp is the water in the interlayer of calcium and silica hydrates. From the grid defects, the one prevailing is the one with the largest concentration in the spatial matrix.

"Linear imperfections" or "Linear dislocations": This abnormality is called so due to the fact that, in terms of geometry, it extends at a length that is multiple of the lattice constant, along one of the three basic directions, while along the two others the imperfection is spatially limited, i.e. it is extended at a distance equal to the lattice constant. The model of this imperfection may partially include the evolution of a basic crack, developing after a mechanical stress to a cbm with significant differences, as previously examined in the same chapter.

Microcracks: In the classification of defects on the basis of complexity of the morphology and spatial area, after the "linear imperfection" the imperfection of the "microcrack" follows. The characteristic aspect of this defect is that its creation and development are procedures accompanied by the breaking of bonds in the crystal materials; while in the cbm, the microcracks are mainly created when, during the drying shrinkage procedure, tensile tensions are developed in the evaporated capillary pores. The participation of the imperfections in the formation of the properties of the crystal materials is definitive. The theoretical approaches regarding conductivity, elasticity, plasticity or strength, lead to conclusions that are compatible with reality only if they accept the presence and inclusion of the lattice defects in these phenomena. For instance, the theoretical study of the fracture phenomenon leads to conclusions compatible with the experiment, only when the presence of microstructures is provided in the bulk under stress. In accordance to the current view, fracture comes after the formation, expansion, and then interaction of these imperfections. The possibility of co-existence with all types of imperfections is realistic. In several instances, there is a

bidirectional relation regarding their creation, expansion, or multiplication. The energy required for the creation and expansion of the microcracks will be available in selected regions of the crystal lattice, such as the regions characterized by intense concentration of stresses - strains. Such areas are also restored and as a result of a respective concentration of linear dislocations. The correlation between the microcracks and the linear dislocations refers to an interesting, in terms of its physical background, procedure: Within the frame of mathematical description, the field of deformations accompanying the presence of the microstructure may be expressed as a sum (integral) of the fields of an equivalent network of linear dislocations, arranged within a microcrack. In terms of physics, this means that some linear dislocations, grouped close to the main dislocation of their network, may extend or form the microstructure.

The interesting fact is that the imperfections do not comprise the fundamental web for the theoretical approach only for "mechanical" phenomena developed during stressing a solid (elasticity, plasticity, fracture). The efforts to understand the mechanisms of electrical emission, activated during stress on crystal materials are based on the imperfections. As will be shown in the chapters with the experimental details, this emission is the precursor phenomenon of fracture. Therefore, the prevailing opinion is that the linear dislocations and the microstructures at the stage of their transfer or opening comprise the fundamental elements of emission, which, in the case of fracture, is the precursor to the emission of electrical currents. The conclusion is that the linear imperfections and the cracks and microcracks are concepts on which the theoretical approaches of the phenomena activated in the initial and final parts of fracture are based, both when they are applied for describing the deformation and fracture and when applied in order to understand the mechanisms of the emission of electrical currents prior to fracture.

2.1.9 The linear dislocation

The topological approach of the crystal lattice justifies the use of the "linear" morphologic definition for the imperfections mentioned with the term "linear approaches". The disturbance of the lattice, next to an "edge dislocation" expands to a region that is morphologically similar to a solid, of cylindrical volume. The axis of the cylinder is the end of an additional level interfering with the normal distribution and its diameter is approx. the "width of the linear dislocation". Even though this deformation

occupies a finite volume of the crystal, the elongated axis of the cylinder is much larger than its diameter; hence the entire disturbance is reasonably called "linear imperfection" or "linear dislocation". The stimulus for introducing the concept of "linear dislocation" was the search for a mechanism that would ensure "drifting" with the most economical, energy-wise, manner. In a perfect crystal devoid of imperfections, drifting may be succeeded if all the atoms of the lattice level located above the drift level simultaneously move to new balance locations, with respect to the atoms of the grid level located exactly below the drift level. However, such a motion requires that all the atoms simultaneously pass the maximum values of the potential obstacle, thus requiring a large amount of energy. However, there is an alternative solution: The gradual performance of this movement (and not by all atoms simultaneously). This alternative capability is equal to the movement of a caterpillar, which does not move its entire body simultaneously; it rather moves successively parts of its bulk. A similar action occurs, as explained below, in the drift procedure of a solid, as long as there are "linear imperfections". It is repeated that the thought leading to the discovery of dislocations was the need to deal with the problem: the manner with which it is possible to perform drifting on a given lattice level most economically energy-wise.

2.1.10 Slip planes

Slip planes are a remarkable point. It is considered on the atomic basis of the strength of materials that very large forces are actually required to pull the atom apart to fracture the brittle material. Especially for the cement mortar and paste materials of the current thesis, the fracture in compressive loading is performed in the maximum shear plane, mainly with respect to the cement mortar, while for the cement paste it is performed in a quasi maximum shear plane.

In a three dimensional crystal usually it is not necessary to exceed the bonding forces for permanent change of shape, that is plastic flow Fig.2.6. When a brittle material (as concrete or mortar) is subjected to compressive loading the main compressive force could be analyzed on the maximum shear plane (45^0) in two component forces P_S+P_V. The P_S is clearly a shear force along the shear plane while the P_V is a compressive component perpendicular to the plane. Thus the growth of shear forces and stresses from a simple compressive force in a brittle sample. A satisfactory simulation is performed by examining atoms or particles that are enclosed in a "bundle" of spheres (Fig. 2.6) and that these spheres, under the effect of shear stresses drift below each

other; this is called slip and the plane slip plane. (i.e. the same with shear plane). While these atoms drift below each other, they move in order to form a "bundle" again.
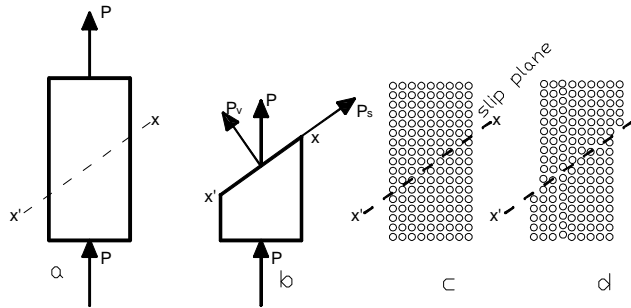
Fig. 2.6: Compressive load and, shear forces with respect to slip plane

For brittle materials, fracture comes at the maximum shear plane or slip plane "bundle" because they are weaker against shearing than against compression.

2.2 Cement based materials microstructure and physical properties

2.2.1. General

In 1937, studies were published dealing with the issue of microstructures and with the natural and mechanical properties of cement, since this material is the basic component of concrete, which at that time started being used extensively. The compound of cement and the properties of cement paste were necessary elements in order to combine the qualities of concrete with the contained cement paste. The participation of water in the procedure of hydration of cement and the resulting creation of voids, in the form of pores were the basic parameters for investigating the properties of cement paste. Water and its relation to cement (w/c ratio), also in accordance to Abrams' law, is very important for hcp. These parameters, in combination with air voids and the interfacial transition zone, the characteristic region between cement and fine aggregates for cement mortar, are responsible for the strength and for various deforming changes of cement paste and cement mortar, and mainly for the change of its volume after the completion of drying, due to the creation of shrinkage, leading to fracture. Other properties were studied also, such as permeability, porosity, etc. With the development of laboratory methods for scanning the elements of cement paste (X rays, scanning

electron microscopy, electronic microscopy), important information came up regarding the cement paste microstructure.

With the emphasis being on the two basic materials involved in the experimental part of the current thesis, which are the hardened cement paste and cement mortar, reference will be made to specific properties of the above materials' microstructure. This reference, as well as any observations regarding issues of the cement paste and cement mortar's microstructure acts as the basis for defining the natural and mechanical properties of the materials under examination, since they are heavily influenced by the cement paste properties. In addition, the special properties of the microstructures of the above materials - samples of the experiments of the current thesis significantly contribute to the process of PSC emission, since the resulting deformations, mainly in the form of evolving cracks after the application of various types of loads, are responsible for the PSC emissions, in accordance with the MCD adopted model.

2.2.2 The heterogeneity of the cement paste - cement mortar samples

Cement products are based on cement, in its hydrated form, having as their final form the hardened cement paste (hcp). This material, through the hydration procedure is changed from having a grain and gel form, through chemical reactions in the cement components, to a hardened cement paste with significant strength after the elapsing of a relative small time period.

The hardened cement paste is a highly complex and heterogeneous product, comprising mainly calcium hydroxide crystals, ettringite crystals and an unformed gel-type mass (C-S-H) as its solid components, along with air void pores, dispersed with various manners and in various sizes inside the mass of the paste, and finally water quantities also dispersed by various ways in its mass. It is clear, that the complexity and heterogeneity of the above components participating in the microstructure of the cement paste hinder the full analysis of its behaviour, along with its simulation within models, in order to be studied. An acceptable model for examining some mechanical properties as the attractive forces between C-S-H and Ca $(OH)_2$ is the Van Der Waals model. This hardened cement paste, either on its own or as a component of cement mortar or concrete, is the weakest material and the first to be deformed; through it, and Interfacial Transition Zone (ITZ), the cement based materials fail. The failure in the hardened cement paste comes with various manners of brittle fracture; one of them is

the fracture level, while in the cement mortar, the fracture will come through the Interfacial Transition Zone, and macroscopically will break in a maximum fracture level very close to main slip plane (shear plane).

Since the deformation procedures until the fracture of the hardened cement paste are very important after the development of existing micro-cracks and the creation of new, for the production and interpretation of the electrical currents during mechanical stress, a detailed analysis shall be performed, regarding the microstructure of the hardened cement paste and of the cement mortar.

2.2.3. Cement paste: crystals or gel

The morphology of cement paste, mainly from information acquired via the electronic microscopy (scanning electron microscopy - SEM) and by the chemical analysis of the cement paste, may be explained in two ways.   The first is that its main structure comprises small needle-shaped crystals (Crystallization theory, Chatellier), while the other view believes that hardening is the result of constriction of the amorphous thick gel mass (Theory of colloids, Michaelis). Based on research with X-rays and electronic microscopy, the result is that both views properly govern the issue of the cement paste structure. This happens because the calcium silicate hydrates, as well as the calcium sulfoaluminate hydrates are of crystalline. However, the size of these crystals is equal to the size of colloids (0.15 μm diameter).

As a result, both simulation models, the Van Der Waals model regarding colloids and the model regarding crystals, may be regarded as compatible concerning deformations.

2.2.4. Phases of cement paste

The entire complex structure of the hcp resulting after hydration is characterized by various phases; the phase of solid products and the phase of voids are of most importance.   Another crucial parameter is the water that remains in various points within the bulk of the paste, where during its partial evaporation it creates serious conditions for failures, mainly due to shrinkage; however, water cannot be regarded as comprising a phase. Various models simulating the cement paste microstructure have been suggested, such as Jennigs, 1994, and Tennis, P 2000.

The basic solid sections forming the hcp core which are practically regarded as the bodies undertaking its intensive conditions are the following:

A. Calcium Silicate hydroxide (C-S-H): This is an amorphous material comprising particles of fibrous form, with a variety of form and dimensions that are relatively very small (0.13-0.22μm); it participates in the entire volume of the hcp at a percentage of 55%-62% depending on the cement type and w/c ratio. These small geometric dimensions and its plastic behaviour register it in the class of colloids, and is mainly the reason for which the component is called a gel. This component is satisfactory addressed with the Van Der Waals model. In regard to C-S-H and its structure, Jennigs, 1994, and Tennis, 2000 consider the construction of a colloid mass with a high porosity (26%-28%) and with a very small diameter, 14-15Å. These pores must not be confused with the capillary pores, which are of significantly larger dimensions. Another view was expressed by Fieldman and Sereda, 1968, supporting that the structure of C-S-H comprises three-dimensional arrangements of C-S-H levels, which at the final phase condensate their levels in thicker layers -this simulation supports the crystal form of C-S-H- the new arrangement of these layers creates interlayer spaces, hence areas where water resides.

B. Calcium Hydroxide-Ca $(OH)_2$ (portlandite). These particles are crystalline with spatial crystals of hexagonal geometry in prismatic form of various heights, that have a relatively large diameter in relation to the fibrous C-S-H (approx. 5-10 times larger), participate at a percentage of 25-30% in the total mass of solids and are dispersed within the body of C-S-H gel, as well as in the various voids formed during the creation of the entire spatial network. The Ca $(OH)_2$ phase is regarded as the weakest in the bulk of hcp.

The above two components are regarded as the basic elements - carriers of hcp, while the following also participate, in a lesser degree:

C. Calcium sulfoaluminates hydrates, a hydrate whose morphology comprises needle-shaped crystals that participate in the final solid matrix of hcp, also randomly dispersed in the matrix; their geometrical dimensions are similar to b. The name of this element is ettringite ($C_6A\hat{S}_3H_{32}$), while in later time phases and especially in Ordinary Portland Cement (OPC), it is converted to $C_4A\hat{S}H_{18}$ crystals, providing the hcp with a relative resistance to sulphate infections. The ettringite, with its crystal form, develops in the gel empty spaces, as well as close to the surface of the aggregates, in cases of mortar and concrete.

The clinker grains are relatively large clinker particles, of >35 μm diameter, with incomplete, or none, hydration, which during their hydration are converted to grains of smaller diameter, and which on later times participate in the bulk of the hcp with a relatively thick mass, which in certain occasions may absorb a small quantity of water from the water encapsulated in the hcp, resulting to dilation, thus increasing its deformation.

The above elements that may be considered as crystals or gel, as stated above in the description of the solid particles, form a complex composite body where various voids - pores are created, with a number of origins and causes; these are the weakest points in regards to hcp's mechanical stresses.

2.2.5 The important role of water.

The most important fact in the water - cement relation is the easiness with which water escapes from the hydrated cement paste.

Three categories have been suggested, classifying water in the hydrated cement paste; these being free water, chemically bound water, and the water in the interlayer spaces of C-S-H (Powers and Brownyard, 1946).

The case of chemically bound water is regarded as part of the solid section of the cement paste and may not be evaporated, unless thermal hydration is applied. Free water is located in the capillary pores, and water in the interlayer spaces of C-S-H refers to water that has been absorbed, as well as water that has been bound by the surface stresses of the cement paste.

The manner through which water escapes cement paste is important, since this is a very important cause for micro cracks created due to drying shrinkage.

Powers' model is one of the most acceptable models in regard to classifying the evaporated water from the cement paste and has practically proven that the water in the capillary pores may be evaporated more easily than in the other types of cement paste water, such as in the gel pores or in the case of chemically bound water.

However, it must be noted that the way of drying plays a significant role in the evaporation of water.

2.2.6 Cement paste, cement mortar, and pores.

The structure of pores in hydrated cement paste and in the cement mortar is very important for the natural and mechanical properties of the above materials. These voids may be regarded as the cement paste point defects, which are examined here as an independent material, as well as a participating entity in the cement mortar, which is the basic component of the experiments of this thesis.

The natural pores created between the structures of the particles C-S-H are of very small diameter (10-20 Å) do not initially seem to play an important role in the strength of C-S-H, which is the basic structural element of the cement paste. However, since water remains from the creation of hydrogen bonds in these voids, when water evaporates under conditions of dry environment, then these elements will constitute the first region where micro-cracks develop, due to the resulting drying shrinkage.

Another important void is created by the capillary pores. These are the voids that cannot be filled by solid parts of the spatial matrix of the cement paste, stated above. Porosity due to such voids includes two very important parameters: a) the diameter of the pores and b) their distribution in the spatial matrix of the cement paste. There are different views about the role of these parameters; the prevailing one is the view that the pores of large diameter, even with a smaller participation in the bulk of the paste related to small diameter pores, at the end create bigger strength problems for the cement paste.

A characteristic diameter value for defining the crucial pores is d> 50-55nm, where it is obvious that greater problems are created in the strength of the paste, than by pores of smaller diameter, such as the development of micro-cracks, either due to shrinkage, creep or due to a combination of both.

Finally, the water temporarily or permanently remaining in the microstructure of the hcp also participates in its weak zone. In particular, when the water is evaporated in the capillary pores, tensile stress will be applied to the perimeter of the pores, resulting to the presence of micro-cracks (drying shrinkage effect). In addition, the water absorbed in the hcp surface, creating hydrogen bonds in atmospheric conditions with relative humidity <35 is lost, and this loss will greatly contribute to shrinkage, starting from surface layers and leading towards the core of the hcp, hence creating regions of micro-cracks.

Another type of void is the air void created while mixing the component; this is of spherical form and its diameter varies between 10μm and 1mm. In terms of mechanics, they are sections trapped during the procedure of mixing the hcp component and will become another weak point in the crack creation process of the paste and mortar, in a completely different way. Finally, the water encapsulated inside the interlayer space in C-S-H is also stated. This is encapsulated with chemical bonds and there is no actual loss; There is only loss in case of mechanical stress that the chemical bonds change resulting in escaping of a small part of water by evaporation, thus, accelerating procedures.

2.2.7. Cement mortar – Interfacial Transition Zone: the weak phase

After extensively analyzing the microstructure of the cement paste, in the case of mortar concrete, there are a number of interfaces; regarding the specific material participating in the experiments of this thesis, the mortar, the interface between the paste and the sand particles are examined.

In the case of the cement mortar (fig 2.7), close to the sand grains there is a zone with a composition and porosity that significantly differs from the remaining mass of hcp, located in the bulk of cement mortar. This zone is the weakest connection in relation to the sand grains and hcp; it is also known as interfacial transition zone (ITZ). There are several aspects defining the role of the ITZ, however, there is a common assumption that the high porosity at the limits with the aggregates reduces its strength.
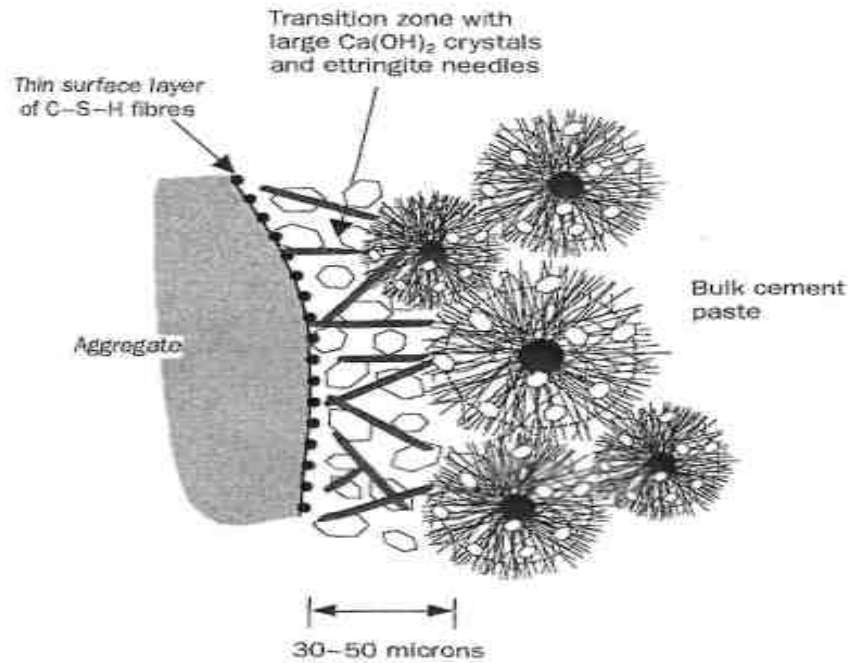
Fig 2.7: *Microstructure simulation of the transition zone at the paste-aggregate interface (De Rooij et al., 1998).*

Having an average thickness of 40-50μm (Olivier, Maso, Bourdette,1995) which is due to the manner with which the cement particles surround aggregates, ITZ presents a larger porosity; however, in certain occasions the thickness may be different, depending on the size of the aggregates and on the w/c ratio.

The microbleeding and wall effect phenomena are those explaining the presence if the ITZ. Wall effect s is created when the small sized cement particles meet an obstacle in the relatively large aggregates and may not easily disperse in the matrix of the cement mortar. The distance of the cement particles from the aggregates results to a high porosity and possible to higher values of water concentration, in contrast to hcp's bulk; it must be noted that the average size of the cement particles is approximately the same with the width of ITZ. (Olivier, Maso , Bourdette.,1995). In addition, microbleeding is a phenomenon that takes place during compaction and vibration of the cement mortar, while manufacturing it .The result of this phenomenon is that a small quantity of water remains in the lower section of the larger aggregates, thus creating conditions for increased porosity, which in these areas is 10% - 20% higher, than in the remaining hcp body (Scrivener, Crumbie , Laugesen, 2004).

As a result, ITZ is the weakest phase in the cement mortar, and generally in the cbm, and has a defining effect for the failure of these materials. An important factor for the formation of the ITZ, hence for its strength, are the aggregates, as well as their grade, the w/c ratio and the mixing and compaction of the separate materials in the cbm, in order to avoid creating continuous paths that increase the risk for a basic crack and the permeability elements, which significantly reduce its strength.

2.2.8 A short reference to Van der Waals bonds

This reference is made because it is assumed that Van der Waals bonds develop in the microstructure of hcp, especially in the hydrated interlayer C-S-H. During the development of cracks in the bulk of a cbm, the first microcracks will be created, since these bonds, as it will be shown below, are weak.

Initially, there are three different types regarding the atomic bonds (covalent, ionic, and metallic) and their appearance results from the need to restore the balance of free electrons. The ionic and covalent bond is of most interest in regard to hcp components.

The bonds of this form are universal along the entire surface of the atoms and molecules, but are practically weak; hence their effect disappears when the initial bonds prevail. These bonds are named Van der Waals bonds. For instance, through the application of the rules for these bonds, the actual gases deviate from the laws governing ideal gases. These bonds result when the electrons of an outer layer of a cloud - shaped element, are placed into orbit. The actual image is that of a cloud with such density, that there is definitely a possibility to meet an electron there. This means that the electrons are "distributed" near the atom, and for a set time period, they are symmetrically dispersed in the electron cloud.

The electron cloud moves and the electrostatic field around the atom continuously changes, thus resulting in a dynamic electric dipole (Fig. 2.8).
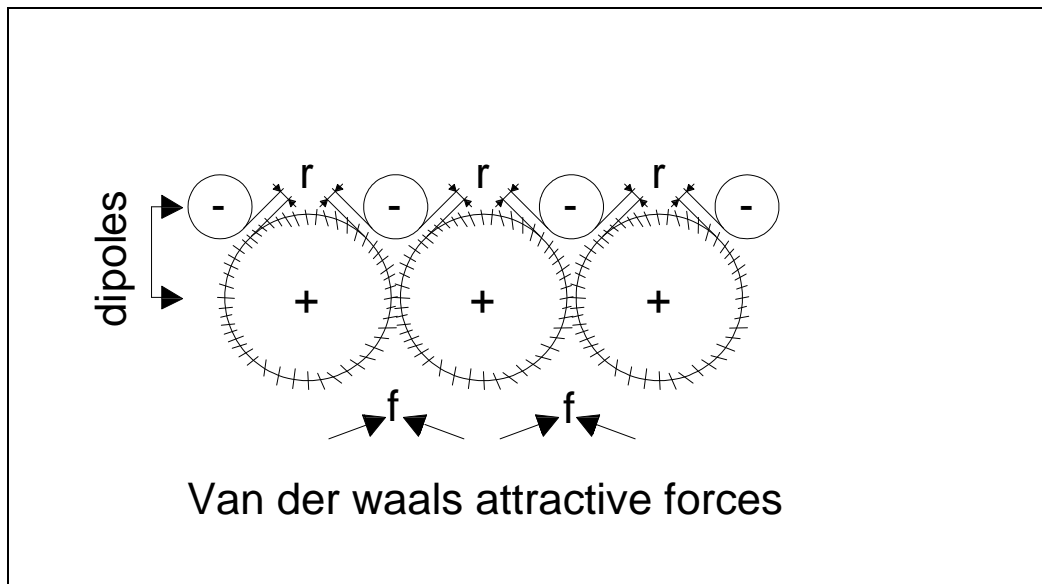
Fig 2.8 *A schematic representation of weak bonds according to Van der Waals model*

.

When another atom is present in the vicinity, the dipoles of the two atoms may interact in an additive manner, thus producing a weak, disoriented electrostatic bond. A very important example of dipole interaction refers to the compounds between hydrogen and nitrogen, fluor or oxygen; it is known as a hydrogen bond and appears due to the simple and small structure of the hydrogen atom. Within these frameworks, the simulated bonds of the basic components of hcp are included, where the created dipoles between the atoms in the interlayer spaces of C-S-H, with the presence of water, present inter-attracting powers -weak due to the power of Van der Waals bonds- as well as incoherent hydrogen bonds. As a result, the $Ca(OH)_2$ crystals initially create voids and then react to CO_2 of the atmosphere, resulting to $CaCO_3$ (calcite).

2.3 Mechanisms of electric current emissions

This section deals with the dominant underlying theoretical models that support electric phenomena accompanying stress application. The Moving Charged Dislocations model explains electric current emissions due to dislocation movements and crack opening and propagation processes. A second potential cause is the electrokinetic effect that can be applied for the cases of fluid flow in solid materials through pores or cracks. The piezoelectric effect dominates the electric current generation in quartz-rich materials. All these phenomena have been studied in depth by several researchers and results have been discussed during the last years.

2.3.1 Moving Charged Dislocations model

The electrification due to imperfections in the structure of a brittle material has been introduced by Slifkin (1993). This approach was improved and further investigated by Tzanis and Vallianatos (2002); and Vallianatos and Tzanis, (1998, 1999).

When brittle materials are stressed, it has been observed that this action is accompanied by an electric current generated within the material. Although there are several theories to explain this phenomenon, the one favored is the Moving Charged Dislocations model (MCD) first described by Vallianatos and Tzanis (1999) as it most closely fits all the experimental data. This model was built based on experimental data from geomaterials. In this work the MCD model is used to examine the health of cement based products. The MCD model seems to explain the observed relationship between current density and strain rate through the propagation of arrays of charged edge dislocations through the material during microfracture. Before the fracture, stress and strain increase and microfracture begins with large numbers of propagating cracks giving rise to electric fields that will superimpose to create pre-fracture electric current emissions. The motion of dislocations occurs parallel to the applied shear stress. This allows for the generation of a dipole electric field, parallel to the slip vector of the moving dislocations, hence quasi-parallel to the slip vector of shear cracks and by the self-similarity of fragmentation and faulting processes, to the slip vector of the upcoming fracture.

Dislocations and other mechanical imperfections may occur in different mechanical process (i.e. tension, compression, bending, and torsion). For instance, the defect could point to any direction, and would move depending on the loading mode. Thus, according to the assumption that the electrical neutrality is maintained around a physical defect for a heavily deformed material when the material does not suffer any mechanical processing this neutrality cannot be further maintained when the bulk structure of the material is deformed due to any kind of mechanical loading (tension, compression, bending e.t.c). The movement in the net of the material structure would generate dipoles of opposite signs and the net polarization would not be zero (Vallianatos and Tzanis, 1999). Clearly, any net electrical polarization of one sign, must be the result of a net excess of charged dislocations with a particular mechanical moment.

Next, consider that the motion of a dislocation or any other kind of physical imperfection may result in crack formation by the piling-up (the Fracture Process Zone) of the linear defects (for cement mortar are microcracks and cracks) when the leading dislocation gets locked by some obstacle (i.e. sand grains). An assumption from the MCD model is that the stress concentrations near the first locked dislocation of an array is equivalent to the product of the applied stress times the number of dislocations in the array. Propagation of cracks occurs when a new dislocation array enters the crack. The dislocation-to-crack process has been considered for interactions along a single dislocation plane, on which dislocations move under the influence of an external stress field. The corresponding processes that take place in cement based materials have been presented earlier in this chapter. It is indicative that the net polarization is produced around the crack formation (fig 2.9)

Generalizing the formalism of the MCD model it can quantatively be described by the following assumptions:

Assume that D describes the electrical properties of the bulk structure of the material. Specifically, it contains the kind and the charge distribution around a crack formation (the stress concentration is the mechanical analogue). When this distribution is distorted due to mechanical stress and crack motion, leading to deformation, a polarization is formed in the bulk. This polarization can be described as $D \cdot \dfrac{\delta x}{\sqrt{2}}$

where δx is the distance a dislocation moves due to mechanical loading. The observed mechanical strain is linearly related to the quantity δx.

Thus since the rate of the polarization change $\dfrac{\partial P}{\partial t}$ describes the flow of the electric current (I) it can be considered that:

$$I = \Gamma \frac{d\varepsilon}{dt}$$

where Γ stands for the physical and electrical parameters of the material charge distribution around and a crack formation .

Since current density is related to the deformation variations it is expected that when external mechanical loading is applied on a sample electric current emissions are expected. When the rate of the applied loading leads to a constant deformation rate, no electric current is expected.
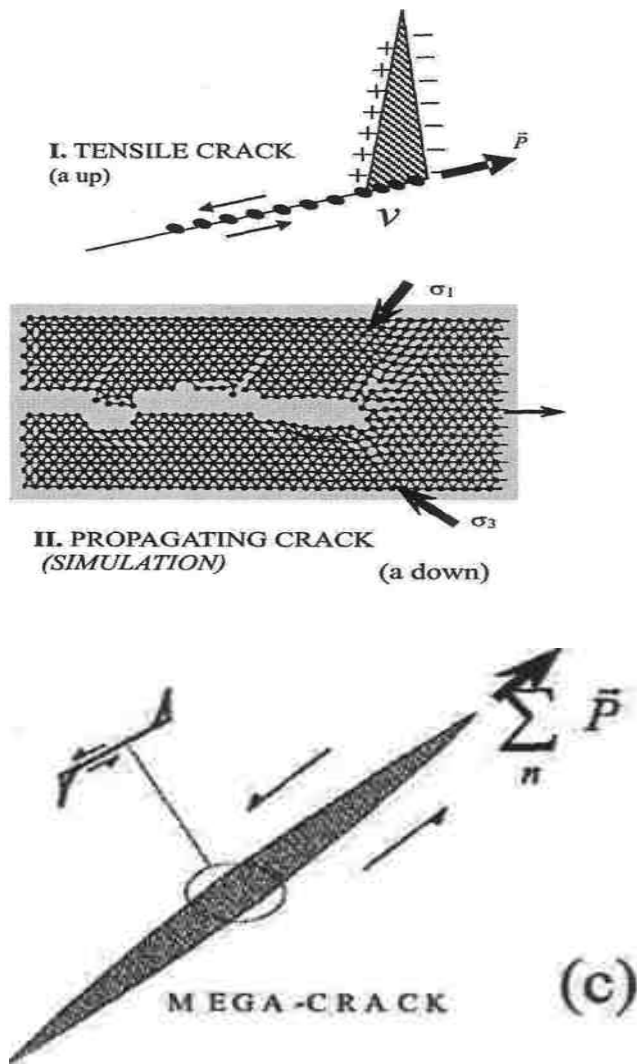
Fig. *2.9: (a) Schematic diagram of the proposed model of electrification by Moving Charged Dislocations during microfracturing. (up) is a simplistic sketch of a tensile crack forming at the tip of a dislocation array. The slip plane is parallel to the applied shear stress and the electric polarization vector is the resultant of the polarization vectors of the v moving dislocations, lying on the slip plane and in the same direction as the slip vector, (down) is a computer simulation of an unstably growing crack in a simple atomic scale, (c). Meso- and mega- scale cracks are fractal ensembles of shear micro-cracks with parallel slip planes; the induced polarization vector is parallel to the slip plane and comprises the resultant of the polarization vectors of N simultaneously propagating microcracks in the ensemble. (Vallianatos and Tzanis, 1999).*

Cracks are fractal ensembles of several shear cracks propagating with parallel slip planes subject to the same external shear stress, as is schematically depicted in fig.2.9 a. By the superposition principle, the electric dipole moment of a material structure will comprise the resultant of all the simultaneously propagating cracks, sub-parallel to the slip plane and in the general direction of the slip vector of the propagating fractures (Vallianatos and Tzanis, 1999).

It has been experimentally verified that when mechanical stress is applied upon a rock or more generally on a brittle material it is accompanied by the production of weak electric variations, most usually by weak electric currents (Pressure Stimulated Currents – PSC).

As the magnitude of stress increases reaching the plastic deformation range of the material, microcracks occur randomly starting at the heterogeneities and spreading within the bulk of the sample. In the beginning, the structural imperfections produced are not linked but as the "stream" of microcracks increases they interact and a correlated microcrack net structure starts appearing. The microcracks eventually coalesce leading to the irreversible fracture process. The same phenomenon but with different procedure has also been observed and presented here in cement product samples.

According to the most dominant model that interprets such electric phenomena there is a relationship between current density and strain rate through the propagation of arrays of charged edge dislocations through the material during microfracture.

This process may scale up to the fracture that occurs within the mass of or cement based material. Before the main crack stress and strain increase and microfracture begins with large numbers of propagating cracks giving rise to electric fields.

According to the MCD model described, the temporal evolution of the emitted PSC(t) during a process that a time varying uniaxial load is applied, can be described by a law of the form:

$$PSC(t) \propto \frac{d\varepsilon}{dt} \qquad\qquad Equation\ 2.11$$

where $\dfrac{d\varepsilon}{dt}$ is the strain rate. For an elastic material Hooke's law is applicable and is written in the form:

$$\sigma(t) = E_0 \cdot \varepsilon(t) \qquad\qquad Equation\ 2.12$$

where E_0 is the modulus of elasticity of the undamaged material. Equation 2.12 is valid only when the applied stress is lower than the "yield stress" ($\sigma \leq \sigma_y$).

Based on Eq. 2.11 and 2.12 for the cases that the applied stress does not exceed the "yield stress" PSC are expected to be emitted. Exceptionally this does not apply when the applied stress rate is very high and practically the sample suffers an abrupt stress increase. Such an abrupt stress change even in this range seems to cause damages into the material and PSC emissions can be detected.

For the case that the applied stress is greater than the "yield stress" ($\sigma \geq \sigma_y$) the modulus of elasticity gradually decreases and the material enters the damage range.

In this case a variable that quantifies the damage grade is introduced as "damage variable" α, (Turcotte and. Shcherbakov, 2006) and is described by the following form:

$$\sigma = \sigma_y + E_0 \cdot (1 - \alpha) \cdot (\varepsilon - \varepsilon_y) \qquad\qquad Equation\ 2.13$$

where $\varepsilon_y = \sigma_y/E_0$. The damage variable varies between 0 and 1. When α=0, linear elasticity dominates. When α approaches to 1 failure occurs. Increasing the value of α in the range 0 to 1 the weakening of the material is quantified and the E_0 becomes lower and is straight forwardly associated with the increase in the number and size of microcracks within the material.

2.3.2 Piezoelectric model

Piezoelectricity has been considered as a phenomenon that takes place when fracture events occur in brittle materials by (e.g. Yoshida, et al., 1994; Yoshida et al., 1997; Nitsan, 1977; Warwick et al., 1982;). the applicability of piezoelectric mechanisms is under investigation since it is possible for the macroscopic electric field to be canceled due to the orientation of quartz crystals. (e.g. Tuck et al., 1977). Several experiments attribute the generation of electric signals to the fracturing of brittle material due to mechanical loading .(e.g. Enomoto et al., 1994; Yoshida et al., 1997 in simulated faults; Sasaoka et al., 1998), with the high stress rate, of a specific distribution and geometry.

Laboratory experiments have been conducted on geo-material samples under mechanical loading and led to the discovery of electric current emissions and electromagnetic activity. A model that explains the generation of electric signals due to the piezoelectric effect has been proposed by (Yosida et al., 1994, Ikeya and Takaki, 1996, Yosida et al, 1997).

Rock samples subjected to static loadings are found electrically polarized in proportion to the stress, but the polarization charges are neutralized by the compensating bound charges which have moved to the quartz surface. Thus the polarization cannot be detected as an electric potential signal outside the rock. When loading variations occur, the neutral state is distorted and a measurable polarization rises due to the bound charges. Despite the fact that this model is based on a well known effect (piezoelectric) it is not applicable for all kinds of materials. In this work electric current emissions were experimentally detected from a quartz-free material like hardened cement paste and cement mortar. It is also known that performing similar tests on other kinds of materials like marble, electric current emission were observed and cannot be attributed to piezoelectric effect since the specific type of material has only 0.40% quartz content. Conclusively, this model is not applicable in our case because the cement paste (hcp) should not give any electric current emission since it does not contain quartz.

2.3.3 Electrokinetic model

Electrokinetic phenomena such as the electrification caused by a flow of water crossing layers of rocky surface - the permeability of rocks may be due either to gravity or deformations due to mechanical reasons (overloads) - have been proven at a satisfactory level in laboratory experiments (e.g. Morgan et al, Jouniaux and Pozzi, 1995a,b, 1997). Practically, the electrokinetic phenomena are favoured close to areas that are prone to earthquakes; the wet models are stated for the preparations against an earthquake (e.g. the Scholz et Al, 1973, model. As a result, the electrokinetic model is a fairly frequently stated mechanism (e.g. Mizutani et al, 1976 Bernard and Le Mouel, 1996, Bernard, 1992 Fenoglio et Al, 1995). Yoshida et al. (1998) suggested the elecrokinetic model as the main source of possible electric potential changes, during the creation of small cracks in hydrated samples of sandstone.

2.4 Electric current emissions from geomaterials

This section presents certain results from measurements performed in marble samples, along with representative plots and certain assumptions that will be an important tool for comparing results with the experiments of the current thesis, which involve hcp and cement mortar samples. The different structure of crystal formed marble, the different

porosity and permeability levels are a challenge for comparing the emitted PSC; this comparison will contribute to the development of future experiments. The experimental results presented here correspond to measurements on marble and have been conducted in the "Laboratory for the study of Electric Properties of Materials" at the Technological Educational Institution of Athens. They have been published in international journals.

2.4.1 Constant stress rate up to fracture

When compressive load is applied on marble samples at a constant stress rate up to fracture the form of the emitted PSC can be seen in Fig. 2.10 which presents the linear increase of the stress (left-hand axis) in MPa, as well as the emitted PSC (right-hand axis) in pA. When the stress exceeds the 70% of the ultimate compressional strength of the sample i.e. to the limit where the stress-strain curve deviates from linearity, significant PSC are developed. The interesting point is that the maximum peak value of the positive current appears before fracture load and immediately changes polarity.
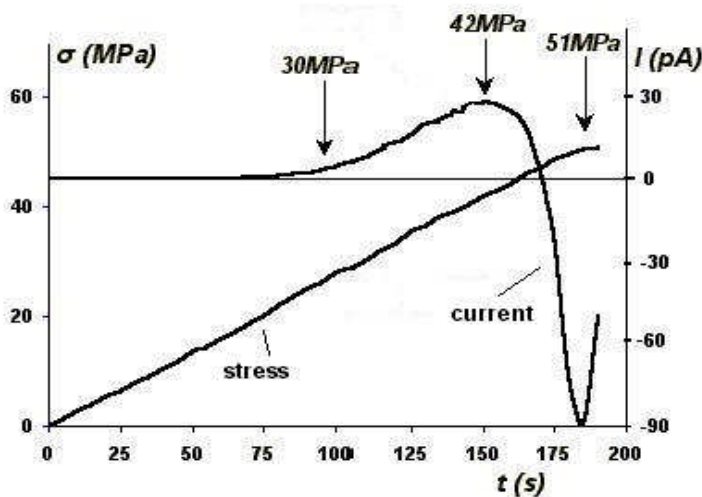
Fig. 2.10: *Correlation of PSC and applied stress with respect to time. The values of the corresponding stress are noted on the PSC curve for the first appearance of PSC, for the maximum PSC and for the fracture. (Stavrakas et al., 2003)*

2.4.2 Abrupt stress steps

When abrupt compressional stress steps are applied on marble in the form of the upper part of Fig. 2.11 a PSC emission like the one presented in the lower part of Fig. 2.11 is

emitted. This Fig. shows the time development of the abruptly applied stress steps (upper part of the Fig.) and the emitted PSC (lower part of the Fig.). It is significant to mention that whenever the applied stress increases the corresponding PSC emission gets to a higher peak. This is attributed to the fact that the sample approaches failure and massive crack formations are produced and develop faster.
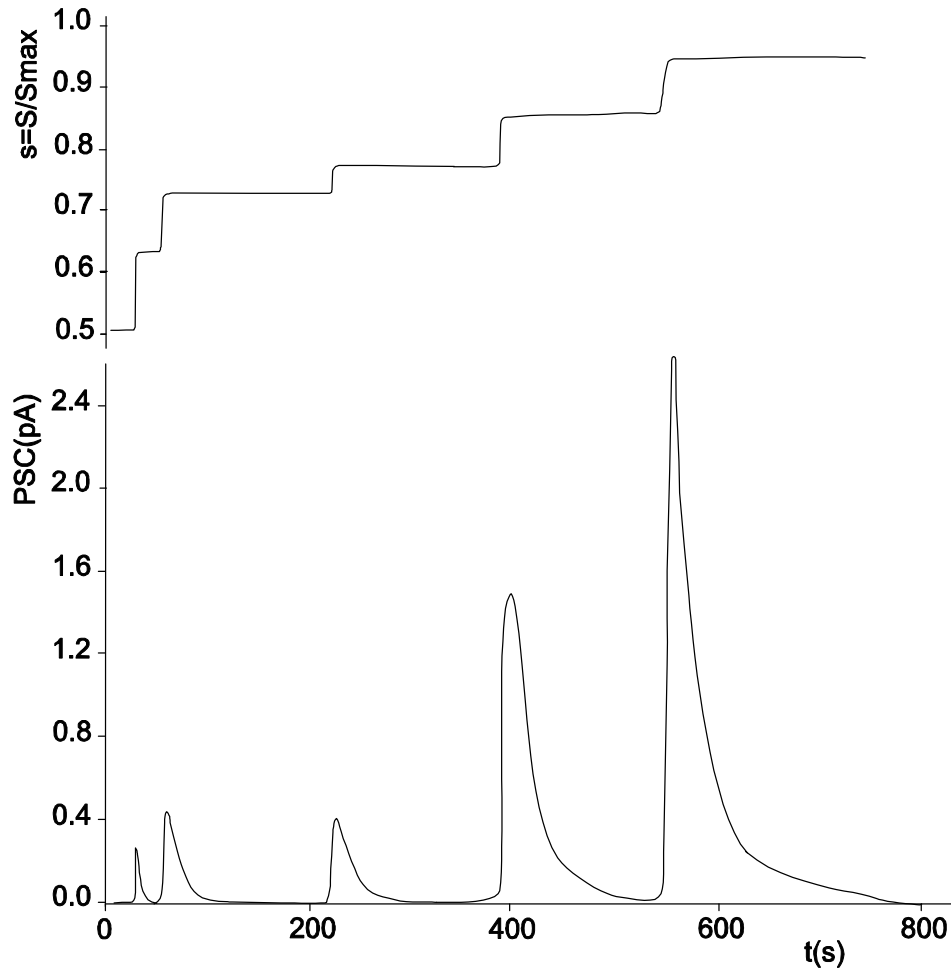

Fig. 2.11: *Abrupt compressional stress steps in the vicinity of fracture (upper part of the Fig.) and the corresponding PSC emission (lower part of the Fig.)(Triantis et al., 2006a).*

2.4.3 Sequential loading cycles

Fig. 2.12 shows the behaviour of the emitted PSC when sequential compressional loading cycles (fatigue) are applied on a marble sample. Specifically, curve **a** corresponds to the first loading cycle, curve **b** to the second and curve **c** to the third. During this last loading the sample was led to fracture and the expected PSC reduction before fracture is obvious in the same Fig. Each loading and unloading is performed at a constant load rate. It is indicative that during each next of the loading processes the

emitted PSC has a lower peak. The authors attribute this phenomenon to the limited number of the remaining crack formations to be activated during each next cycle. Since cracks are the stimuli of the emitted PSC and they cannot be further activated when the sample has already suffered the same stress levels it is expected for the electric current to become lower when these formations are limited.
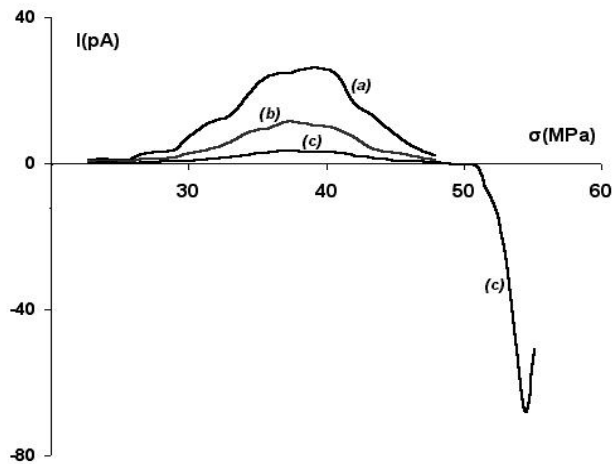

Fig. 2.12: Consecutive PSC curves at a constant stress rate indicative of the results of the "fatigue "procedure. (a) Initial compression, (b) Second compression, (c) Final compression up to fracture (Stavrakas et al., 2003).

3. Experimental methods of measuring Pressure Stimulated Currents (PSC)

3.1 Introduction

In this chapter, the behaviour of cement product samples under various modes of stress is presented. The modes of the applied stress and other experimental details like the sample composition will be described. Additionally, a detailed description of the experimental arrangement (i.e. both the mechanical and electronic parts) and the custom made software that is used to handle the devices and to collect the measurements of the stress, the strain and the PSC will be given.

3.2 Arrangements

A description of the arrangements used in the laboratory for realizing the PSC and BSC experiment is described below. Specifically, the mechanical arrangements, methodology, and specialized electrical measurements are described. In addition, the electric insulation and protection from external interference is described, along with a presentation of the recording and data processing software.

3.2.1 Mechanicals

The experimental apparatus and technique supports the detection and recording of the weak currents during laboratory experiments. Fig. 3.1 shows the experimental setup.

The experiment has been conducted within a Faraday shield to prevent from electric noise. The noise-protected system comprised a uniaxial hydraulic load machine (Enerpac-RC106) that applied compressional stress to the cement samples. Depending on the experimental technique that was occasionally applied each sample was placed between two thin plates of teflon, in the direction of stress, in order to provide electrical insulation.

Stress was to be applied to the cement paste and cement mortar samples following two kinds of loading, abrupt stepwise and monotonically increasing at constant rate. The manual pressure machine (Enerpac P-142) was deemed most appropriate to achieve sudden increases in pressure for the abrupt stepwise method.

The electric pump (Enerpac PUJ-120E) was deemed most appropriate in delivering approximately constant rate increases in pressure over the duration of an experiment that might last 15 min. before it reached failure.
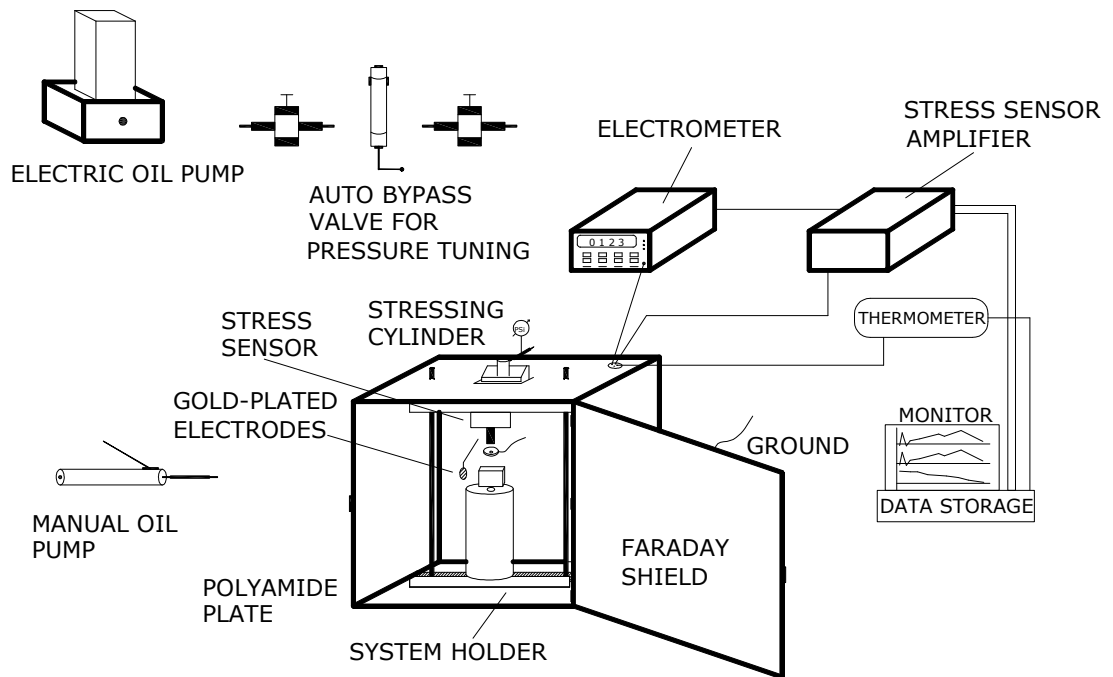
Fig. 3.1*: The experimental apparatus for measuring Pressure Stimulated Currents (PSC)*

Mechanical valves were used to control the oil flow in the hoses. In the first arrangement a valve (Enerpack V66) was used to cut the flow of the oil to or from the pressure cylinder (Enerpac cylinder R-106) abruptly, thus creating ideal step changes. In the second arrangement the flow of oil to the pressure cylinder could be more accurately controlled for constant rate of increase by running the pump at a higher rate and bypassing part of the stream back to a storage tank through a valve (Enerpack V82). In cases when pressure was to be maintained for an extended period, a non – return valve (Enerpack V152) was used between pump and pressure cylinder.

3.2.2 Electronic measurements

A pair of gold plated electrodes was attached to the cement mortar and paste sample, using conductive paste. The electrodes were attached depending on the applied technique either in a direction perpendicular to the axis of the applied stress or at the upper and the lower sides of a sample beam when applying bending tests. For the electrical measurements sensitive programmable electrometers Keithley 617 and 6514

were used. The electrometers used exhibit low input voltage burden and extremely low input offset currents. This is achieved by measuring current as a feedback type Pico ammeter. This is in contrast to the shunt method used by many digital multimeters. The used electrometers can resolve currents from 0.1fA to 20mA in 11 ranges.

The equivalent electric circuit of the system (i.e sample, electrodes, electrometer), as well as the current measuring stage of the electrometer is shown in Fig. 3.2.

All the recordings originating from the electrometers were stored in a PC through a GPIB interface.

The values of the externally applied stress were measured using a stress sensor, with values recorded onto PC through an A/D card. Sets of axial strain gauges were attached to the sample in the middle of each surface. A manometer was used to measure the oil pressure in the hoses.

The strain was measured using Kyowa strain gauges attached on the Microlink-770, 120Ω resistors bridge while the bridge distortion was directly recorded on the PC through a 8 differential channel, high sampling rate and 500x maximum amplification, Keithley A/D converter. The same A/D converter recorded the stress level.

During the experimental procedure a camera was installed in the Faraday shield where the sample was compressed and real time video was recorded.
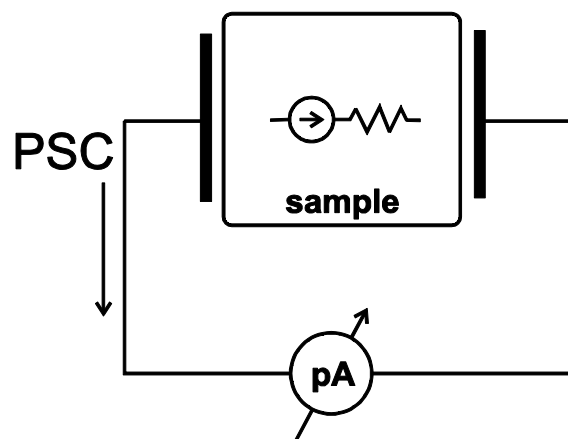

Fig. 3.2: *Electrical equivalent of the measuring system, current measuring stage.*

3.2.3 Shielding and Protection

It is very important to cater for the protection of the measurements realized during the experiments from various noises of the surrounding area, as well as from various

electric, electromagnetic, or other radiations that could affect the relatively small values of the emitted currents. For this reason, a Faraday shield was used, as described below. The Faraday shield has dimensions 500x500x600mm. Two layers of ferromagnetic metal sheet prevent electric and magnetic noise. The shield was selected to be able to reduce the electromagnetic interference of frequency lower than 2GHz to levels below the threshold of the measuring system. The sides of the shield have been ruggedized in order to prevent from several damages from fragments of cement samples during the experiments. The shield has been grounded using thick copper wire. Electrical interference, in the experiment is minimized by placing only the essential parts of the equipment inside the shield while all other electronic devices and the oil pumps were kept outside. All wires have been carefully led out of the shield using the appropriate interfaces.

At very low current signal levels, noise generated in the cable can affect measurements. The source of this current is generated by triboelectric effects which constitute a primary cause of noise currents generated in connecting cables. These currents are generated by charges created at the junction between a conductor and an insulator because of friction. Coaxial and triaxial cables are especially prone to such noise currents due to cable flexing. To minimize these effects, the cable used has been fixed firmly to minimize any flexing. However, even with low noise cables, cable movements can generate several tens of femptoamps of noise currents.

3.2.4 Software for conducting the measurements.

Custom made software was used to handle the electronic equipment, to set the parameters of the experiments to store and roughly analyze the measurements. Fig. 3.3 shows the interface of this software. The upper plot of the software depicts the measured currents at a primary and a secondary axis depending on the number of the used electrometers. The entire axis and the colours of the graphs are adjustable during the experimental procedures. Moreover, during the experimental procedure the axis can change from linear to log or the limits of the axis can also change. The second plot area contains the temporal variation of the stress (primary axis) and the temporal variation of strain (secondary axis). The lower plot provides a preliminary view of the $d\varepsilon/dt$ quantity.
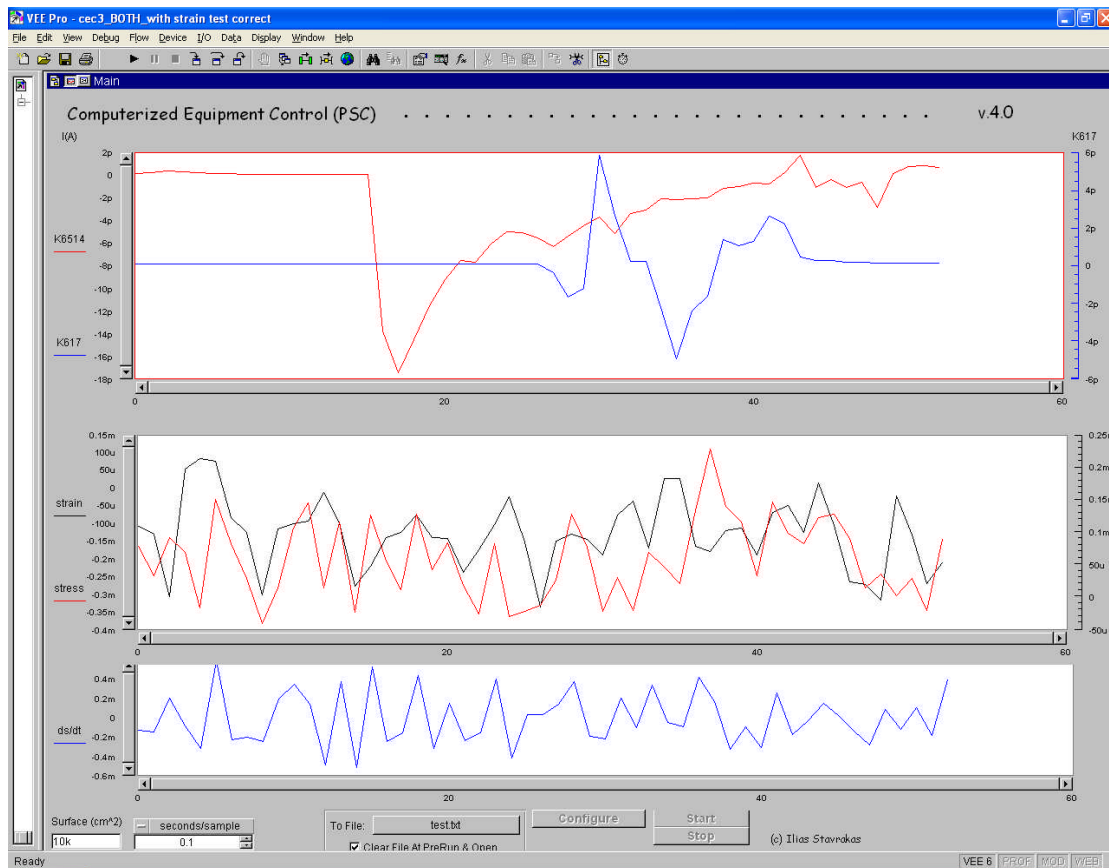
Fig. 3.3: *Snapshot of the software that is used to perform PSC measurements.*

3.3 Samples under test preparation and specifications

During this work two types of cement based materials are studied in depth.

a) Cement mortar samples

b) Hardened Cement Paste (hcp)

All the used samples (a: cement mortar, b: cement paste) that were used for conducting the experimental work of this thesis were classified depending on their dimensions in 6 categories: CM70, CM50, CM160, CP40, CP50 and CP100. The CP or CM prefix defines the material. Specifically CM stands for Cement Mortar and CP for Cement Paste. The number that follows this prefix describes the length of the sample in mm. Table 3.1 contains the above six categories of materials providing also information regarding their dimensions, the applied experimental technique as well as the maximum stress or load values the sample suffered before fracture.

Table 3.1

Description of the used samples depending on the applied experimental technique.

Material	Category	Dimensions (mm)	Fracture limit	Technique
Cement mortar	CM70	50x50x70	50-60 (MPa)	LSRT
		50x50x70	46-53 (MPa)	ASST sequential steps up to fracture
	CM50	50x50x50	25-30 (MPa)	LSRT with constant stress that remains at a high level up to fracture
	CM160	40x40x160	1.4-1.6 (kN)	Three point bending tests
Cement paste	CP40	40x40x40	25-29 (MPa)	Loading – unloading with constant stress rate
	CP50	50x50x50	28-35 (MPa)	ASST with sequential steps up to fracture
	CP100	40x40x100	1.05-1.25 (kN)	Three point bending tests

What follows is a description of the used cement samples that were prepared by the research team of TITAN (Greek cement industry) as well as representative stress strain curves as produced at the Laboratory of Electric Properties of Materials of the Electronics Department of the Technological Educational Institution of Athens.

All the samples were provided by the same manufacturer and are of comparable characteristics concerning their composition and ingredients.

The used OPC (Ordinary Portland Cement) consisted of: (symbols in parentheses are typical shortcuts) $3CaO.SiO_2$ (C3S) 54%, $3CaO.Al_2O_3$ (C3A) 19%, $2CaO.SiO_2$ (C2S) 17%, and $4CaO.Al_2O_3.Fe_2O_3$, (C4AF) 9%. Various physical properties of the cement paste are shown in Table 3.2.

Table 3.2

Physical properties of cement and recommendations for OPC -43 grade cement

Property	Value	EN-197-1 cement codes recommendations
Fineness, %(residue on 90 µm sieve)	2.70	<10
Standard consistency , %	27.50	-
Setting times		
(a) Initial (min)	120	≥ 30
(b) Final (min)	210	≤ 600
Specific gravity	3.10	-
Compressive strength compared to the ultimate compressional strength		
(a) 3 days	53%	≥ 23.00
(b) 7 days	76%	≥ 33.00
(c) 28 days	100%	≥ 43.00

Fig 3.4 presents a representative typical stress strain curve extracted from the used cement mortar sample. The axis of the axial compressional stress is normalized and represents the relative compressive stress $\hat{\sigma}$ that defined as:

$$\hat{\sigma} = \frac{\sigma}{\sigma_{max}}$$
Equation 3.1

were σ_{max} is the ultimate compressional stress strength that corresponds to the value the failure occurs. After conducting stress strain tests to cement paste samples and comparing them to those of the cement mortar it was concluded that for both categories of the samples (cement mortar and cement paste) the value of the relative yield stress that is given as

$$\hat{\sigma} = \frac{\sigma_y}{\sigma_{max}}$$
Equation 3. 2

corresponds to the range $0.1 < \hat{\sigma} < 0.7$ where the stress is linearly related to the strain. The value of the cement paste Young's modulus is $E_0 = 260\sigma_{max}$.
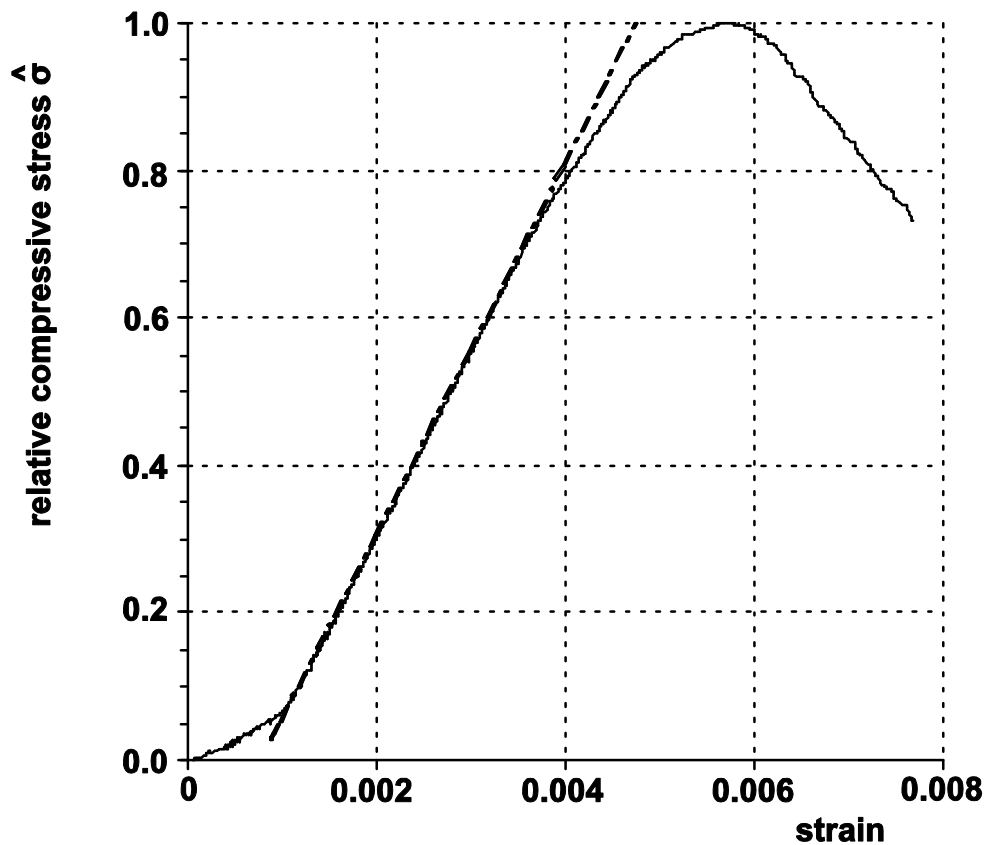
Fig. 3.4: _A representative curve that describes the relative compressional stress with respect to strain for the used cement mortar samples._

3.3.1 Cement paste

The used cement paste had the following characteristics:

For all the samples, OPC Portland cement was used, from the laboratories of TITAN Greek cement industry. The water / cement ratio 0.50 and the mixing time through the use of a metallic mixer lasted for approx. 2 minutes. After the completion of the mixing, the mix was cast to properly formatted moulds that had been internally lined with proper form-work oil. The metallic moulds were of cubic and orthogonal prismatic form in order to serve the compressive and bending tests. When the sample was placed inside the moulds, compaction was effected through the application of a small-sized vibrator for two additional minutes, in order to remove the air. The samples were removed from the moulds after 24 hours and were cured by remaining in an area with stable temperature and wet environment, securing a humidity of 75 - 80%; the samples remained in this area until the time for the experiments.

3.3.2 Cement mortar

For all the cement mortar samples, OPC Portland cement was again used, from the laboratories of TITAN Greek cement industry. The ratio (weight) of the separate materials was: 3 parts of fine aggregates - sand, 1 part of cement and 0.50 part of water. The maximum diameter of sand grains was 3mm and in the granulometric composition, the last sieve was 600 μm. In regard to the sand, its fineness was 2.8 and its special gravity was 2.60, while the density was 2.20 and its porosity was evaluated at approx. 8%.

The mixing of the solid sand and cement ingredients lasted for approx. 1 minute and then, with an appropriate mixer, some further mixing with gradually adding water occurred for 2 more minutes. The mixing was performed with a slow speed for better moisturizing the cement grains. Afterwards, for 1 minute, the mixing in the mixer's quick spinning rate was performed leading finally to casting the sample in metallic moulds, with oiled internal surface, of cubic and rectangular form for the cubic samples in the compressive tests and for the rectangular samples at the size of a small beam. In order to improve compaction, a desktop vibrator was used, in order to remove the air trapped in the bulk of the mixture with the best possible manner. The samples remained in the moulds for one day and then, after being removed from them, were placed in a room with a steady ambient environment, and with 75-80% humidity. They stayed there until the time for the experiments, which was 100 days; during this period, the samples reached 90-95% of their total strength.

3.4 Applied techniques

Based on the above an attempt was made to investigate the behaviour of cement based materials with respect to the detected PSC when these samples are subjected to temporal axial loading in the linear and non-linear regions of the stress-strain curve as well as slightly before failure, and the transition phenomena between the linear and non-linear stages.

Additionally the PSC emission was studied during the application of constant and high axial loading in the vicinity of failure. Further experiments were also conducted to show the change in the characteristics of the currents, which depends on pre-existing damage of a sample (work hardening) or the irregular longitudinal splitting, which was observed during failure.

For the very first time current emissions were studied when cement based sample was subjected to three point bending stress (load) in the linear and non-linear regions as well as slightly before failure, and the transition phenomena between the linear and non-linear stages. The above experiments were rendered under the term Bending Stimulated Currents.

Electric current emissions were monitored throughout a series of experiments in which the samples were subjected to a variety of time varying forms of compression and bending in different region of strain for the sample, linear, non-linear, fracture. Stress was applied in different modes as follows:

a. Application of axial compressional loading with constant stress rate and concurrent PSC recordings (Low Stress Rate Technique, LSRT).

b. Current emission recordings during abrupt, axial, compressional load application (with high stress rate) from an initial stress level to a higher one (Abrupt Step Stress Technique, ASST).

c. Current emission recordings while the stress was maintained practically constant in the range where the sample reaches its ultimate stress strength.

d. Current emission recordings on experiments sequential loadings and unloading at relatively high stress level.

e. Current emission recordings in three point bending tests with constant and stepwise stress increase on cement paste and cement mortar samples.

The first four cases are known as Pressure-Stimulated Current (PSC) technique while the fifth is rendered under the term Bending Stimulated Current (BSC) Technique.

A typical sample setup to conduct experiments using the PSC technique can be found in Fig. 3.5. In this experimental technique, a pair of gold plated electrodes was used, placed perpendicular to the stress axis. The electrodes were circular with a 20mm diameter. Each electrode was placed at the center two opposite sides of the sample. Strain gauges were placed at the center of one of the free sides of the samples.

It is also common to add Teflon plates between the stressing system and the sample to provide electrical insulation. This causes differences to the fracture layers of the samples since it increases the friction force between the load cylinder and the sample. Sequential experiments showed that the qualitative characteristics of the emitted PSC when using or not Teflon are not influenced.
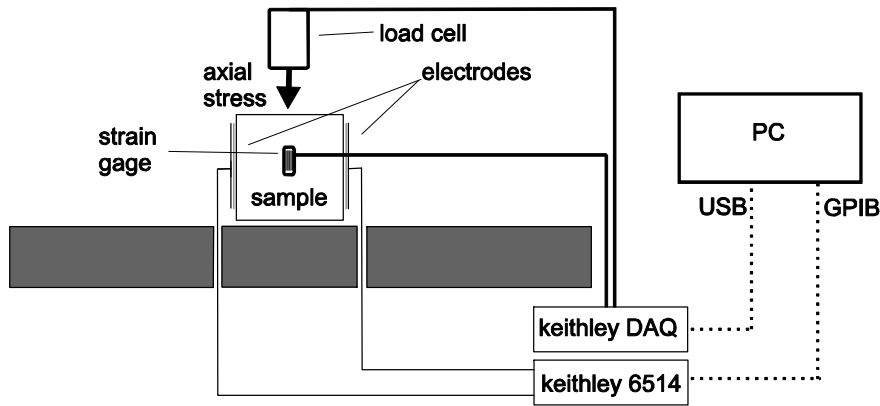
Fig. 3.5: Schematic representation of the sample set-up when applying uniaxial compressional stress and performing PSC experiments.

The experimental setup is different when conducting BSC experiments. In this case two electrometers are used that are connected to two sets of electrodes. The first electrode is connected to the upper side of the sample and the second set is connected to the lower side of the sample (see Fig. 3.6). The surface area of all the used electrodes for the bending tests was the same and equal to 120mm^2. The electrodes were gold plated and were attached onto the sample as it is illustrated in the Fig below. The sample is placed on two prisms and the load is transferred on the sample through a third pin. The two lower prisms are placed at equal distances from the prism where the load was applied. Specifically, each pin is placed 70mm away from the central axis. The upper side and the lower side electrodes were attached symmetrically with respect to each other. The electrodes are placed 20mm away from the central axis.
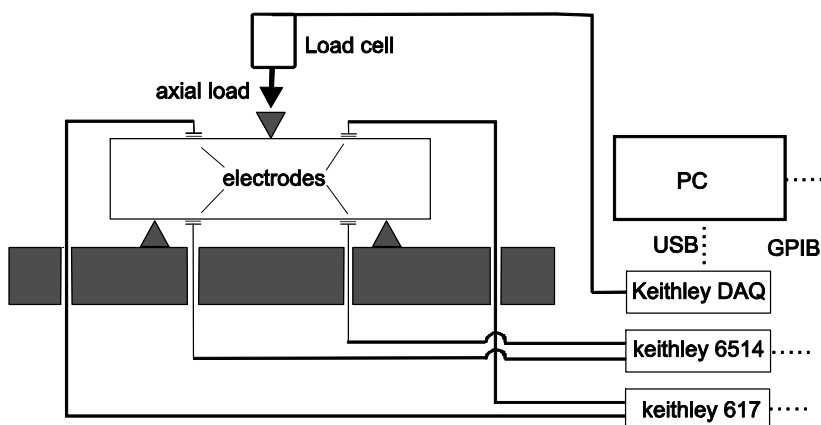

Fig. 3.6: Schematic representation of the sample set-up when applying bending loading.

3.4.1 Low Stress Rate Technique (LSRT)

In this technique a stress increase is applied to the sample from early stress levels up to fracture. The uniaxially applied stress is increasing linearly at a slow rate described by:

$$\sigma = a \cdot t \qquad\qquad\qquad \textit{Equation 3.3}$$

the a is the stress rate, the values of which do not usually exceed 500kPa/s and the ordinary values are around 100kPa/s. Failure occurs at time $t = t_f = \sigma_{max}/a$, where σ_{max} is the ultimate compressional stress strength.

This stressing technique causes gradual failure of the sample without forcing non-linear dynamic phenomena that are caused due to fast stress application. According to the Eq. 2.11 this technique is suitable to study only the non-linear ($\sigma > \sigma_y$) range of the materials behaviour since the emitted PSC is expected only when $d\varepsilon/dt$ is not constant. This experimental technique henceforth will be referred as Low Stress Rate Technique (LSRT).

3.4.2 Abrupt Step-Stress rate Technique (ASST)

In this technique while the sample is in a state of constant uniaxial stress σ_k, an abrupt stepwise stress increase of short duration Δt is applied so that the uniaxial stress increase by $\Delta\sigma = \sigma_{k+1} - \sigma_k$, where σ_{k+1} is the new state after the application of the stress increment (see Fig. 3.7). It must be noted that the new stress state σ_{k+1} remains constant until the PSC restores to a low level. The aforementioned temporal variation of stress σ, which was recorded during this experimental procedure could be described in a good approximation by the following equation.

$$\sigma(\tau) = \begin{cases} \sigma_k = \text{constant} & \text{for } t < t_k \\ \sigma_k + b(t - t_k) & \text{for } t_k < t < t_{k+1} \\ \sigma_k = \text{constant} & \text{for } t > t_{k+1} \end{cases} \qquad \textit{Equation 3.4}$$

where b is the stress rate during the stress increase from an initial level σ_k to a final σ_{k+1}. Typical values of stress rate b vary between 1.5MPa/s and 5MPa/s and are always greater than those of the LSRT technique. A series of sequential abrupt steps of stress can be applied on the sample under test and evaluate the PSC emitted for all applied stress ranges from very low stress levels up to very high, near the vicinity of fracture. This experimental technique henceforth will be referred to as (ASST).
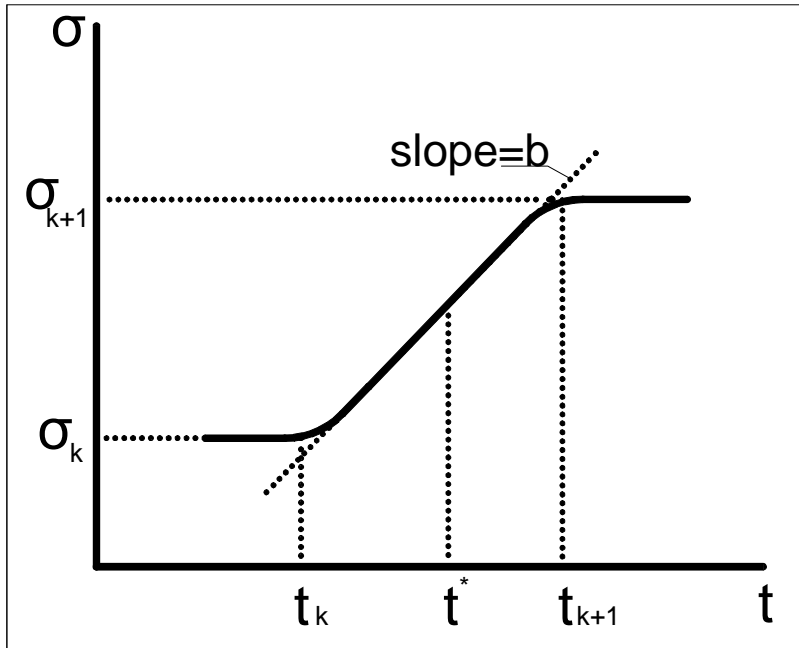
Fig. 3.7*: Schematic representation of the variation of stress σ with respect to time as it was recorded experimentally.*

3.4.3 Study of the creep phenomenon

Another common test to study the PSC emissions is the application of constant uniaxial compressional stress in the vicinity of the sample fracture and cause fracture due to early creep mechanism. The sample arrangement for these tests can be any of the aforementioned. These tests were conducted for both cement paste and mortar. This kind of test provides information regarding the way that non-linear fracture processes dominating this stress range influence the emitted PSC since cracks develop and create new formations while stress is practically maintained constant. Significant information was retrieved when strain gauges were attached to the samples and the strain was recorded while the stress was constant. It was observed that despite the fact the dσ/dt=0 the strain rate dε/dt was not zero. Significant PSC emissions were recorded during these tests, which as it will be obvious to see from the experimental results they are correlated with strain rate changes.

3.4.4 Loadings and unloading.

This experimental technique is applied to study the so-called memory effect regarding the PSC emissions. Specifically, sequential loadings and unloadings are applied on the sample using both uniaxial compressional stress at stress level adequate to cause generation and propagation of microcracks. During this procedure the emitted PSC and the stress of the sample are recorded. Compared to what is known from the Acoustic Emissions (AE) during the PSC emissions the Kaiser effect (Kaiser 1950) seems to apply similarly. Moreover, as can be seen from the experimental results a significant reduction of the PSC peak magnitude with respect to the repetition number of loadings and unloadings is observed. Each loading and unloading is conducted using the same upper and lower stress levels as well as the same stress rate.

3.4.5 Three Point Bending Technique (3PBT)

During this experimental technique a sample beam is supported over two prisms. A loading step is applied on the upper part of the middle of the beam (see Fig. 3.6) and is maintained constant. This process continues up to sample failure.

The technique adopted for the experimental loading of the samples is based on the increase of the load in abrupt steps and it is implemented as follows. The beam under test is initially subjected to loading of a constant value (relatively small with respect to the ultimate strength). An abrupt stepwise load increment is applied and the load increases to a new state. It must be noted that the new stress level is close to the strength of the sample and remains constant until the sample fails.

For the implementation of this experimental technique two pairs of electrodes are used (see Fig. 3.6) in order to study the regions where maximum compressional stress was applied (upper part of the beam) and where maximum tensile stress was applied (lower part of the beam). The tensile strength of the mortar is much less than the compressive strength and fracture occurs when a flexural tensile crack at the bottom of the beam propagates upwards through the beam (A. Griffith, 1920; M. Saito, 1988). In this case Teflon plates are installed between the prisms that support the sample and the stressing system. This has no impact on the mechanical behaviour of the sample since the Teflon does not come in contact with the sample.

4. Results and Discussion on PSC recordings with LSRT tests

This section examines the recordings of the electric currents in cube - shaped cement mortar samples, when they are subjected to a compressive load, which evolves linearly, up to the failure of the sample. A compressive load was applied on two identical samples with fast and slow loading rates in order to study the corresponding PSC emissions. The importance of the Teflon electric isolator is mentioned, along with the manner through which it affects the recordings of the electric signals; in addition, the interferences from electrical noises and their effect on electrometers are commented on. For this reason, an experiment was performed with both a loaded and an unloaded sample, in order to verify the accuracy of the measurements. The experimental procedure follows, where results are presented and commented on, while in the end a second experiment is carried out by applying a compressive load on two identical samples, with fast and slow loading rates, in order to compare.

4.1 The influence of Teflon stress interfaces

The need for a) proper electrical insulation in order to avoid any external interference, and b) avoiding the PSC leakage from the frame of the compressive machine and collecting it by the electrodes, led to the selection and installation of Teflon plates of thickness 2mm between the compressive metallic plates, presenting high conductivity, and the sample, presenting relatively low resistance.

A significant problem for realizing the compression test is the friction developed between the sample sides and the compressive metallic plates. Teflon affects only the mechanical fracture manner, but not the value of the emitted PSC since dielectric polymers like Teflon, PVC and Plexiglas do not affect that type of electric measurements. In particular, by using the above material, friction between the compressive metallic plates and the sample is increased; the latter is led to fracture within a shorter time and in a different fracture level, a characteristic of the quasi brittle materials, such as of the experiment. The correlation of the experiment results regarding the PSC emissions with other results that did not include the intervention of Telfon as an electrical insulating material shows that the relation $PSC(t) \propto \dfrac{d\varepsilon}{dt}$ relation still applies.
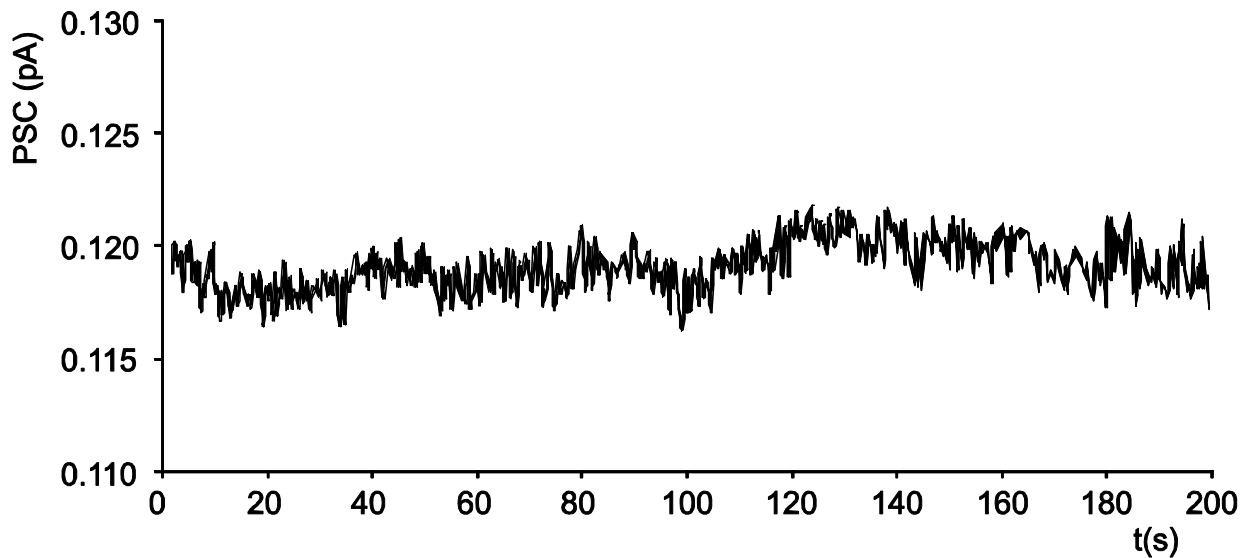
Fig. 4.1: *Temporal variation of the PSC emissions when a Teflon sample is subjected to compressional stress at a constant rate up to 60MPa.*

Fig. 4.1 depicts the temporal development of the PSC emitted when a Teflon sample, with the same dimensions with the samples under test, suffered mechanical stress at a constant rate of 0.3 MPa/s approximately up to stress levels of 60MPa. The electric current recorded during the above procedure shows no PSC excitation. The order of the recorded electric current (0.1pA) is in the lower limits of the measuring capability of the electrometer, and it constitutes noise.

4.2 Evaluation of Electric noise interference

In testing measurements within the Faraday shield, two samples were placed, one of which remained unloaded; the recording of the emitted PSC was performed from both samples in an identical time window.

The results are depicted in Fig. 4.2 and clearly show that in the first sample that the compression load was applied, the PSC presented the expected development (Fig. 4.2a); in the other sample, the electric emission remained stable and close to background levels of approximately 0.6-1pA (Fig. 4.2b).

From the electrometer data, as presented by the specifications table of Keithley electrometer, and based on the two lowest values of currents, the instrument may measure with a much greater accuracy (four orders of magnitute) 100 αA.
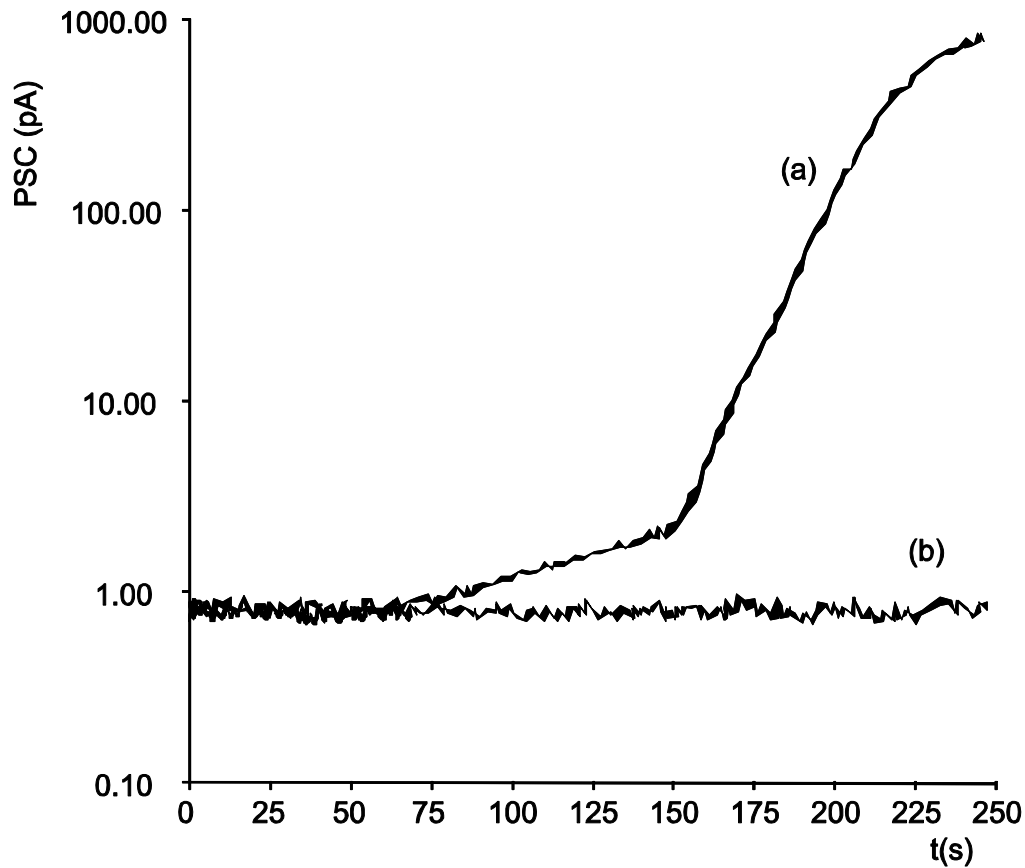
Fig. 4.2: *(a) is the emitted PSC from the loaded sample (b) is the corresponding emission from the sample that was also placed in the Faraday shield but remained unloaded.*

4.3 Constant stress rate tests

A representative PSC recording is described here when the LSRT was applied on cement mortar samples of the category CM70 (see table 3.1). The applied stress rate was 0.18±0.01 MPa/s and the failure occurred at 59MPa.

Fig. 4.3 depicts the temporal recording of the PSC emitted in a logarithmic scale along with the compressional stress σ (fig.4.3a). The ultimate compressional stress was achieved at time t_f=320s and the sample failed for stress equal to 60MPa approximately. Fig4.3 curve b that depicts the temporal variation of the emitted PSC shows clearly that slightly before the sample failed the PSC became maximum. The significant change of the PSC values was observed at time 210s approximately that corresponds to a stress value of 42 MPa approximately which corresponds to a relative compression stress value $\hat{\sigma}$=0.7. Fig. 4.4 shows the behavior of the emitted PSC with respect to the applied relative compressional stress. Particularly, as long as the sample is stressed uniaxially at low stress values corresponding to $\hat{\sigma}$ lower than 0.70, the PSC values (I) are very small.
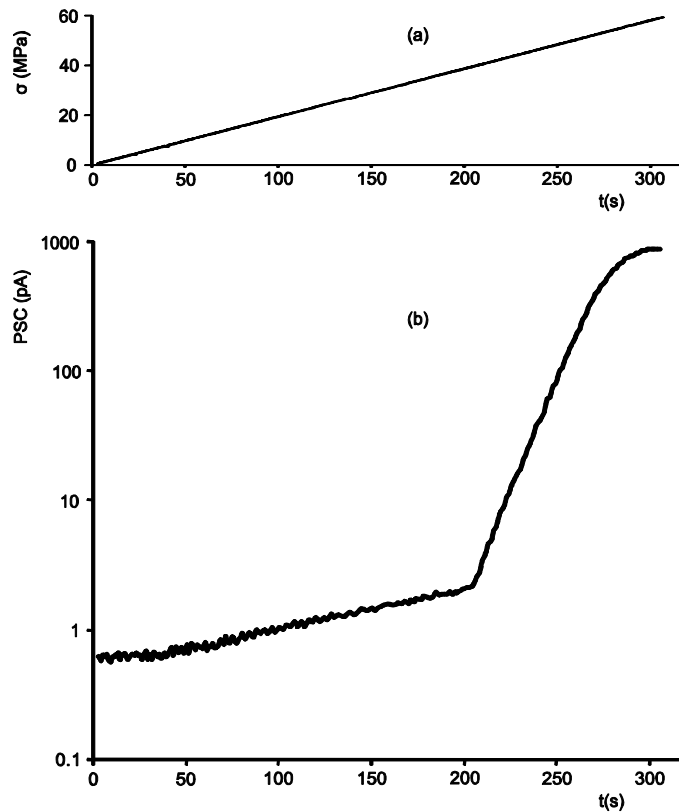
Fig 4.3: *The temporal variation of the applied compressional stress (curve a) and the concurrent PSC emission (curve b)*
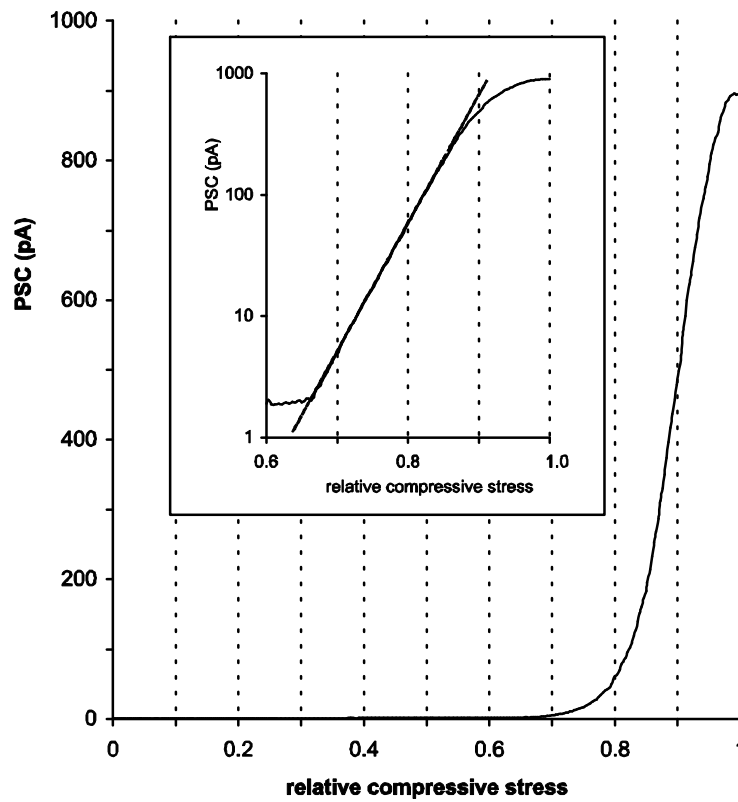

Fig. 4.4: *The behaviour of PSC with respect to linearly increasing stress (Low Stress Rate Technique). In the inset graph the PSC is shown on a logarithmic axis for* $\hat{\sigma} > 0.6$

Particularly in the limits $0<\hat{\sigma}<0.25$ the values of PSC do not exhibit significant variations and these are close to the background of the electrometer noise. As the applied stress increases ($\hat{\sigma}>0.25$) the PSC values tend to exhibit a small incremental process (for exponential increase), that can be described as follows:

$$I = I_0 \cdot \exp(a \cdot \hat{\sigma}) \qquad\qquad \textit{Equation 4.1}$$

where I_O is a current constant and a is a characteristic exponent describing the magnitude of the PSC increase in the referred range. Computer fitting in the recorded values I vs $\hat{\sigma}$ for a series of experiments show a value for the exponent factor a in the range between 1 and 2.

As the MCD model suggests, as Eq. 2.11 indicates and given that in the LSRT technique $\dfrac{d\sigma}{dt}$ = const and the strain rate in this stress range ($\hat{\sigma}<0.7$) is constant no PSC appearance should be expected. There is a weak but distinguishable PSC which is recorded, and it must be a part of consequences of the activation of some microcracks, that are either generated due to the shrinkage in the preparation stage or start from the interfaces between grains and cement especially in regions of the material near the surface of the compressed faces of the sample.

When the relative compressional stress upon the sample in the range between 0.65 to 0.70 then the PSC values increase with a very intense exponential rate which is directly related with the fact that the material has been driven into the non linear strain range (see inset of Fig. 4.4).

In this range the Young's modulus gradually decreases and the strain rate is no more zero. Consequently a significant PSC emission is also expected by Eq. 2.11. The PSC values increase rapidly and continuously up to the failure limit. In this range microcracks occur. During a microcrack opening two fresh surfaces are produced in the bulk of the material since the lattice is destroyed and the bonds are broken. These new surfaces are responsible for the charge separation phenomenon (A.A. Griffith, 1920). On the other hand it has been observed on cement mortar samples that no measurable compressional stress – induced cracks have been formed before stress approaching 70% of the ultimate stress had been reached (C.D. Pomeroy, 1980).

The new surfaces created during the crack opening processes are responsible for local polarization (Vallianatos and Tzanis, 1999; Whitworth, 1975; Slifkin, 1993). The charges of the appearing dipoles interact instantaneously causing weak electric currents

to flow in order to get the distorted equilibrium state to a new stable equilibrium state (Anastasiadis et al., 2007b). In this way the measured PSC can be interpreted. During microcrack generation a time-varying microcurrent appears around the microcrack. The superposition of these microcurrents corresponds to the measured PSC. Its magnitude depends on the microcrack concentration in the dominant direction of the microcracks propagation. Although the creation and propagation of a microcrack is a random phenomenon in the catastrophic process, nevertheless, there is always a first microcrack, which develops to a main – mother – crack defining a dominant orientation. Consequently there must be a dominant current component whose orientation is related with the mother crack orientation.

The relation of PSC values with the relative compressional stress values $\hat{\sigma}$ in the range $0.7 < \hat{\sigma} < 0.85$ (nonlinear deformation zone) they can be described by an exponential law of the same form with Eq. 4.1. differentiated by a characteristic exponent a that describes the magnitude of the PSC increase in the referred range, (after fitting) and from series of experiments was found to vary between 20 and 25 (see appendix B –A3) while for this case it has a value a ≈ 24 approximately.

The deviations of PSC values from the exponential law are evident when the relative compressional stress becomes greater than the value ($\hat{\sigma} > 0.85$), a value corresponding to a interfacial transition zone signaling the onset of unstable crack growth and the material enters a Fracture Process Zone (localized failure crack zone). In this range the PSC values stay on increasing intensely and as the ultimate strength point is reached, the PSC gets to a maximum. From the complete set of the PSC recordings that were conducted it was clearly shown that slightly before the fracture and for compressional relative stress value $\hat{\sigma} > 0.96$ the PSC values were non-deterministic (unstable) especially when the applied stress rate was very low. This fact clearly manifests the forthcoming fracture.

4.4 The influence of the stress rate on the PSC

PSC emissions were detected and are presented here when cement mortar samples were subjected to stress from early levels up to fracture at various stress rates. It was observed that only the maximum value of the PSC emission is affected by the stress rate.

A representative experiment that contributes to the aforementioned observations will be described. The used samples were from the category CM50 (see table 3.1). The first sample CM50-1 suffered compressional stress at a constant stress rate 0.72MPa/s and the fracture occurred when the stress reached 30MPa. The second sample CM50-2 suffered compressional stress at a constant stress rate 0.14MPa/s and the fracture occurred when the stress reached 25MPa.

Fig. 4.5 depicts two temporal recordings of PSC on logarithmic PSC axis (PSC1 and PSC2), that correspond to the two samples CM50-1 and CM50-2. In the same figure, the temporal variation of the uniaxial compressional stress for both rates is also depicted. Particularly the PSC1 starts to excite significantly from the time t=25s that corresponds to compressional stress $\hat{\sigma}$=20MPa approximately while for the PSC2 the corresponding time is t=115s and the stress is $\hat{\sigma}$=17.5MPa approximately. This observation becomes even more obvious when the emitted PSC is plotted with respect to the relative stress (see Fig. 4.6) shows the two PSC emissions with respect to the relative uniaxial compressional stress on a logarithmic (PSC) plot.

Fig 4.6 shows the behavior of the above two PSC recordings for different stress rates with respect to the relative compressional stress. The principal characteristic of both PSC recordings is that the emission initiates to appear from the background level when the relative axial compressional stress becomes higher than 0.7 approximately (see Fig. 4.6).
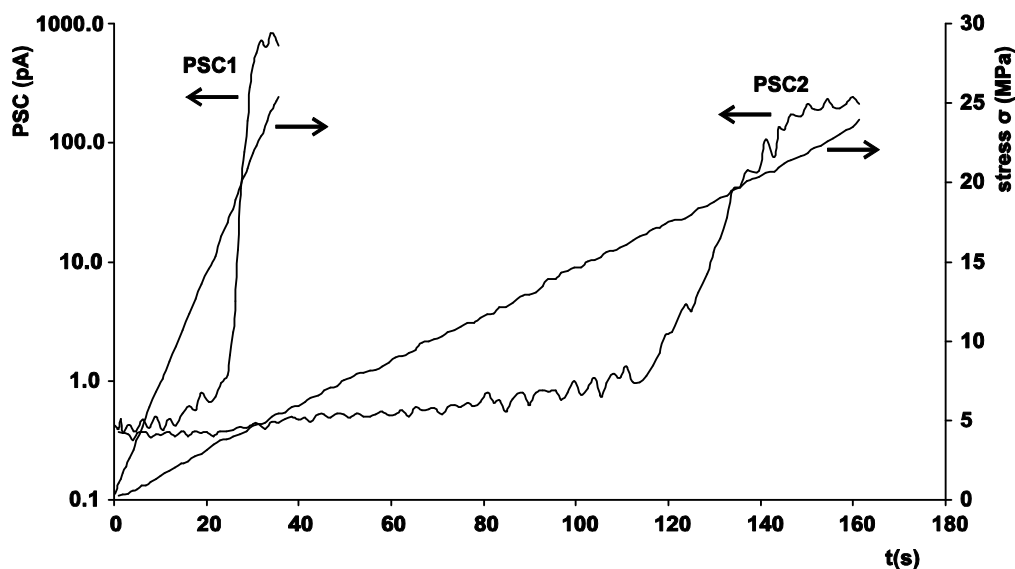

Fig. 4.5*: PSC recording taken for two different stress rates. The secondary axis is calibrated in stress units.*
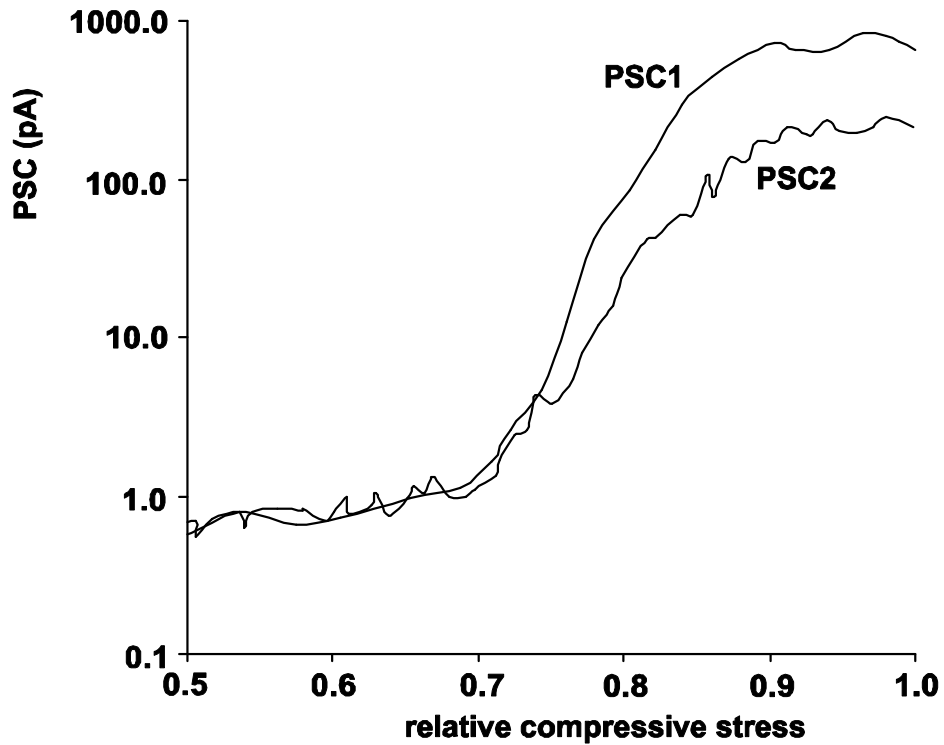
Fig. 4.6: Two PSC recordings for different stress rates with respect to the relative compressional stress.

Despite the fact that the maximum values (PSC$_{max}$) of the PSC are different for the described recordings, the most characteristic fact is that the totally released charge, in the time window from to that the PSC starts to excite t=t$_0$ from background level ($\hat{\sigma} > 0.7$) up to the fracture t$_f$, is practically the same. Accurately, the calculations show that $Q = \int_{t_0}^{t_f} I(t)dt$ is constant and irrelevant to the stress rate for both PSC recordings

The integral value that corresponds to the total charge is approximately 4.3nC. This characteristic property has also been observed in relevant experiments that were conducted on marble samples and has been discussed and interpreted (Triantis et al., 2006a).

5. Results and Discussion on PSC recordings using ASST

Here, the case of abrupt compressive step loading is presented in three modes. They are all performed with cube-shaped samples. The first test on a cement mortar sample includes the application of abrupt loading steps in four increasing levels up to fracture, and the PSC emissions are recorded. The second mode refers to a fatigue test with a hardened cement paste sample, where three abrupt successive loadings and unloadings are performed from a given stress level up to a higher one, close to fracture. The values are recorded and the relative comments are presented. The third mode involves three successive increasing compression loadings, at levels close to fracture, on a hardened cement paste. Observations are made and significant conclusions are drawn with respect to the emitted currents.

5.1 Gradually increasing stress levels (steps)

The discussions on a representative experiment with this technique follow. The used sample was of the category CM70 (see table 3.1). Four sequential abrupt stress increments at a constant rate (b=5MPa/s approximately) were performed (see Fig. 5.1a). It was ensured that the stress rate during each abrupt stress increase was the same in order for the PSC peak maxima to be comparable. The temporal variation of the PSC during the above procedure is depicted in the plot of Fig.5.1b. When each abrupt uniaxial compressional load is applied on the sample, simultaneous and similar abrupt current spikes appear, and having peaks at value PSC_{peak}. It should be noted that the appearance of these small PSC is due to the abrupt application of stress even at low stress levels. This experiment shows that during microcrack creation and the consequent charge production, a time-varying microcurrent appears around the microcrack. The recorded PSC is the superposition of such microcurrents. Its magnitude gets to a maximum when the concentration of microcracks gets also to a maximum. Particularly, when a crack meets a hard aggregate particle like sand grain, crack branching can occur so that instead of a single crack advancing, a whole family of cracks could gradually be formed. This requires larger forces and uses more energy. Accordingly, after the appearance of PSC peak, relaxations of a complex exponential decrease law to background level follow, with an initially short relaxation time τ_1 followed by a fairly longer τ_2. Fig. 5.2 depicts the PSC recording of the fourth abrupt

uniaxial compressional stress step, on a logarithmic current axis with respect to time. Fitting PSC values as a function of time indicates that an exponential relaxation law should exist, with an initially short relaxation time τ_1 followed by a fairly longer τ_2. Such a relaxation can be empirically described by the following relation:

$$I(t) = \begin{cases} A_1 \cdot \exp\left(-\dfrac{t}{\tau_1}\right) & \text{for } t > t_m \\[2em] A_2 \cdot \exp\left(-\dfrac{t}{\tau_2}\right) & \text{for } t \gg t_m \end{cases}$$

Equation 5.1

where A_1 and A_2 are constants and t_m is the time that the PSC becomes maximum.
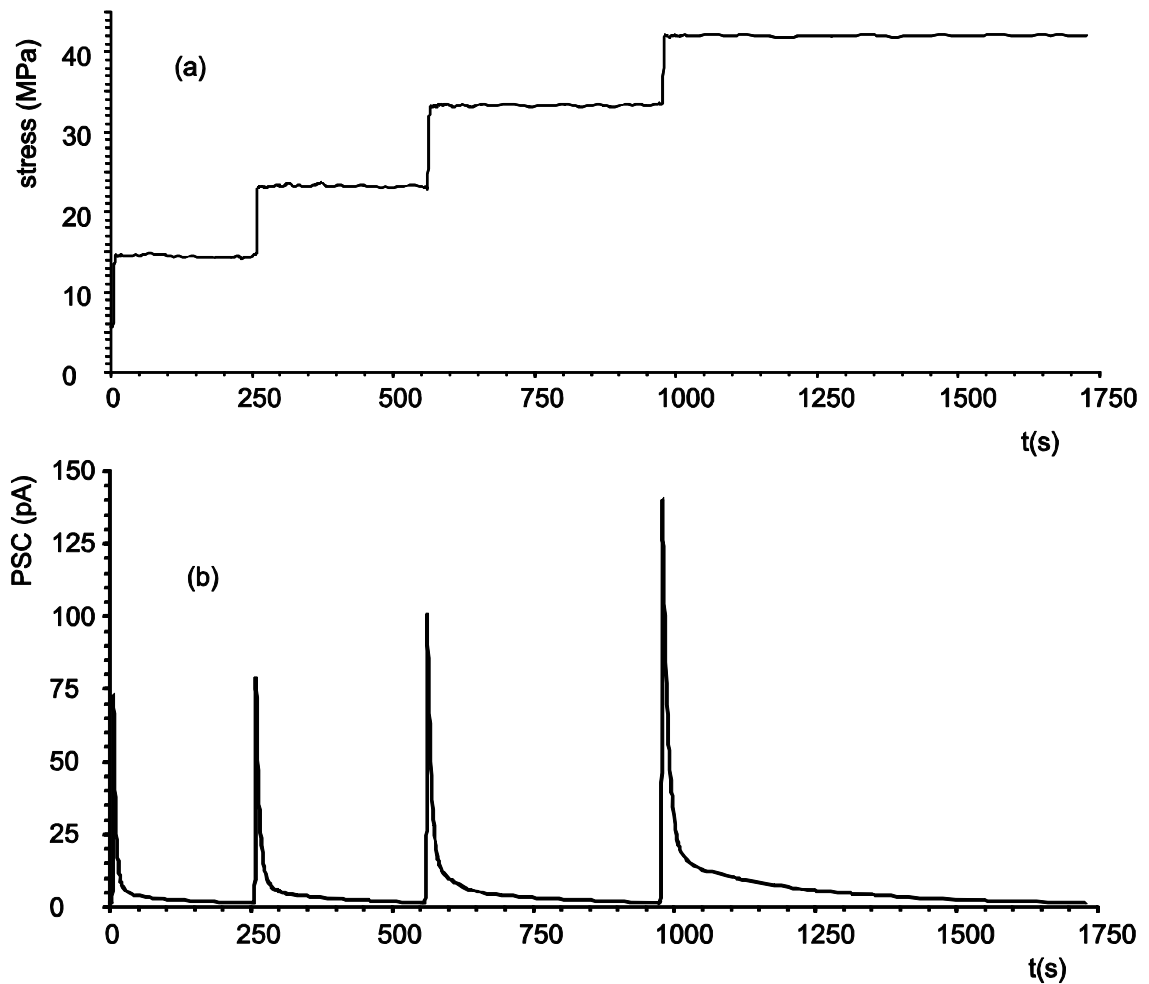

Fig. 5.1*: Depicting of the abrupt stepwise stress steps **(a)** and the corresponding PSC emissions recordings, with respect to time **(b)**.*

After the maximum value and considering that the stress remains constant through Fracture Process Zone production, the stress rate decreases rapidly and consequently

the PSC decreases and the short relaxation time is τ_1. This decrease does not continue at the same rate because due to the complexity of cement mortar fracturing another mechanism maintains the PSC emissions for a long time, so, that the PSC relaxation takes place with a longer time constant τ_2. A probable cause is the continuing material strain, even at a very low rate, although stress is unchanged. The process of new microcracks that continue appearing produces new microcurrents and as a result the PSC conserved at relatively high values and these values do not permit a direct relaxation to noise level. This fact is even more significant when it refers to an abruptly increasing stress that its higher level is in the vicinity of fracture. Systematic experiments show that for abrupt stress increases with relative values greater than $\hat{\sigma}=0.9$ this general observation is no further valid but instead abrupt PSC spikes are detected. Such an observation will be described in the following sections.
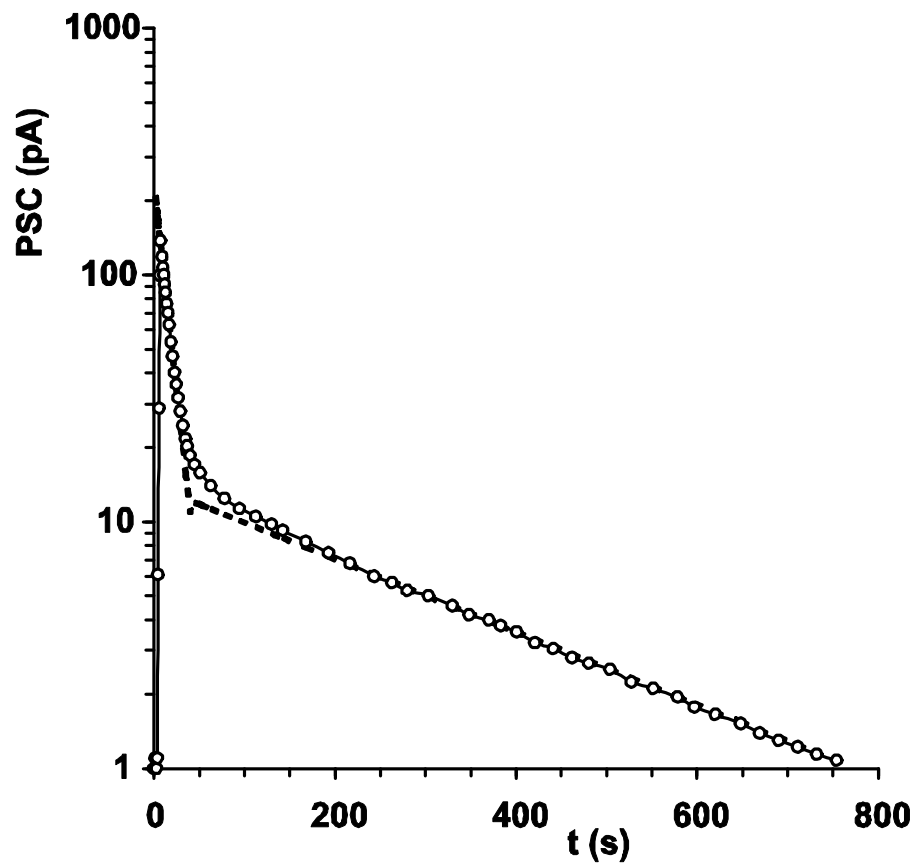

Fig. 5.2: *PSC recording of the fourth abrupt uniaxial compressional stress step with respect to time, on a logarithmic current axis*

The PSC peak value of each PSC following the application of an abrupt stepwise uniaxial compressional stress depends on the final state σ_{k+1}. In Table 5.1, PSC peak

values can be read with respect to the initial σ_k and the final σ_{k+1} states of each stress step, as well as with the respective relative compressive stress states $\hat{\sigma}_k$ and $\hat{\sigma}_{k+1}$ of stress.

Table 5.1: *Values of the parameters of the SST technique. (b≈5MPa/s)*

step	σ_k (MPa)	σ_{k+1} (MPa)	$\hat{\sigma}_k$	$\hat{\sigma}_{k+1}$	PSCpeak (pA)	τ_1 (s)	τ_2 (s)	Q(pC)
1	5.5	14.5	0.11	0.30	70.5	5.6	159	954
2	14.5	23.0	0.30	0.48	77.1	7.4	182	1385
3	23.0	33.5	0.48	0.70	98.0	9.1	227	2250
4	33.5	42.0	0.70	0.88	137.5	13.1	294	5340

Fig. 5.3 depicts graphically the PSC peaks, values with respect to the corresponding values of the final state σ_{k+1} of each step. The final states σ_{k+1} of steps 3 and 4 correspond to stress values which have driven the material into the non linear deformation range ($\hat{\sigma}_{k+1} > 0.7$). The PSC peak values are evidently greater than the initial. A similar behaviour has been observed in laboratory experiments using the SST technique on marble samples (Anastasiadis et al., 2004).
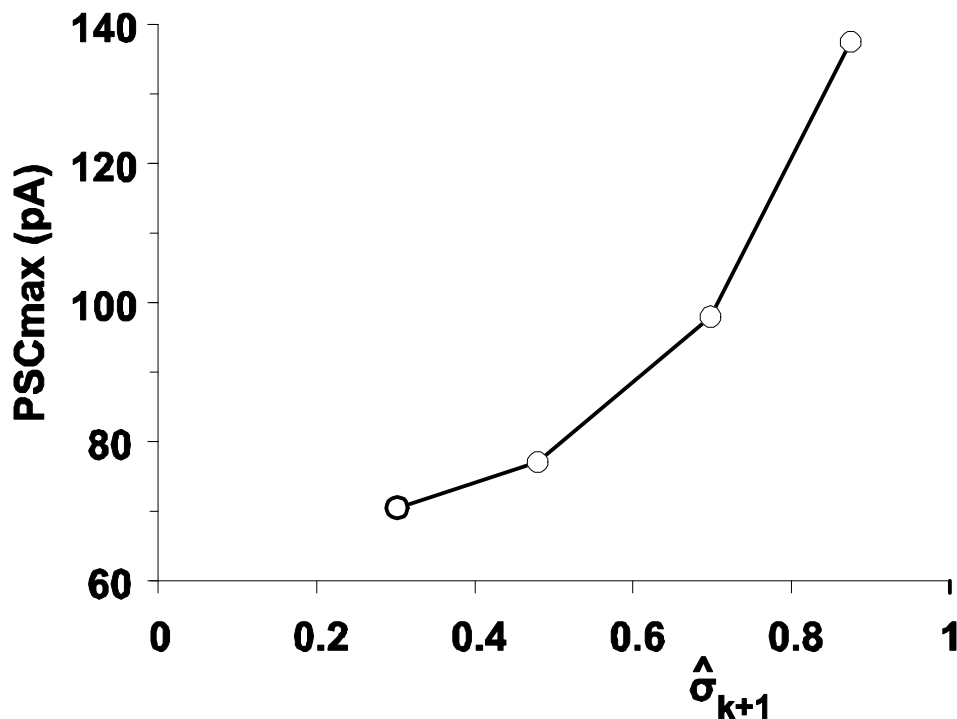

Fig. 5.3: *Correlation of the PSC peak values with respect to final stress level $\hat{\sigma}_{k+1}$.*

In the last column of Table 5.1, one will notice the calculated values of the totally emitted electric charge Q during the four sequential abrupt stress increases as well as the values of the relaxation time constants τ_1 and τ_2.

An intense increase of the electric charge can be observed (Fig. 5.4), as long as the value of the final state σ_{k+1} in which the material relaxes after the abrupt stepwise uniaxial compressional stress procedure. Such an increase is directly related to the continuously increasing PSC peak value (Fig. 5.3), and with the values of the relaxation time constants τ_1 and τ_2, which, as it becomes evident from Table 5.1, keep on increasing with the value of the final state σ_{k+1}.

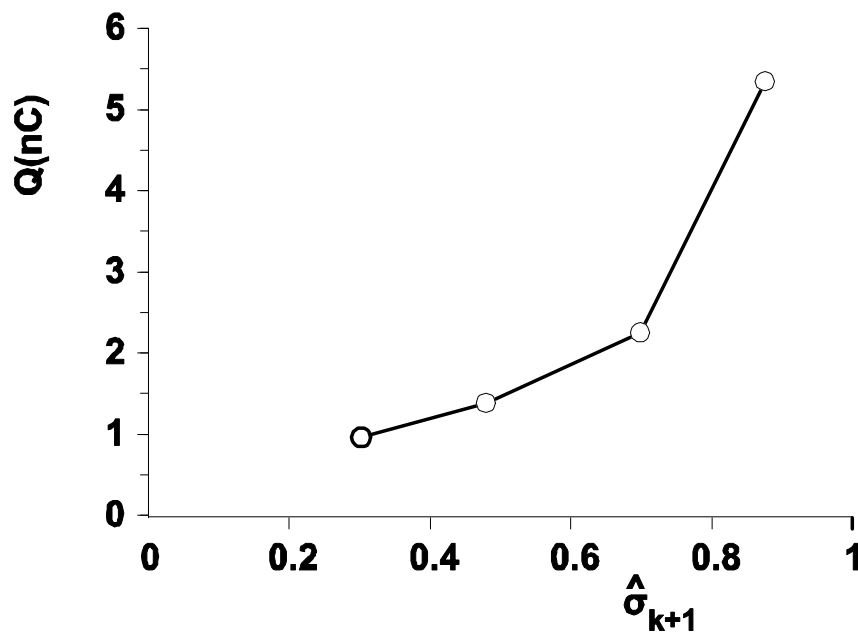***Fig. 5.4****: Correlation of the totally emitted electric charge values with respect to the final stress level $\hat{\sigma}_{k+1}$.*

5.2 Loading and unloading tests

Systematic PSC recording were conducted on cement based materials using the technique of applying sequential loadings and unloading.

The loading is conducted abruptly with a stepwise form from an initial stress value $\hat{\sigma}$ up to a higher final value that is in the limits of the Crack Propagation Zone (CPZ) ($0.75 < \hat{\sigma} < 0.85$).Representative PSC recordings on CP40 and CP50 type of samples follow.

The used sample (type CP50) was subjected to three sequential compressional loadings and unloadings. The levels of the applied stress varied in the range of 18MPa as initial stress value of each stress step up to 26MPa as the higher level of the each stress step. After maintaining the stress at its high value (26MPa) for about 8 minutes in order for the emitted PSC to fully restore a slow unloading was applied. The rate of the unloading was low in order not to disturb the emitted PSC.
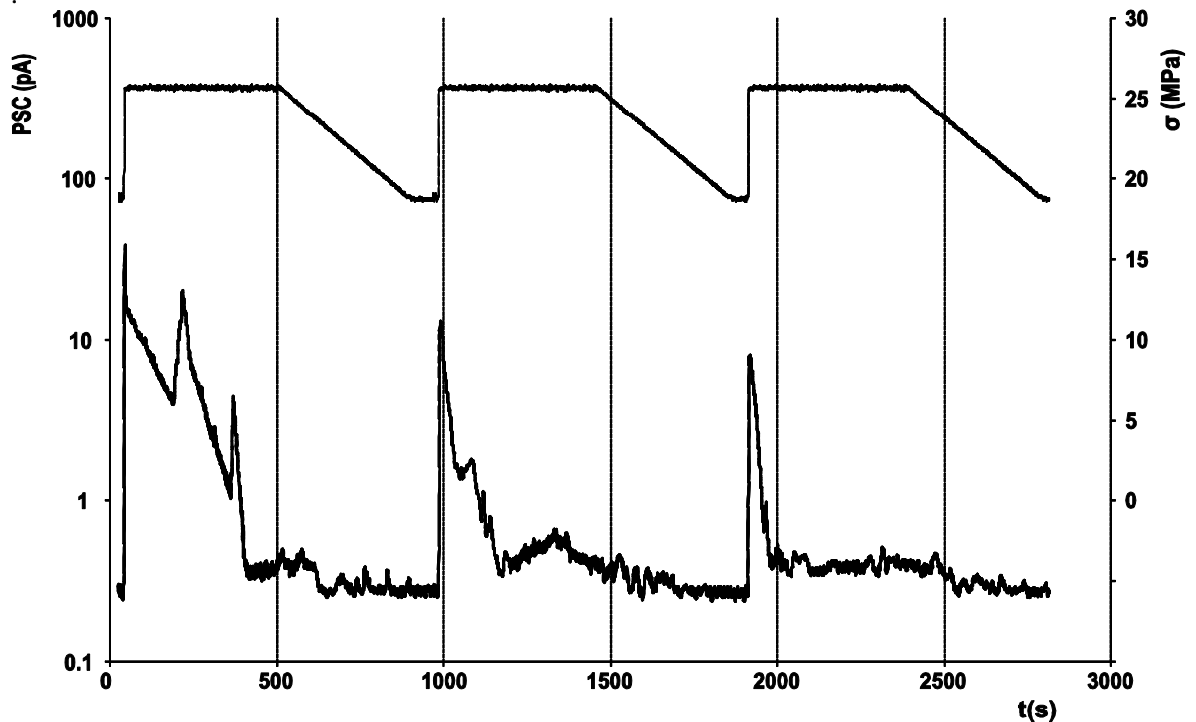

Fig. 5.5: *The temporal variation of the applied compressional stress during all the three sequential loadings and unloading and the corresponding emitted PSC.*

Fig. 5.5 depicts the temporal variation of the three repetitive compressional loadings and the corresponding emitted PSC. The right axis is graded in pA and the left axis in MPa. The PSC is depicted in semi log plot. It is obvious that the emitted PSC during each loading becomes lower but it retains its qualitative characteristics.

After the PSC gets to a maximum it gradually returns back to its background level.

5.3 Three sequential loadings near fracture

Three PSC recordings are described in the Fig. 5.6 These recordings correspond to a sample of the type CP40. Three temporal variations of the stress from a lower stress

value (12MPa) up to a higher (16.5MPa) were conducted. Each stress increase and its stay at the high stress level (16.5MPa) lasted 7 minutes approximately.
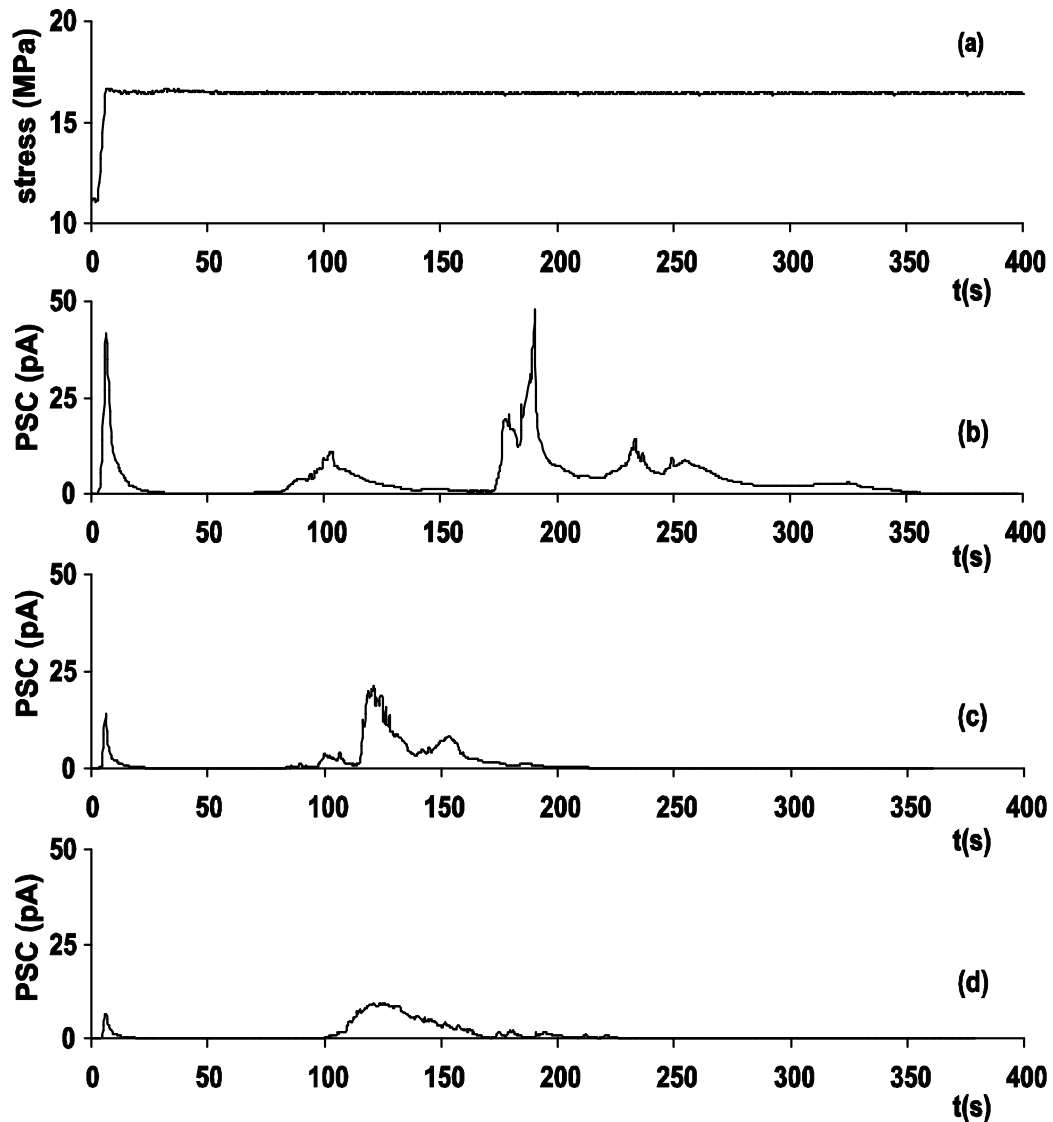

Fig. 5.6: *Depict of a representative stress step (curve a) with a three times repetition and the corresponding primary and secondary PSC emissions during the first stress step, the second and the third (curve b) (curve c) , (curve d) respectively.*

A slow unloading followed to the value of 12MPa and then a new loading/unloading process started. Fig. 5.6 describes this experimental procedure. Specifically, the upper (a) graph corresponds to the applied compressional stress in MPa while the three lower curves (b,c and d) correspond to the emitted PSC in pA during the three repetitive compressional loadings. It is obvious that the emitted PSC during each loading becomes lower but it retains its qualitative characteristics.

Two characteristic kinds of PSC emissions are depicted in Fig. 5.6. Especially, a primary main current that is emitted simultaneously with the stress increase, from the

lower to the higher level at a relatively fast process of restoration and a secondary emission that takes place while the stress as in short time creep tests is maintained practically constant. It is characteristic and demonstrated that both primary and secondary PSC emissions during each loading get lower.

The primary PSC emission is attributed to the crack formation and propagation processes that are directly plotted into corresponding deformation changes. Each loading and the sequential stay of the stress at its high value had 7minutes duration.
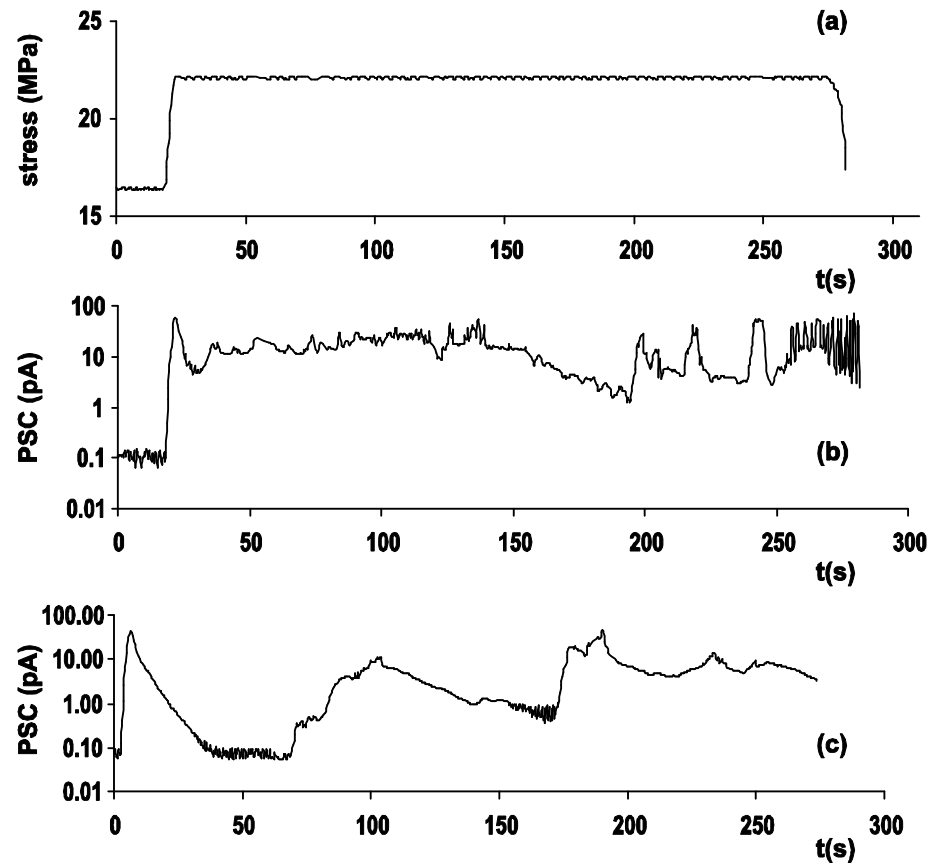

Fig. 5.7: a) The final stress step (16.5MPa-21MPa close to fracture and b) the corresponding emitted PSC, c) the PSC emission during the initial stress step (12MPa-16.5MPa) at a lower stress level so its observed in the time window between the primary and the secondary PSC emissions.

On this procedure after the third loading/unloading cycle a new abrupt stress increase was applied up to 21 MPa. This upper stress level was selected considering that the fracture limit of this category of the samples would lower than 25MPa (see Table 3.1) since the sample had already suffered significant damages due to the sequential loadings.

Fig. 5.7 depicts the last stress step (curve a) that was conducted from 16.5MPa up to 21MPa approximately. The sample was subjected to this loading for 5min and

77

consequently it failed due to short creep and fatigue. During this compressional stress step a significant PSC emission was demonstrated and lasted until the sample fracture. During this procedure sequential PSC peaks were recorded (Fig. 5.7b). It is characteristic that the initial peak that corresponds to the instant the abrupt compressional stress step was applied tended to restore but instead several more peaks followed. During this final stress step the primary PSC emission is overlapped by the secondary and cannot be distinguished. The fact that the duration of the emissions is relatively long (from the initial stress change until fracture) and its high magnitude in combination with the fact that the primary PSC emission never restored are parameters that ensure the fracture of the sample at the time t_f=270s (see Fig. 5.7a). Another observation is that before the sample failure the secondary emission has a brush-like form as a prediction of the upcoming fracture. This PSC emission before fracture (curve b) is in contrast to the first stress step PSC emission (curve c) in order to explain the changes in the form of the emitted PSC slightly before fracture to become quite clear. The deformation, after a compressional load application with a step like form, continues to vary (phenomenon of hysteresis). This phenomenon becomes more intense during the ultimate stress application on the sample. The secondary emissions are phenomena predicting that when the sample is close to fracture limits these emissions will be more intense.

6. Results and Discussion on PSC recording in the vicinity of fracture

This chapter examines the behaviour of a cubic sample made of cement paste, which, after the compressive load, has remained for a significant time period within a range of values close to the fracture limit. The sample fails while it is subjected to a load smaller than its compressive strength. Therefore, the creep phenomenon is detected. Additional interesting points are the peaks of the emitted PSC during the test. At the same time, with the help of a camera placed in the Faraday shield, the different stages of the development of the surface cracks are recorded and a correlation is made with the recordings of the PSC emitted.

Given that PSC becomes maximum near fracture, it was interesting to focus and study PSC emissions while maintaining the uniaxial compressional stress constant, on the condition that this relatively high value of the stress would be in the vicinity of fracture limit. A representative recording of a sample of type CP40 followed. This process was recorded with a camera installed in the Faraday shield. A stepwise stress increase was applied from an initial stress level of the order of σ_k=20MPa up to a higher stress level of the order of σ_{k+1}=25MPa, at a low stress rate $b = 14\text{kPa}/\text{s}$. Considering that the mean fracture limit varies from 25 to 29MPa (see Table 3.1), the upper stress level for this experiment was selected to be 25MPa in order for the relative compressional stress to correspond to at least 0.86. After this stress level was maintained on the sample for a relatively long time (approximately 30min), an attempt to increase stress by 0.7MPa led to the fracture of the sample. This means that the fracture limit of the sample was 25.7MPa.

Fig. 6.1 shows the complete temporal variation of the PSC during the described experiment while the secondary axis shows the values of the uniaxial compressional stress. When the stepwise stress increase started, an abrupt increase of the PSC was recorded and maintained its high value exhibiting also repeated spikes in the range of 160 pA to 180pA. Since the applied stress was in the vicinity of fracture, these spikes can be attributed to the non-linear processes that take place when the material is severely damaged and is led to failure. Once the emitted PSC is directly related to the damages taking place in the bulk of the material these spikes illustrate severe sequential localized damages or extension of the existing ones. When stress is stabilized around 25MPa, the PSC starts to decay and at t=1400s it returns to its background value (1 to 2pA approximately).
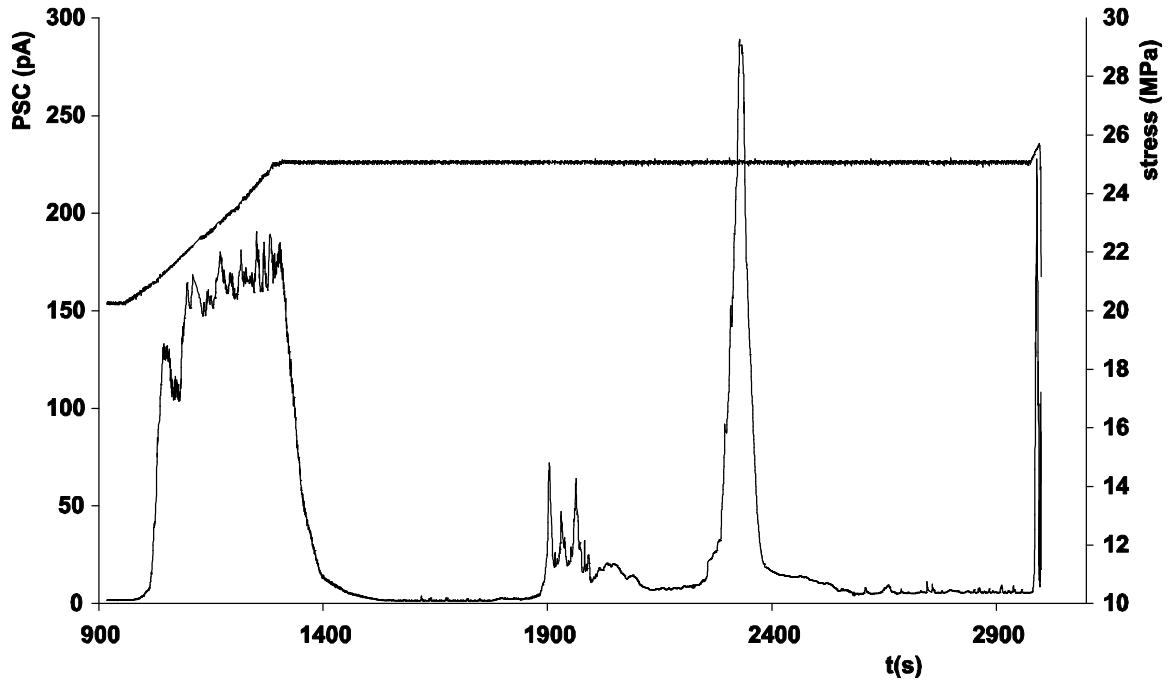
Fig. 6.1*: PSC emission when stress varies in the vicinity of sample fracture. PSC recordings during a process of stress increase and stabilization very close to fracture.*

Fig. 6.2 illustrates the temporal relaxation of the PSC on a logarthmic axis, once stress reaches the value of 25MPa. Two logarithmic branches depicting PSC relaxation processes, a fast and a slow one can be observed. Similar results have been observed in past experiments conducted on materials like marble and amphibolite (D. Triantis et al., 2007; P. Kyriazis et al., 2006). As can be derived from Fig. 6.2 when the emitted current begins to decay, its values follow an exponential law in the general form of $PSC(t) \propto exp\left(-\dfrac{t}{\tau}\right)$ that corresponds to a relaxation time $\tau \approx 30s$, while consequently and until the PSC is fully restored to its background value the relaxation time becomes significantly longer, 70s approximately.
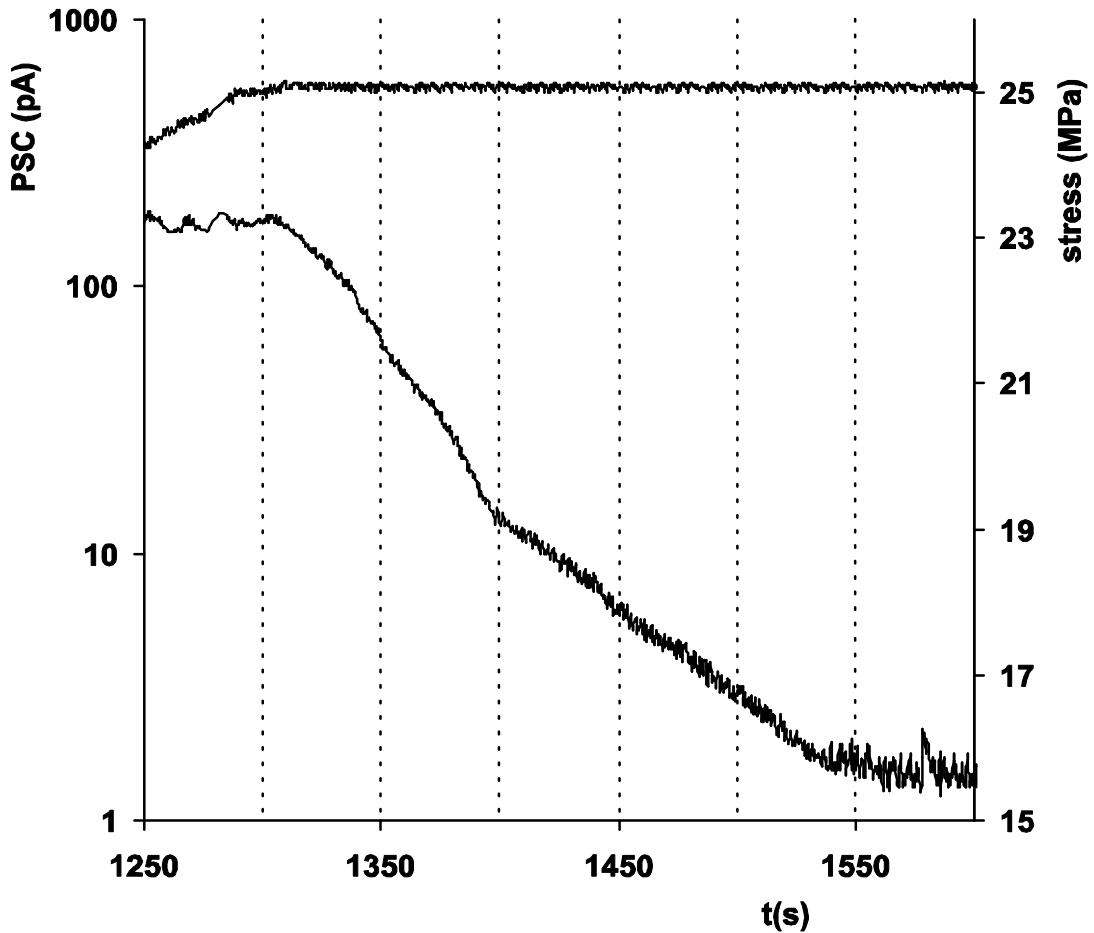
Fig. 6.2*: PSC relaxation after stabilizing the stress at 25MPa.*

After stabilizing the stress at the value of 25MPa and while the PSC is being restored, a surface crack appears at the video recording (see Fig. 6.3a). This capture is taken at t=1500s. This surface crack becomes more obvious later at (t=2100s) and while the cement mortar sample is still suffering the high level stress of 25MPa (see Fig. 6.3b).

In the meantime between the captures of Figs. 6.3a and 6.3b (i.e. 1850s-2100s) a PSC excitation develops (see Fig. 6.1, time interval between 1900s to 2000s). Consequently at the time interval 2300s-2400s a sharp intense PSC peak shows up with maximum value of 285pA approximately (see Fig. 6.1). The surface view of the sample after this PSC peak is depicted in the capture of Fig. 6.3c (t=2800s). A new surface crack becomes obvious at the lower right corner of the sample. Maintaining constant stress for another 400s at 25MPa did not yield any PSC emissions. Similar experiments on other materials show similar PSC recordings with qualitatively but not quantitatively comparable results. The experimental experience manifests that while the applied stress is maintained in the vicinity of fracture the frequency of PSC excitations is higher.
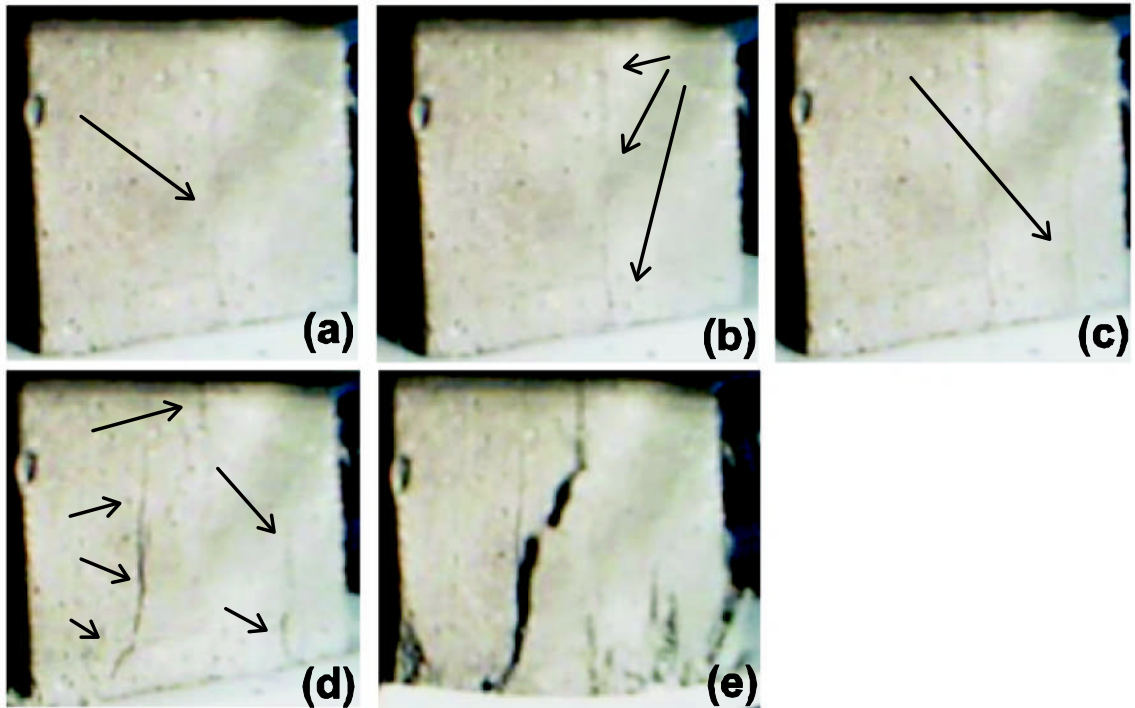
Fig. 6.3: *Photo captures for various stress levels. Surface damages make clear the gradual sample collapse and potential PSC sources.*

Attempting a further increase to the applied stress, fracture of the sample occurred accompanied by an abrupt increase of the PSC (see Fig. 6.1). Fig. 6.3d, e shows the localization of the cracks and the state of the sample 2s and 1s before the sample failure respectively.

7. Results and Discussion on the correlation of PSC and strain

In this technique a correlation is attempted between the strain rate and PSC. Successive slow rate stress steps were performed and the strain was measured simultaneously with PSC. In conclusion, the linear relation between the strain rate and PSC (MCD model) is not valid only at very high deformation levels close to fracture.

The fact that while the stress is constant in the vicinity of fracture, PSC emissions are observed, and since the emitted PSC is related to the strain rate according to Eq. 2.11 an experimental procedure was planned during which simultaneous PSC, stress and strain measurements were conducted. The selected technique for applying the mechanical load was low rate stress steps. The low rate was selected in order to follow in detail the temporal development and the consequent variation rate of the strain. For these experiments samples of the category CP50 were used. Initially the samples were subjected to a stress level of the order of 29.5MPa. This stress corresponds to relative compressional stress $\hat{\sigma} \approx 0.8$. Maintaining the stress at this value for a long time (15 min approximately), a procedure of sequential abrupt stress increases were applied at a mean stress rate of 20kPa/s until the sample failed. After each abrupt stress increase to the next higher and before the new stress step the stress was also maintained constant for a relatively long time. After applying 29.5MPa three sequential stress steps (step1, step2 and step3) were applied but when attempting a final fourth one (step 4), the sample collapsed at a stress value of 37MPa.

The temporal variation of the stress at the above described procedure is depicted in Fig. 7.1a while the corresponding temporal variation of the deformation is depicted in Fig. 7.1b. The recorded PSC is shown in Fig. 7.1c.

It is clear that strain and stress do not exhibit similar behaviour. Despite the fact that the stress is maintained practically constant after each stress step the strain continues to increase proving that constant stress will produce damages in the bulk of the sample. The recorded PSC signal is described in Fig. 7.1c. An interpretation of the mechanisms that dominate the generation of the PSC peaks is the following:

The experimental results illustrate two principal observations:

1. PSC peaks can be observed not only during the stress step but even when the stress is constant (see Fig. 7.1 time period 6800s to 6900s)

2. Every PSC excitation and its consequent low or high peak is related to an increase of the strain rate. When the deformation rate reduces (this is a

characteristic observed at the completion of each stress step) then the PSC starts to decrease gradually.

It is characteristic that during the initiation of step1 a PSC perturbation is detected in the form of a low PSC peak (PSC1a), while it is followed by a peak (PSC1b) that is emitted during the stress increase from 29.5 to 33MPa
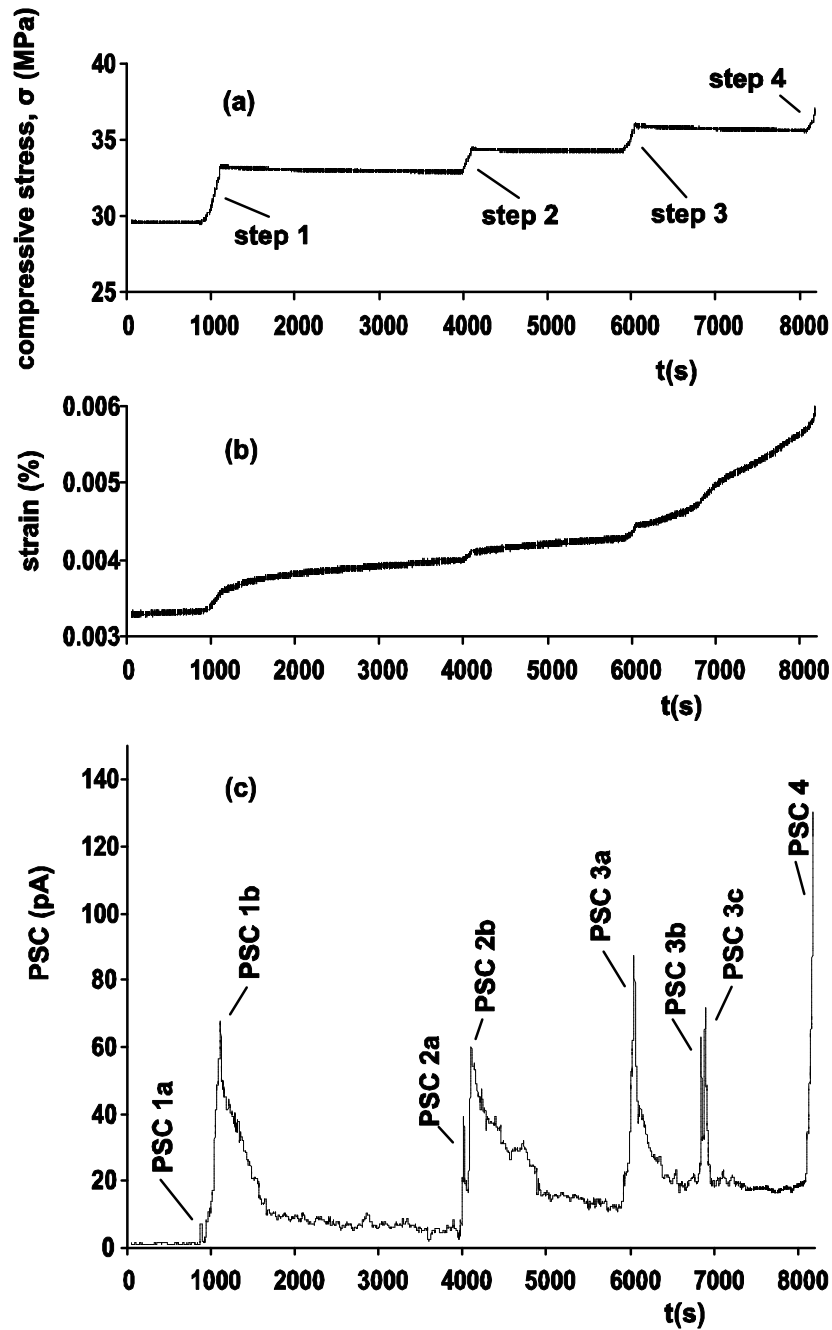

Fig. 7.1: *Temporal recordings of **a)** Stress, **b)** strain and **c)** PSC during sequential abrupt stepwise stress increases illustrating the behaviour of the strain with respect to stress when the latter is maintained practically constant.*

Fig. 7.2 further supports the above, illustrating the PSC recording during step1, with the corresponding strain on a secondary axis.
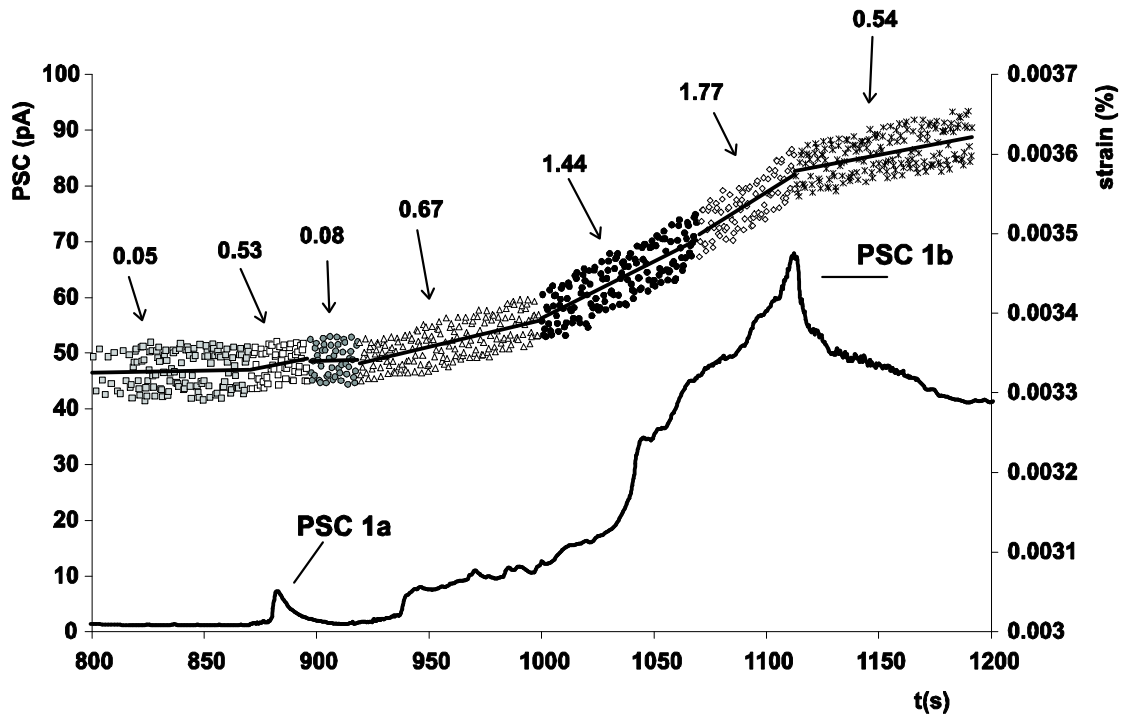
Fig. 7.2: *Temporal variation of PSC and strain during the first stress step. The strain rate is also depicted using windowed linear fitting*

During this procedure two PSC peaks are revealed, a weak one PSC1a and another significantly higher PSC1b. At the time PSC1a showed up the trend line of the mean temporal strain increases. Before the PSC1a excitation the sample is subjected to a mean strain rate of the order of $0.05(\mu s)^{-1}$. This rate increases to $0.53(\mu s)^{-1}$ (when the PSC1a is observed) and then decreases to $0.08 (\mu s)^{-1}$ leading the PSC to decrease. Consequently the strain rate becomes gradually higher until the stress step is completed and the stress reaches its maximum step value at 33MPa yielding this way the PSC1b. When the stress restores at the value of 33MPa the mean strain rate is significantly lower $0.54(\mu s)^{-1}$, than the corresponding rate (i.e. $1.77(\mu s)^{-1}$) slightly before the PSC became maximum (see Fig. 7.2). The behaviour of the PSC with respect to strain is similar during the following procedures in the stress steps 2 and 3 (see Fig. 7.2).
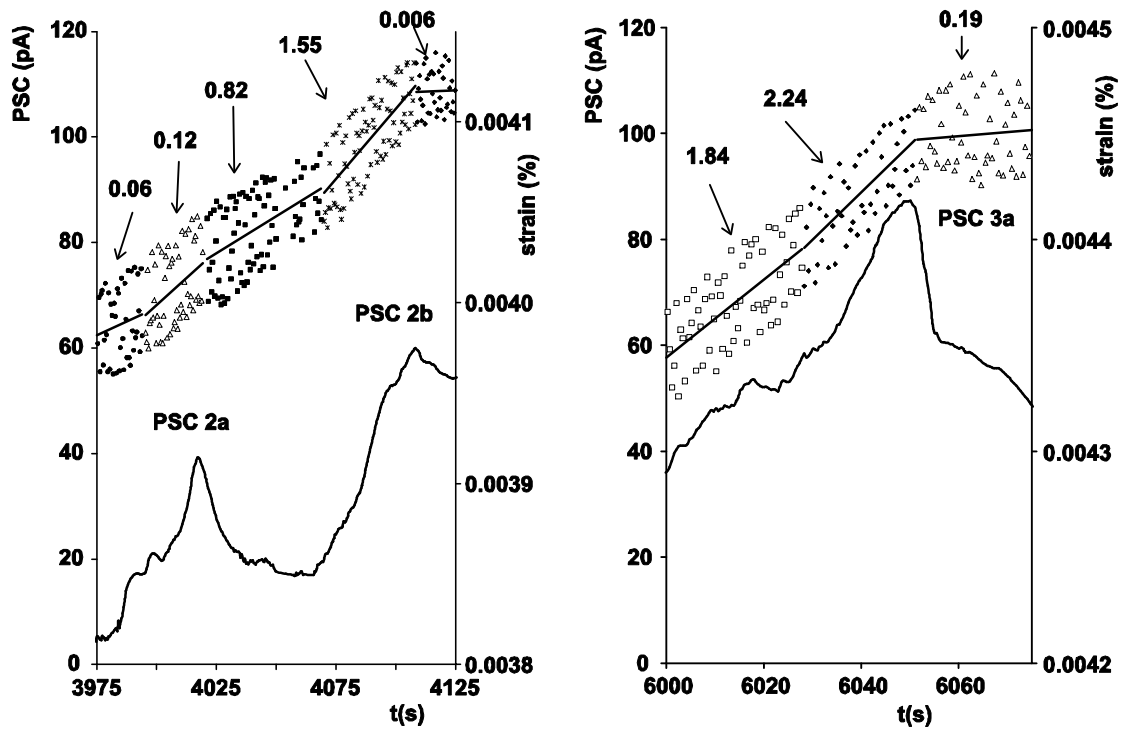
Fig. 7.3: *Temporal variation of PSC and strain during the second and the third stress steps. The strain rate is also depicted using windowed linear fitting*

It is very interesting to focus after stress step 3 and while stress reaches its maximum step value 33MPa and remains constant and the PSC tends to restore at a low level, an abrupt PSC excitation is observed (see Fig. 7.1) that comprises two sequential maxima(PSC 3b and PSC 3c). A detailed view of them with respect to emission mechanisms is depicted in Fig. 7.4, in combination with the temporal variation of strain. It is clear that both PSC (PCS 3b, PSC 3c) are related to the change of the strain rate. The mechanisms of these PSC emissions can be attributed to the redistribution of charges caused by the dynamic change of the lattice of the bulk of the sample during the formation of the new microcracks and the extension of the existing ones.

Table 7.1 contains the value of the maximum PSC (PSC_{max}), as well as the mean strain rates yielded after the windowed linear trending of the temporal variation of deformation curve for each of the observed PSC maxima.
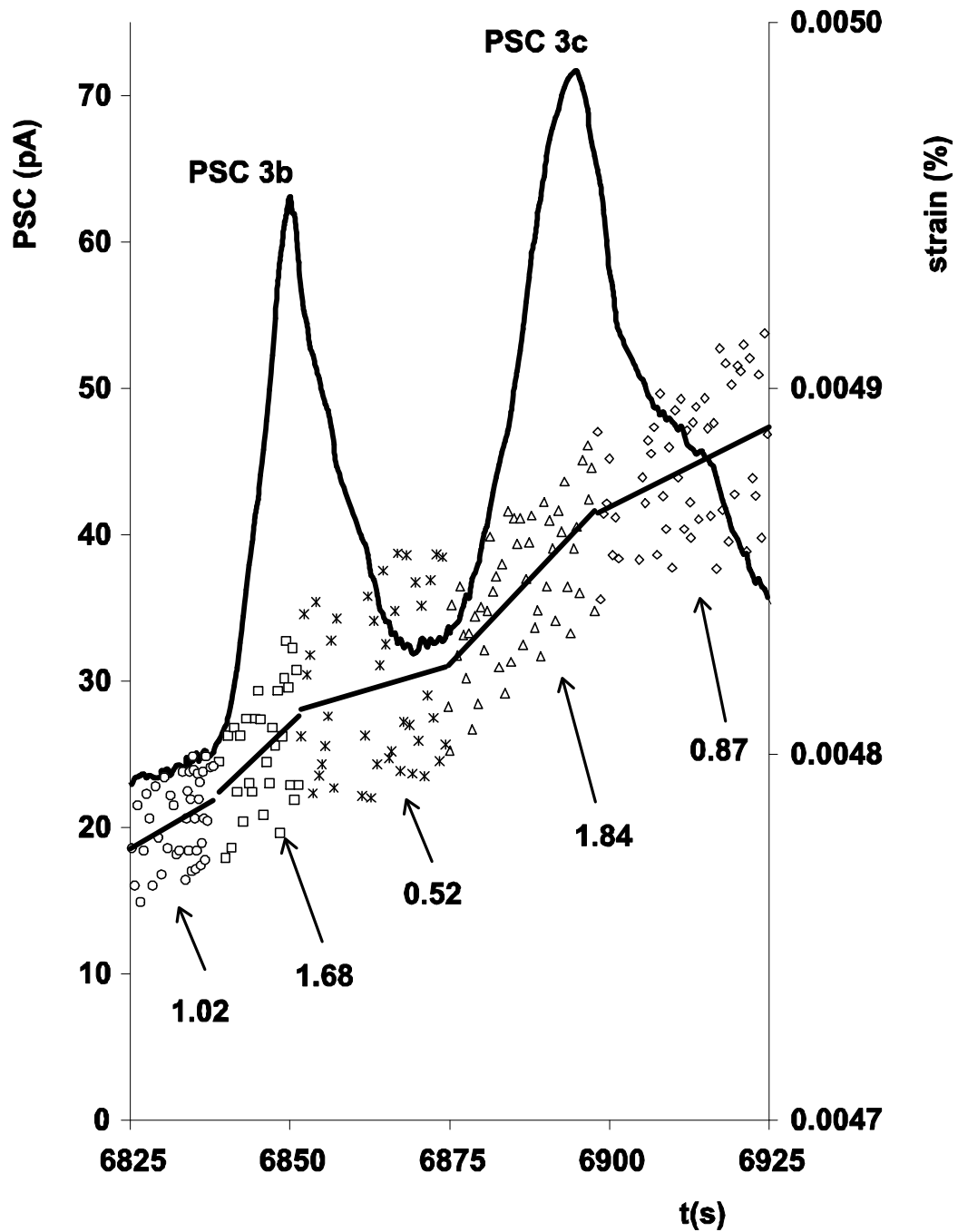
Fig. 7.4: *Temporal variation of PSC and strain after the third stress step and while the stress is maintained constant. The deformation rate is also depicted using windowed linear fitting*

A satisfactory linear relation between the PSC_{max} and the strain rate $\dfrac{d\varepsilon}{dt}$ is verified through the experimental results (see Fig. 7.5), a fact that confirms the MCD model applicability and theoretical support, as can be attributed to Eq. 3.1.

Table 7.1: *Characteristics of the applied stress steps the corresponding strain and PSC.*

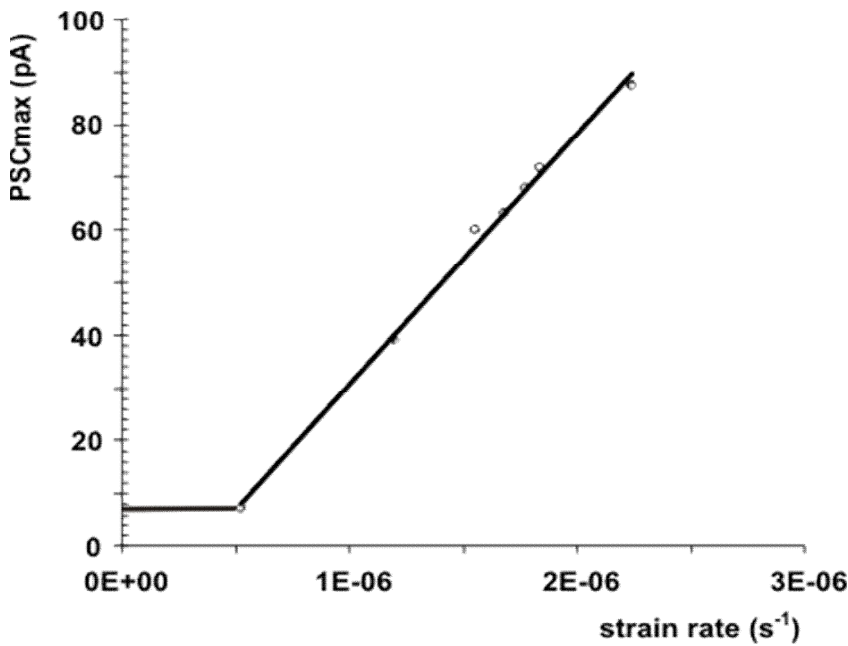| Stress - Step	PSC - peak	strain rate (s^{-1})	PSC$_{max}$ value (pA)
1	PSC1a	5.26E-07	7.32
1	PSC1b	1.77E-06	67.90
2	PSC2a	1.20E-06	39.20
2	PSC2b	1.55E-06	59.95
3	PSC3a	2.24E-06	87.30
3	PSC3b	1.68E-06	63.10
3	PSC3c	1.84E-06	71.70

Fig. 7.5: *Correlation between the strain rate and the maximum value of each PSC peak. Only the PSC peaks that correspond to stress levels before the vicinity of fracture are plotted*

The PSC emission during the last stage, slightly before sample fracture (final stress step) will be discussed. In this procedure the strain rate is significantly higher than those of the previous stress steps. From the instant the stress starts to increase the strain has a value of $1(\mu s)^{-1}$ and becomes an order of magnitude higher during the instant of fracture (see Fig. 7.6). Respectively, the PSC values increase and three seconds before fracture a peak at 130pA is observed and is consequently reduced. This reduction is

always observed before fracture predicting this way the inevitable failure, a phenomenon recorded on other brittle materials also (Stavrakas et al. 2003).
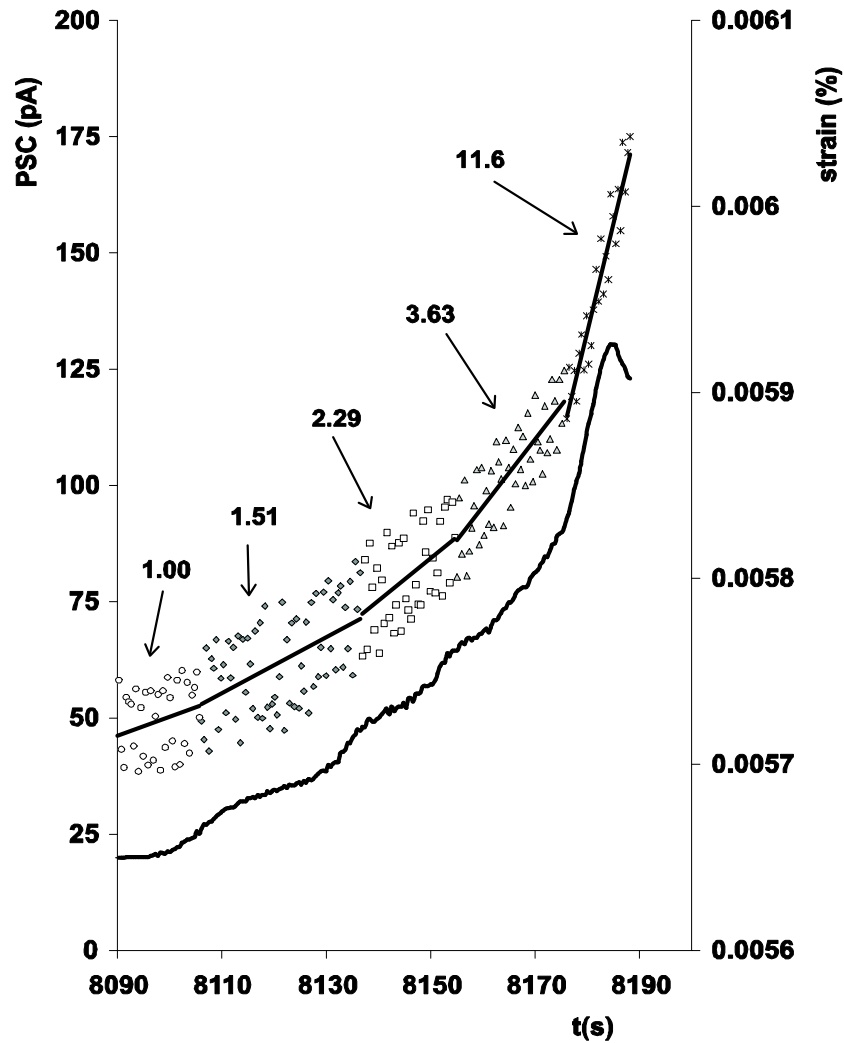

Fig. 7.6: *Temporal variation of PSC and strain slightly before sample failure. The deformation rate is also depicted using windowed linear fitting*

This phenomenon can be attributed to the fact that the failure plane is already guided and surrounded by macrocracks limiting this way the available path for the charges to move and polarization to be built obstructing this way the detection of PSC. Attempting a correlation of the deformation rate with the corresponding values of the PSC no linear relation is yielded (see Fig.7.6), when the deformation rate becomes higher than $1(\mu s)^{-1}$. Attempting to correlate the value of the emitted PSC peak of 130pA with the corresponding strain rate of 11.6 (μs^{-1}) we can observe that this pare of values is not linearly related with previous value as can be seen in Table 7.1. This experimental fact shows that the PSC peak slightly before failure does not obey Eq. 3.1. Fig. 7.7describes the behaviour of the emitted PSC during each stress step with respect to the strain rate.
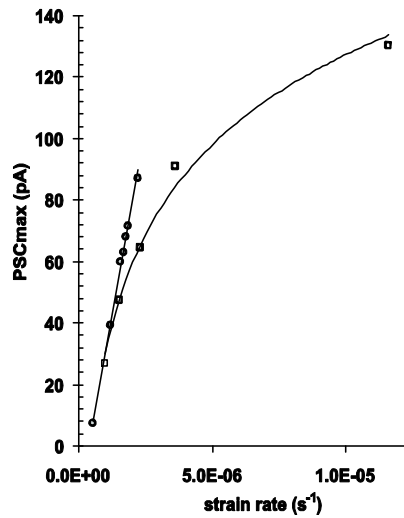
Fig.7.7: *The maximum value of the emitted PSC during each sequential stress step with respect to the mean strain rate during each stress step.*

It can be clearly seen from the figure that the relation between the emitted PSC and the strain rate deviates from linearity and the MCD model no further supports the experimental results. This can be attributed to the massive damages in the bulk of the samples that are concentrated around the main crack that guides the fracture plane.

In other words, what is most important, when the stress acquires high values approaching the fracture limit, then, a deviation from the linear relationship between PSC and the strain rate shows up which in turn gives rise to the prediction of the failure of the material specimen? The formation of the fracture plane that takes place at high stresses and the extensive cracking that is guided through the shear stress plane, limit the available conductive path in the sample bulk and a consequent obstacle on the emitted PSC is created leading to PSC reduction.

Thus, the described technique of relating the magnitudes of PSC and the strain rate can quantify the damage state of the material specimen.

8. Results and Discussion on Bending Stimulated Currents using 3PBT on cement based materials.

Experimental laboratory measurements of electrical signal emissions were conducted on cement based materials in a three point bending procedure. Electric current emissions were recorded at both the upper surface (compressive zone) and lower surface (tensional zone). The qualitative and quantitative characteristics of the electric recordings are correlated with the mechanical state of the samples. The electric current is attributed to crack formation and propagation from low load level up to fracture.

8.1 Bending Stimulated Current in cement paste samples

The 3PBT was applied on cement paste beams of the category CP100. Systematic tests on a series of cement paste beams have shown that the maximum bending strength was 1.1 ± 0.1 kN. The beam was supported by two deform-proof cylinders placed 70mm apart.

A series of experiments were conducted applying the aforementioned configuration on cement paste samples. The load on the beam was initially increased up to the level of 0.3kN and no significant electric current emission was observed at both the compressed and tensed zones. The load on the samples was maintained practically constant at this level for 1.5min approximately.

Fig. 8.1 shows a representative recording of the emitted electric signals as well as the corresponding increasing temporal stress development.

Consequently, the load was increased at a rate of 34N/s until fracture of the beam. The temporal variation of load is depicted in Fig. 8.1, curve a. The same figure shows the appearance of the electric current emissions on both compressional and tensional sides of the beam due to the application of the load. Curve b, describes the electric current collected by the pair of electrodes that were positioned on the upper surface, which corresponds to the compressed region of the beam. Curve c describes the current collected by the pair of electrodes that were positioned on the down surface of the beam, which corresponds to the tensed region.

Clearly, the current emission at the compressed surface lags that of the tensed surface. Since the tensile strength of the cement paste is much less than the compressional strength and fracture occurs when a flexural tensile crack emerges at the bottom of the

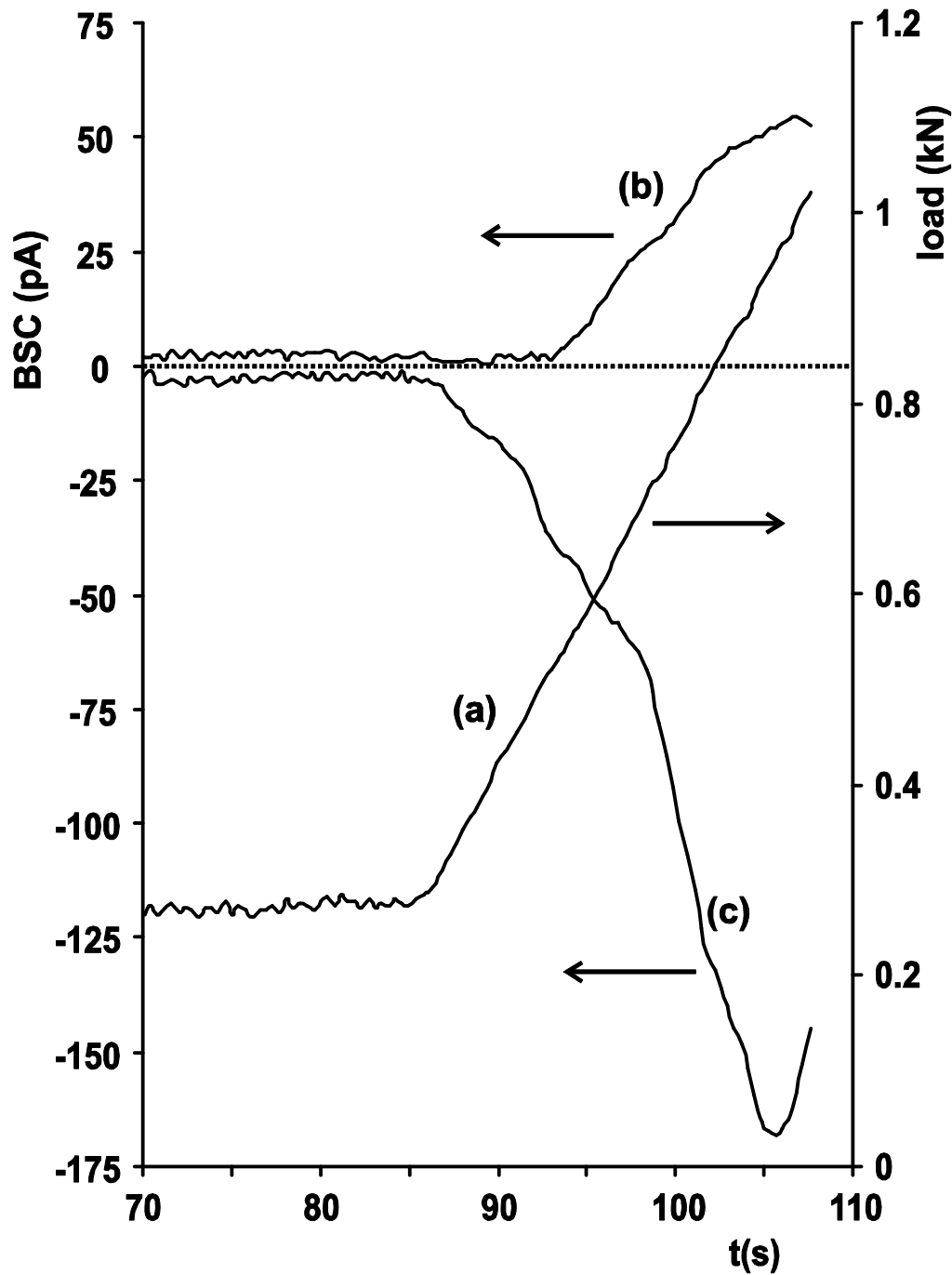beam and propagates upwards through it the sample exhibits earlier deformation at the tensed surface.

Fig. 8.1: a) Temporal variation of stress, b) the electric current collected from the upper electrode corresponding to the compressional zone, c) the corresponding electric current collected from the lower surface (tensile zone).

It is characteristic that the two recordings are of opposite polarity. This phenomenon seems to be compatible with the fact that the electric currents are proportional to the

deformation rate as referred in the corresponding chapter. It must be noted that at the upper surface (compressional) the ratio $d\varepsilon/dt<0$ is negative while at the tensed surface $d\varepsilon/dt>0$. Another observation is that the electric emissions show a peak slightly before the ultimate bending strength is reached.

The electric emission recorded at the tensed surface is of significantly higher magnitude than the respective one at the compressive surface. This can be attributed to the fact that due to the extensional deformation (bending deflection) of the lower part of the beam a larger number of microcracks take place and the escorting dislocations find easier their way to move apart than those in the compressed region.

8. 2 Bending Stimulated Currents in cement mortar samples

A series of experiments were conducted on cement mortar samples of the category CM100. The experimental results are presented here. Fig. 8.2 depicts the temporal variation of the BSC recorded during the third type of experiments (3PBT), employing the application of a constant load to bend a cement mortar beam. The use of the third technique was accomplished by applying a force step at an increase rate equal to 0.14 kN/s up to a maximum 1.3kN approximately. (see Fig. 8.2a). It should be noticed that the value 1.3kN is slightly smaller than the force adequate to cause fracture to the beam. This fact was tested experimentally and the fracturing force was found to be equal to 1.5kN.

Fig. 8.2b shows the appearance of BSC on both opposite sides of the beam due to the load application. The solid curve was recorded by the pair of electrodes that were positioned on the upper surface of the beam which corresponds to the compressed region of the beam (where $d\varepsilon/dt<0$). The dotted curve respectively, was recorded by the pair of electrodes that were positioned on the lower surface of the beam which corresponds to the tensed region of the beam (where $d\varepsilon/dt>0$). It is a characteristic fact that the two recordings are of opposite polarity. This is in agreement with the experimental results of the cement paste samples and Eq. 2.11 which comes from the MCD model.
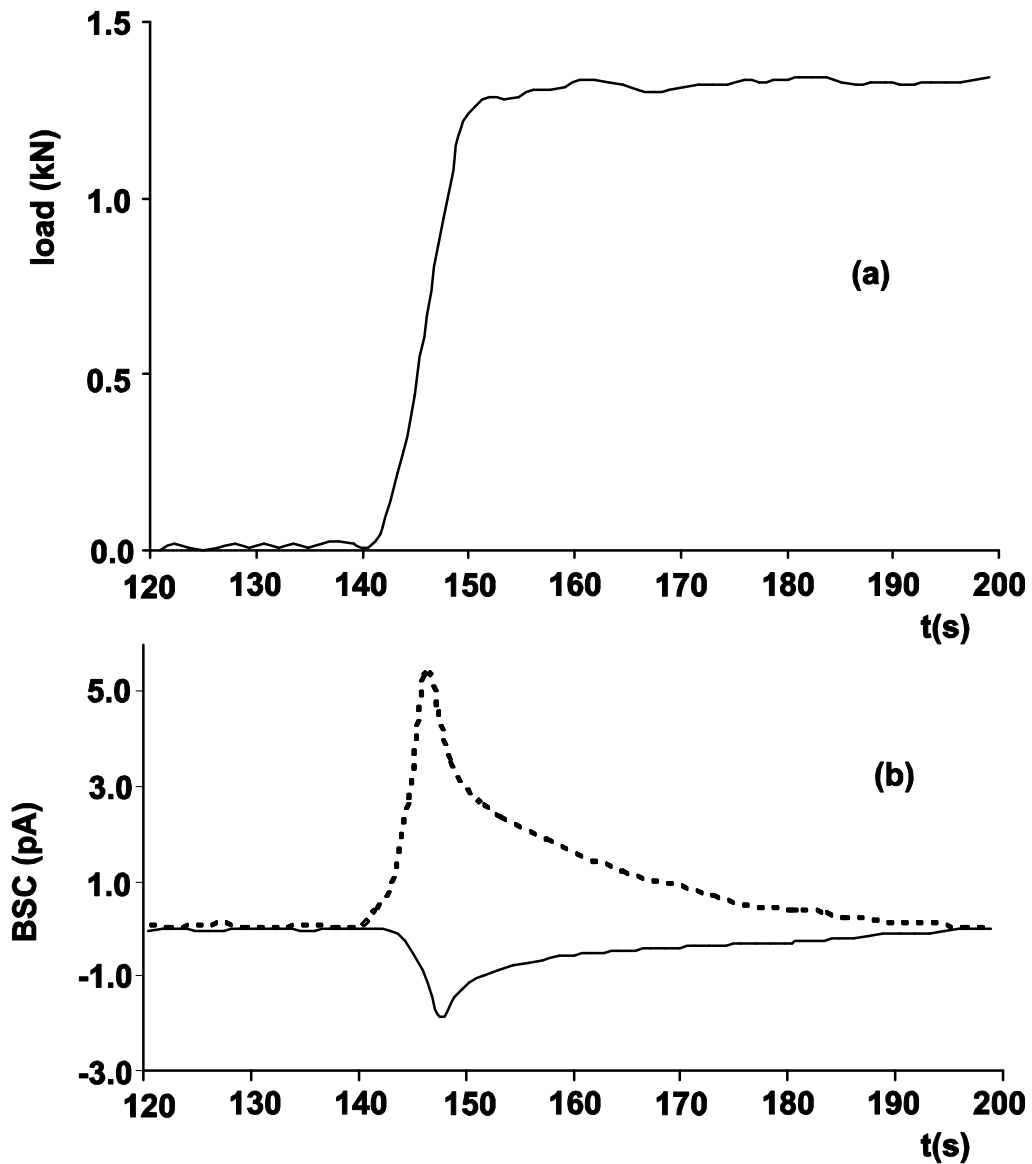
Fig. 8.2*: BSC emissions from a cement mortar beam. a) the temporal development of the applied load. b) the corresponding BSC emissions at the upper (compressed) surface of the beam (solid line) and the lower (tensed) surface of the beam (dotted line).*

The maximum value of the curve corresponding to the tensional region is more than twice as large as that of the compressional region. This fact gives rise to the hypothesis that due to the extensional deformation of the lower part of the beam a larger number of microcracks take place and the escorting dislocations find easier their way to move apart than those in the compressional region (Griffith, 1920; Landis and Baillon 2002). Consequently, the electric current (BSC) recorded in the tensional region is larger than that recorded in the compressional region.

Another noticeable fact is that both PSC recordings get to a maximum at the same instant before the applied force takes its final value. Then, both pressure stimulated currents enter relaxation.

9. Comparative results Cement based samples and marble samples

9.1 Comparative Results using LRST technique

In order to evaluate the validity of the theoretical model and provide more accurate results, sets of new experiments as well as the experimental results of already published works have been used to compare the PSC recordings from cement products and marble samples.

Specifically, Fig. 9.1 and Fig 9.2 are representations of the emitted pressure stimulated current as a function of the relative compressional stress both cement mortar and marble samples, applying stress with constant rate (LSR Technique). The used samples were of the same dimensions as well as the used electrodes had the same active areas in order to achieve comparable electric current qualitative results.
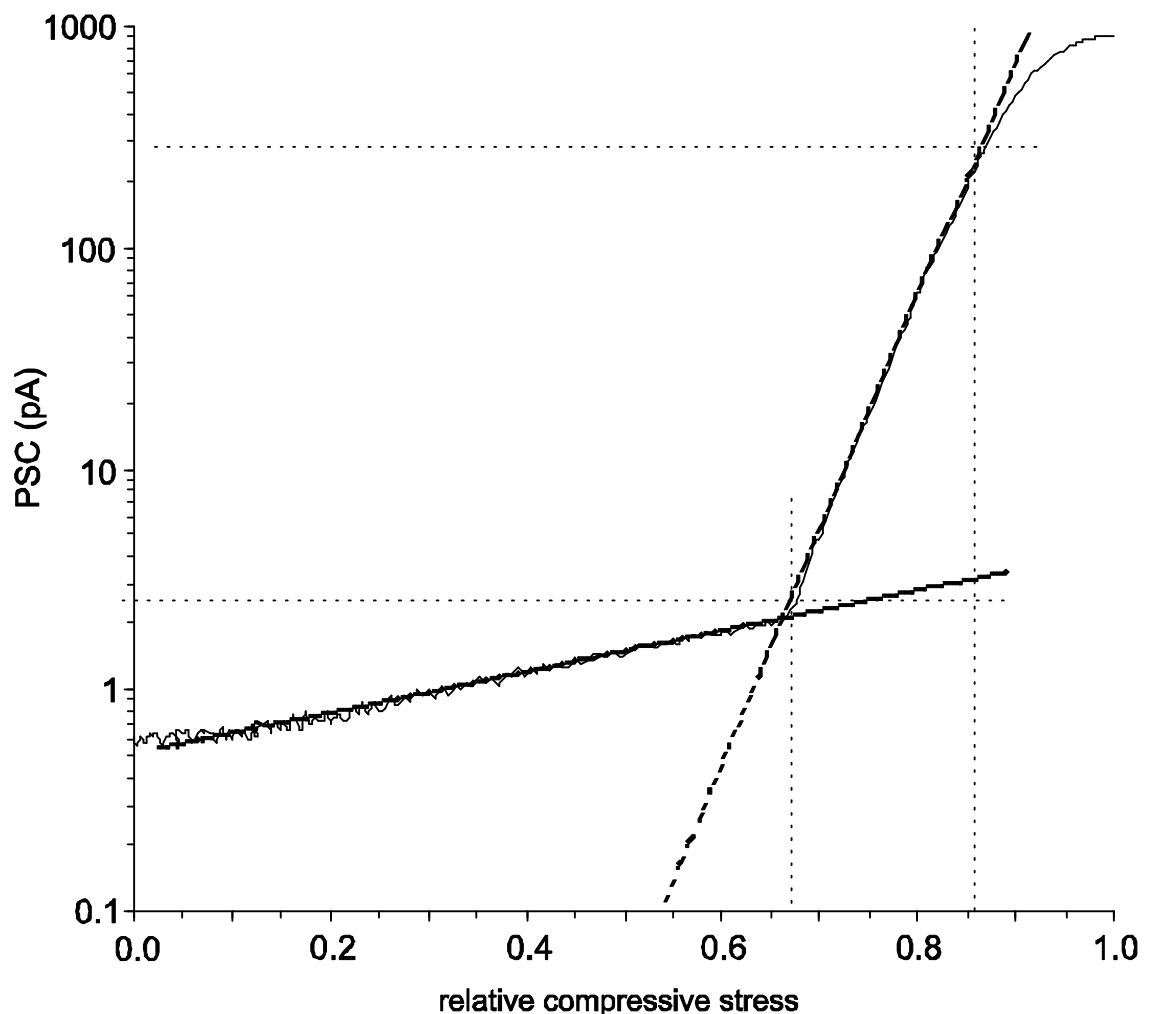

Fig. 9.1: *Correlation of PSC and relative compressional stress on cement mortar samples. (Triantis et al., 2006b)*
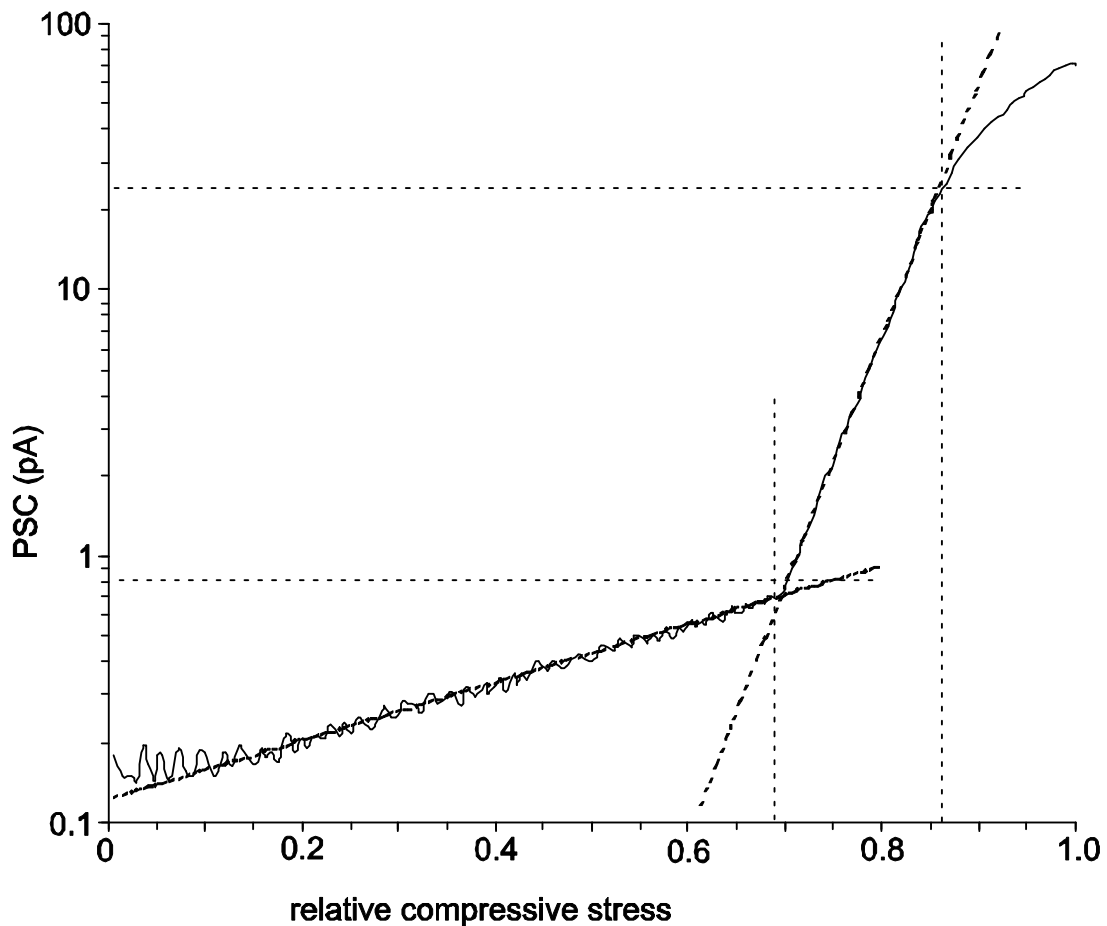
Fig. 9.2: *Correlation of PSC and relative compressional stress on marble. (Triantis et al., 2006b)*

In the same diagrams, the PSC excitation appears approximately in the range 0.70 to 0.75 after the beginning of the compressive stress increase process. In this range both materials practically start deviating from the linear behaviour range regarding the stress strain curve during which the growth and propagation of microcracks is evident and according to the MCD model PSC is expected to grow.

Another remarkable observation is PSC magnitudes on cement and marble differ significantly. In particular, the cement PSC curve attains larger values than those of the marble sample. A significant factor that influences and causes this difference is the enclosed water that participates in the cement products. On the other hand the extremely low porosity of the order 0.4% of the marble reduces fluid transportation or humidity levels increasing in the samples' bulk. The higher PSC level at the cement samples can also be interpreted in terms of the different microstructures of the two materials.

More analytically, the chemical bonds of calcite are stronger and more cohesive than those of cement mortar which is made of cement, sand and water establishing a much more porous solid. As a result, the bulk has a great probability to form more microcracks. Moreover, the pre-existing microcracks in the aggregate transition zone increase in length and width resulting in a progressively increasing contribution to the overall strain. Thus, new microcracks appear corresponding to more released electric charge and consequently to a larger PSC magnitude up to fracture limit of the material sample.

9.2 Comparative results with Abrupt Step Stress Technique. (ASST)

Figs. 9.3 and 9.4 describe the temporal behavior of cement (Fig 9.3) and marble (Fig. 9.4) PSC emissions when the samples are subjected to time varying stress in a stepwise form (conducting ASS Technique). The applied normalized stress never exceeded the 0.9 which was decided in order to avoid secondary PSC emissions due to extensive damaging and creep effect.
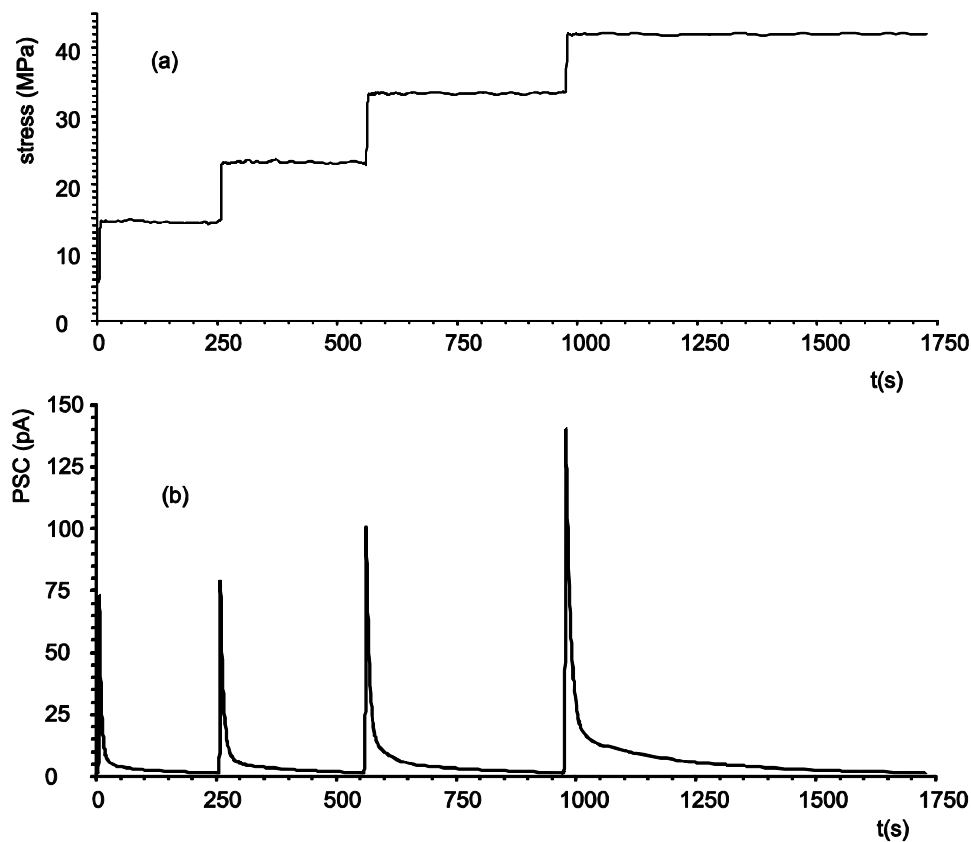

Fig 9.3: *Increasing stress loadings (a) and the emitted PSC (b) during an ASST process of mechanical loading on cement based samples.*
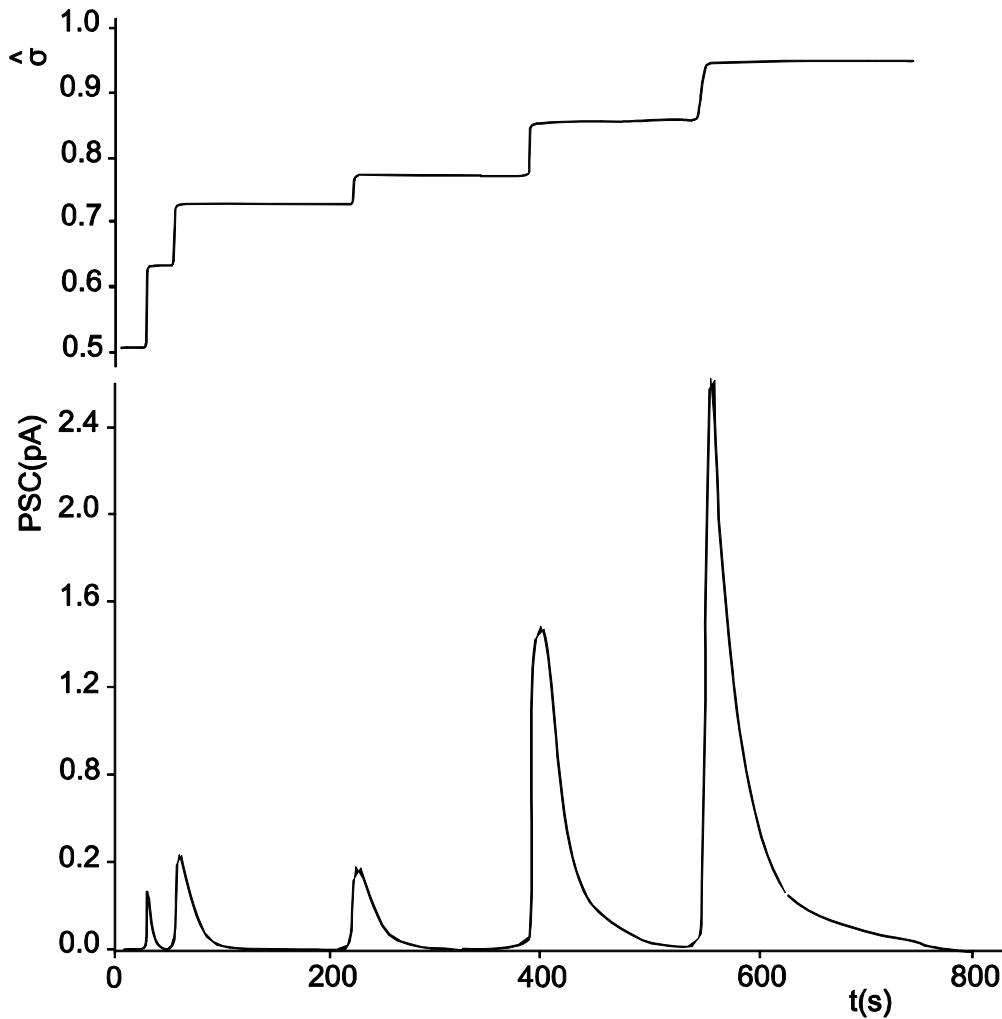
Fig 9.4: *Increasing stress loadings (a) and the emitted PSC (b) during an ASST process of mechanical loading on marble samples (Triantis et al., 2006b).*

The upper part of each figure describes the stress temporal development while the lower the corresponding PSC. It is significant to mention and observe that both emissions obtain the same qualitative characteristics since during each stress step and regardless of the used sample the emitted PSC reaches rapidly a maximum and then decays at a lower rate. The formalisms that the PSC decays after each stress step at cement samples have been discussed in the results section of this thesis.

Since the used samples were of the same dimensions and the same electrodes were used to conduct the experiments the quantitative results are also comparable. As it becomes clear by inspective the Figures the PSC emissions from cement based samples when applying the ASST technique is also higher than the PSC emitted from the marble samples. This can be attributed to the same factors as mentioned in the previous paragraph.

9.3 Comparative results applying sequential Loading – unloading cycles.

Fig. 9.5 clearly shows the behavior of the PSC emission during repetitive loading and unloading cycles for cement based samples (curve a) and for marble samples (curve b).
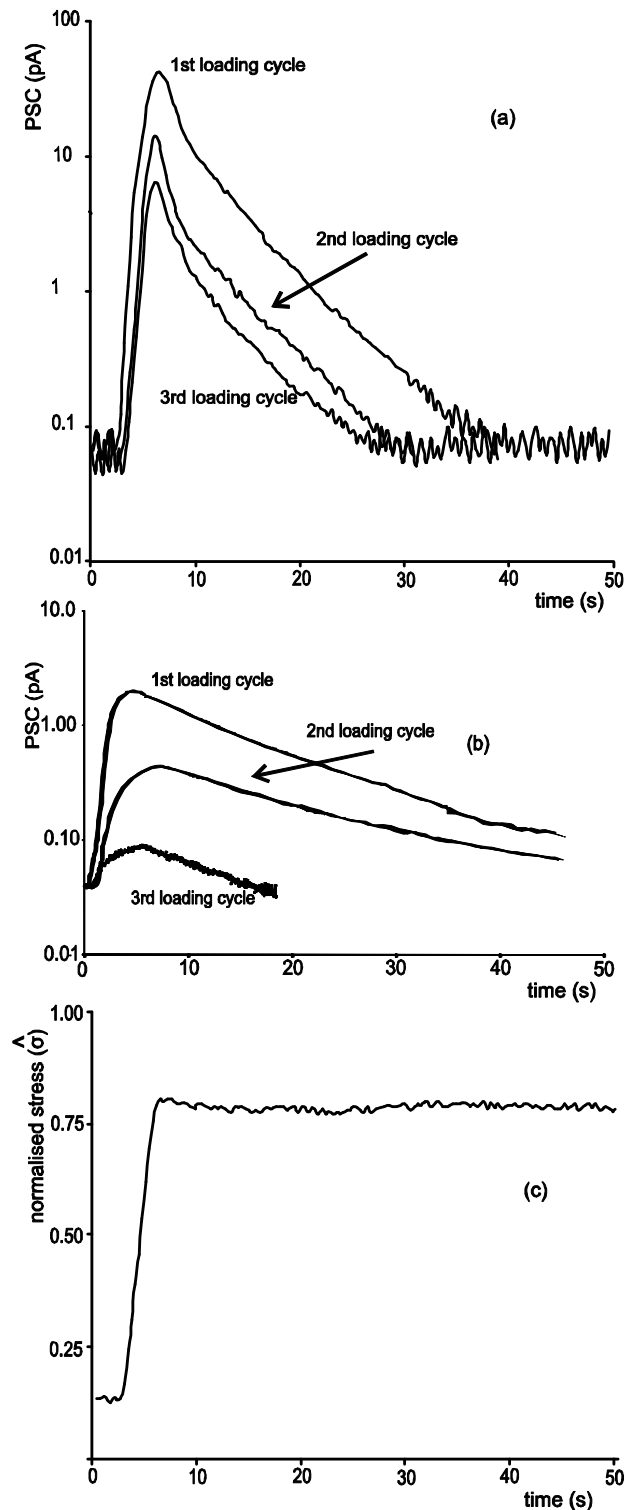

Fig 9.5: *The behavior of the PSC emitted during three sequential loadings and unloading on a cement based sample (curve a) on a marble sample (curve b). Each stress had a form similar to the one presented in curve c.*

The samples suffered stress in the same stress ranges three consecutive times. The obtained PSC becomes lower during each next loading cycle. This observation is valid for both of the samples. Observing curves a and b it can be concluded that when a brittle material suffers a repetitive loading and unloading process in the same stress limits it remembers the higher stress it has suffered and until this point the PSC emission becomes gradually lower. The reason for this phenomenon concerning the marble samples has been discussed in the results section of this thesis and regarding the corresponding results for the marble samples it has been reported and discussed by Vallianatos et al., 2004.

10. Conclusions

1. It is the very first time that weak electric current emissions are detected during mechanical stress application on cement based materials.

2. The above electric current emissions have been compared with corresponding electric emissions on geomaterial samples and show that they have a magnitude up to twice as large but they have similar qualitative characteristics. This difference is due to the different microstructure of cbm and geomaterials and also due to larger porosity and consequently increased presence of water in cement based materials.

3. The experiments provided a relationship between the electric current emissions and the applied stress.

4. A detailed study was made in order to show that the origin of such emissions is the crack opening processes. Several experimental techniques and methodologies (some of them novel) were applied on typical cement mortar and paste samples.

5. It was experimentally verified that PSC depends on strain variations of the sample during mechanical loading.

6. When the samples are subjected to monotonically increasing stress from early stress levels up to fracture, a concurrent electric emission is detected when the relative compressional stress becomes larger than the value that indicates the entrance into an interfacial transition zone. The electric emission gets to a maximum in the vicinity of fracture.

7. Additionally, experiments for the investigation of the fatigue process in the near fracture range were conducted and the emitted electric currents were studied.

8. Finally, three point bending tests showed the significance and the influence of the compressional and tensile zones on the emitted electric currents. The experiment showed that on both types of the used samples electric current emissions of the same form but of opposite polarity were emitted from both the compressional (upper) and the tensional (lower) zones.

9. The above described and proposed methodology can become a very powerful tool in studying and monitoring the health of cement based materials. It can also be used as a prediction methodology indicating the stress state and the consequent damage status of the material or construction. Thus, if the

methodology used in this thesis is enriched with tests on larger and different samples i.e. concrete, it could be the basis for the development of a new NDT-NDE tool.

Further work is recommended to be done for completion of the methodology using:

- Larger samples
- Concrete
- Higher stress
- Field tests

It is clear that research will not end and will always tend to more complete proposals.

References

Anastasiadis, C., Triantis, D., Stavrakas. I., Vallianatos, F., *Pressure stimulated currents (PSC) in marble samples after the application of various stress modes before fracture*, **Annals of Geophysics**, 47, 21-28, 2004.

Anastasiadis, C., Triantis, D., Hogarth, C. A., *Comments on the phenomena underlying pressure stimulated currents (PSC) in dielectric rock materials*, .**Journal of Materials Science**, 42, 2538-2542, 2007a.

Anastasiadis, C., Stavrakas, I., Triantis D., and Vallianatos, F., *Correlation of Pressure Stimulated Currents in rocks with the damage parameter*, **Annals of Geophysics**, Vol. 50, pp. 1-6, 2007b.

Bella, F., Biagi, P.F., Caputo, M., Della Monica, G., Ermini, A., Plastino, W. and Sgrigna, V., *Electromagnetic background and preseismic anomalies recorded in the Amare cave, (central Italy)*, in Hayakawa, M and Fujinawa, Y. (eds), **Electromagnetic Phenomena Related to Earthquake Prediction**, Terra Scientific Publishing Co., Tokyo, 181-192, 1994.

Bernard. P., *Plausibility of long distance electrotelluric precursors to earthquakes*, **J. Geophys. Res**, 97. 17,531-17.546. 1992.

Bernard, P. and Le Mouel, J.L.: *On electrotelluric signals, in Sir J. Lighthill (ed.), A critical review of VAN*, **World Scientific**, Singapore, 118-152, 1996.

Brady, B.T., Rowell, G. A.,: *Laboratory investigation of the electrodynamics of rock fracture*, **Nature** 321, 448-492, 1986 .

Chatelier, H. *Le Crystalloids against colloids in the theory of cements*. **Trans. Faraday Soc.**14 1–2, pp. 8–11, 1919.

Chen, D., Zhang D.,and Sun, Z., *ULF electric potential changes prior to fracture in rock samples*, in Hayakawa, M and Fujinawa, Y. (eds), **Electromagnetic Phenomena Related to Earthquake Prediction, Terra Scientific Publishing Co.**, Tokyo, 323-329, 1994.

Chuy, G., Cannard, J. Robert, L. and Rossi, P., *"Experimental investigations on the damage of Portland cement concrete made with natural aggregates"*, **Mater. Struct.**. 22, 98-106, 1989.

Cress, G.O., Brady B.T. and Rowell, G.A., Sources *of electromagnetic radiation from fracture of rock samples in laboratory*, Geophys**. Res. Lett**., 14, 331-334, 1987.

De Rooij, M.R. and Bijen, J.M.J.M. and Frens, G. *Introduction of syneresis in cement paste.* **Proc. Of Int. RILEM Conf. on the Interfacial Transition Zone in Cementitious Composites**(eds A. Kartz, A. Bentur, M. Alexander and G. Arliguie), Israel, March,E &FN Spon, London,pp. 59-67, 1998.

Enomoto, J. and Hashimoto, H.: *Emission of charged particles from indentation fracture of rocks*, **Nature,** 346, 641, 1990.

Enomoto, Y., Shimamoto, T. Tsutsumi, A.and Hashimoto, H. *Transient electric signals prior to rock fracturring:* Potential use as an immediate earthquake precursor, in Hayakawa, M and Fujinawa, Y. (eds), *Electromagnetic Phenomena Related to Earthquake Prediction,* **Terra Scientific Publishing Co.**, Tokyo, 253-259, 1994.

Faraday, M.: *Experimental Researchers in Electricity* Vol 1, sec 284 (**E.p Dutton New York**, 1940), 1983.

Feldman R. F. and Sereda P. J*., A model for hydrated Portland cement paste as deduced from sorption-length change and mechanical properties,* **Materials and structures** 1(6):509-520, 1968.

Fenoglio, M. A. Johnston, M. S. and Byerlee. J. D. *Magnetic and electric fields associated with changes in high pore pressure in fault zones: Application to the Loma Prieta ULF emissions*, **J. Geophys. Res**. *100,* 12,951-12.958. 1995.

Fiffolt, D.A., Petrenko, V.F. and Schulson, E.M. *Preliminary study of electromagnetic emissions from cracks in ice*, **Philosophical Magazine** *B*, 67, 289-299, 1993.

Finkelstein, D., Hill R.D. and Powell, J.R., The *piezoelectric theory of earthquake lightning*, **J. Geophys. Res.,** 78, pp. 992-993, 1973.

Freund, F.: *Time-resolved study of charge generations and propagation in igneous rocks*, Vol. 105(B5), 11001-11019, 2000.

Glucklich, J., *"Fracture of Plain Concrete* " **Proceedings of the American Society of Civil Engineers**, Vol. 89, No. EM6, pp. 127-138, 1963.

Griffith, A. A., **Philosophical Transactions of the Royal Society**, Vol. A221, p.163, 1920.

Guo, Z., Liu. B., and Wang, V., *Mechanism of electromagnetic emissions associated with microscopic and macroscopic cracking in rocks, Electromagnetic Phenomena Related to Earthquake Prediction*, Edited by M.Havakawa and Y.Fujinawa,. **Terra Scientific Publishing** Co., Tokyo, pp.523-529, 1994.

Hadjicontis, V., Mavromatou, C.: *Transient electric signals prior to rock failure under uniaxial compression*, **Geophys. Res. Letters**, 21 1687-1990, 1994.

Hadjicontis, V. and Mavromatou, C.: *Electric signals recorded during uniaxial compression of rock samples: Their possible correlation with preseismic electric signals*, **Acta Geophys.** Polon., 43, 49-61,1995.

Hadjicontis, V. and Mavromatou, C., *Laboratory investigation of electric signals preceding earthquakes,* in Sir J. Lighthill (ed.), A critical review of VAN, **World Scientific**, Singapore, 105-117, 1996.

Hardy, H.R.Jr (ed.) *Acoustic Emission/Microseismic Activity in Geologic Structures and Materials*, **Proceedings of the 4th Conference. Trans Tech Publications**, Clausthal- Zellerfeld, pp. 711, 1989.

Hilleborg , A., Modeer, M., and Petersson, P.E.,"*Analysis of Crack Formation and Crack Growth in Concrete by Means of Fracture Mechanics and Finite Elements*", **Cement and Concrete Research**, Vol. 6, No. 6, pp.773-782, 1976.

Ikeya, M., and Takaki, S. *Electromagnetic fault for earthquake lightning*, **Jpn. J. Appl. Pins.** *35.* 355-357, 1996.

Jennigs, H.M and Tennis, P.D. *Model for the developing microstructure of Portland cement pastes.* **Journal of the American Ceramic Society** 77, (12):3161-3172,1994.

Jouniaux, L., and . Pozzi. J. P., *Permeability dependence of streaming potential in rocks for various fluid conductivities*. **Geoplns. Res. Lett**.. 22, p:485-488. 1995a.

Jouniaux, L., and Pozzi, J. P., *Streaming potential and permeability of saturated sandstones   under triaxial stress: Consequences for electrotelluric anomalies prior to earthquakes*, **J. Geophys. Res.** 100*.* 10,197-10,209, 1995b.

Kaiser J: *Ph.D thesis* : *Untersuchungen über das Auftreten Gerauschen bei Zugversuch*, **Technishe Hochschle, Munchen, Germany, 1950.**

Kotsovos, M.D.,"*Effect of testing techniques on the post-ultimate behaviour of concrete in compression*", **Materials and Structures**, Vol.16, no.91, pp.3-12, 1983.

Kyriazis, P., Anastasiadis, C. Triantis, D. Vallianatos, F., *Wavelet analysis on Pressure Stimulated Currents emitted by marble samples*, **Natural Hazards and Earth System Sciences**, 6, 889-894, 2006.

Kyriazis, P. Stavrakas, I. Anastasiadis, C. Triantis, D. "*Identification of deformation stages in rocks by means of weak electric current emissions using wavelet analysis*", **EGU General Assembly** 2007, Vienna, Austria 15 – 20 April 2007.

Landis, E. and Baillon, L.: *Experiments to Relate Acoustic Emission Energy to Fracture Energy of Concrete*, **Journal of Engineering Mechanics** Volume 128, Issue 6 698-702, 2002.

Lavrov, A.: *Fracture-induced Physical Phenomena and memory Effects in Rocks: A Review*, **Strain** 41, 135-149, 2005.

Lockner, D.A., Johnson. M.J.S., and Byerlee J.D., *A mechanism to explain the generation of earthquake lights*. **Nature,** 302, p. 28-33,1983.

Lockner, D. *The role of acoustic emission in the study of rock fracture.* **Int. J. Rock Mech. Min. Sci. Geomech.** Abstr. 30, 883–899, 1993.

Mavromatou, C. and Hadjicontis, V. *Laboratory investigation of transient electric signals detected by VAN network in Greece, Electromagnetic Phenomena Related to Earthquake Prediction*, Edited by M.Havakawa and Y.Fujinawa, **Terra Scientific Publishing** Co., Tokyo, pp 293-305, 1994.

Merchant, I.J., Macphee, D.E. Chandler, H.W.,Henderson, . R.J., *Toughening cement-based materials through the control of interfacial bonding*, **Cement and Concrete Research** 31, 1873–1880, 2001.

Michaëlis, W.S. *The setting of calcareous hydraulic cements.* **Z. Chem. Ind. Kolloide** 5, pp. 9–22, 1909.

Mizutani, H., Ishido, T. Yokokura T. and Ohnishi, S., *Electrokinetic phenomena associated with earthquakes*, **Geophys. Res. Lett**., 3, pp. 365-368, 1976.

Midness, S. and Diamond, S.,"*The Cracking and Fracture of Mortar*": **Matèriaux et Consructions**, Vol 15, no. 86 pp. 107-113, 1982.

Moavenzadeh, F. and Kuguel, R.,"*Fracture of Concrete*", **Journal of Materials**, Vol. 4, pp. 497-519, 1969.

Newman, K, *Concrete Systems, in Composite Materials*, **ed. L. Hollaway), Elsevier**, London 1966.

Nishioka, K., Yamakawa, S., Hirakawa, K., and Akihama, S., "*Test method for the Evaluation of the Fracture of Steel Fibre Reinforced Concrete* ", **Testing and Test Methods of Fibre Cement Composites, RILEM Symposium 1978, The Construction Press**, UK,pp. 87-98,. 1978.

Nitsan, U. *Electromagnetic emission accompanying fracture of quartz-hearing rocks*, **Geophysical Research Letters**, 4 333-337, 1977.

Ogawa, T., Oike, K. Mirura, T.: *Electromagnetic radiations from rocks*, **J. Geophys. Res**. 90, 6245-6249, 1985.

O'Keefe, S.G. and Thiel, D.V., *A mechanism for the production of electromagnetic radiation during fracture of Brittle materials*. **Phys. Earth Plane. Inter**., 89. p. 127-135, 1995.

Olivier, J.P. Maso, J.C. and Bourdette, B., *Review article –interfacial transition zone in concrete*. **Advanced Cement Based Materials**, 2(1):30-38, 1995.

Pomeroy, C.D. *Physics in cement and concrete technology* **C.D. Pomeroy Physics Education** 15(3), 171-176, 1980.

Powers, T.C. and Brownyard, T.L.. *Studies of the physical properties of hardened Portland cement pastes.* **Journal of the American Concrete Institute Proceedings** Volume,43:469-504,1946.

Saito, M., *Tensile fatigue strength of the mortar-aggregate bond*, **Cement and Concrete Research**, 18 () 710-714, 1988.

Sasaoka, H., Yamanaka, C.and Ikeya, M., *Measurement of electric potential variation by piezoelectricity of granite*, **Geophysical Research Letters**, *25*, 2225–2228, 1998.

Scholz, C. H., Sykes. L. R. and Aggarwal, Y. P., *Earthquake prediction: A physical basis*. **Science.** *181.* 803-810, 1973.

Scrivener K.L. Crumbie, A.K, and Laugesen P., *The interfacial transition zone (ITZ) between cement paste and aggregates in concrete*. **Interface Science** 12(4):411-421, 2004.

Shah, S.P., and McGarry, F.I., "*Griffith Fracture Criterion and Concrete*", **Journal of the Engineering Mechanics Devision, ASCe**, Vol. 97, pp.39-44, 1971.

Shah, S.P.,S Wartz, S.E., and Ouyang, C., "*Fracture Mechanics of Concrete: Applications of Fracture Mechanics to Concrete, Rock and other Quasi- Brittle Materials*" **John Wiley & Sons Inc.**,552p., 1995.

Slifkin, L., *Seismic electric signals from displacement of charged dislocations.* **Tectonophysics,** 224, 149-152, 1993.

Sok, C. and.Baron, J., *'Mecanique de la rupture appliquee au beton hydraulique'*, **Cem. Concr. Res.** 641-648, 1979.

Stavrakas, I. Anastasiadis, C. Triantis, D. and Vallianatos F.: "*Piezo Stimulated currents in marble samples: Precursory and concurrent – with – failure signals.*" **Natural Hazards and Earth System Sciences**, 3, pp. 243-247, 2003.

Stavrakas., I. Triantis, D., Agioutantis, Z., Maurigiannakis, S., Saltas, V., Vallianatos, F., Clarke, M., *Pressure stimulated currents in rocks and their correlation with*

mechanical properties, **Natural Hazards and Earth System Sciences**, 4,563–567, 2004.

Stepanov, A.W.: **Z. Physics** 81, 560, 1933.

Sun M., Li Z., Song X., *Piezoelectric effect on hardened cement paste*, **Cement and Concrete Composites**, 26, 717-720, 2004.

Sun M., Wang X., Zhao K., Li, Z., *Electrically induced temperature difference and deformation in hardened cement pastes*, **Cement and Concrete research**, 36, 2164-2168, 2006.

Takeuchi, A. and Nagahama, H.: *Voltage changes induced by stick slip of granites*. **Geopphys. Res. Lett**. 28, 3365-3367, 2001.

Tatum, P. J., *The measurement of acoustic emissions to detect embrittled brazed joints*, **Strain** 39, 79–82, 2003.

Teisseyre, R. and Nagahama. H. *Dislocational models of electric field generation in a seismic source zone, in M. Hayakawa* (ed.), *Atmospheric and Ionospheric Electromagnetic Phenomena Associated with Earthquakes*, **Terra Scientific Publishing Co**, Tokyo, 271-285, 1999.

Tennis, P.D. and Jennigs H.M, .*A model for two types of calcium silicate hydrate in the microstructure of Portland cement pastes* .**Cement and Concrete Research**, 30(6):855-863,2000.

Triantis, D., Anastasiadis, C., Kyriazopoulos A.and Vallianatos F.: "*An analysis of Pressure Stimulated Currents (PSC), in marble samples under mechanical stress*", **Physics and Chemistry of the Earth,** Volume 31, Issues 4-9, 234-239, 2006a.

Triantis, D., Anastasiadis, C. Kyriazopoulos, A. and Stavrakas, I.: "*The ascertainment of the presence of damage processes using the Pressure Stimulated Current (PSC) technique on marble and cement samples*", **9**[th] **ECNDT 2006, Berlin**, 25 – 29 September 2006b.

Triantis, D., Anastasiadis, C. Vallianatos, F. Kyriazis, P. Nover G.: "*Electric signal emissions during repeated abrupt uniaxial compressional stress steps in amphibolite from KTB drilling*". **Natural Hazards and Earth System Sciences**, vol. 7, pp. 149-154, 2007.

Turcotte D.L. and Shcherbakov R., "*Can damage mechanics explain temporal scaling laws in brittle fracture and seismicity?*" *Pure Appl. Geophys.*, **163** (2006) 1031-1045.

Tzanis A. and Vallianatos, F., *A physical model of electrical earthquake precursors due to crack propagation and the motion of charged edge dislocations*, in M. Hayakawa and O.A. Molchanov (eds), **Seismo Electromagnetics: Lithosphere-Atmosphere-Ionosphere Coupling, TERRAPUB**, Tokyo, pp. 117-130, 2002.

Vallianatos, F. and Tzanis. A., *Electric current generation associated with the deformation rate of a solid : Preseismic and coseismic signals*, **Phys. Chem. Earth**, 23, 933-938, 1998.

Vallianatos, F. and Tzanis. A., *A model for the generation of precursory electric and magnetic fields associated with the deformation rate of the earthquake focus, in M. Hayakawa* (ed.), **Atmospheric and Ionospheric electromagnetic phenomena associated with Earthquakes, Terra Scientific Publishing** Co, Tokyo 287-305, 1999..

Vallianatos, F. Triantis, D., Tzanis, A., Anastasiadis, C., Stavrakas, I., *Electric Earthquake Precursors: From Laboratory Results to Field Observations*, **Physics and Chemistry of the Earth**, 29, 339-351, 2004.

Warwick, J.W., Stoker C. and Meyer, T.R., *Radio emission associated with rock fracture : Possible application to the great Chilean earthquake of May 22, 1960*, **J. Geophys. Res.,** 87, No B4, 2851-2859, 1982.

Wittmann, F.H., *Observation of an electromechanical effect of hardened cement paste*, **Cem. Concr. Res.**, 3, 601-605, 1973.

Whitworth, R.W.*: Charged dislocations in ionic crystals.* **Adv. Phys**. 24, 203 304, 1975.

Yamada, I., Masuda, K., and Mizutani, H., *Electromagnetic and acoustic emission associated with rock fracture*, **Phys. Earth Planet Inter**., 57, pp. 157-168, 1989.

Yoshida, S.,Manjgaladze, P., Zilpimiani, D., Ohnaka M. and Nakatani. M.. *Electromagnetic emissions associated with frictional sliding of rock, in Hayakawa, M and Fujinawa, Y.* (eds), **Electromagnetic Phenomena Related to Earthquake Prediction, Terra Scientific Publishing** Co., Tokyo, 307-322, 1994.

Yoshida, S., Uyeshima, M. and Nakatani M*., Electric potential changes associated with a slip failure of granite : Preseismic and coseismic signals*, **J. Geophys. Res**., 102, 14883-14897, 1997.

Yoshida, S., Oswald, C.C. and Sammonds, P.R.: *Electric potential changes prior to shear fracture in dry and saturated rocks*, **Geophys. Res. Lett**., 25(10), 1557-1580, 1998.

APPENDIX A

Experimental Instrumentation and arrangements

The following pictures are taken in the Laboratory Environment where the experiments have been conducted.
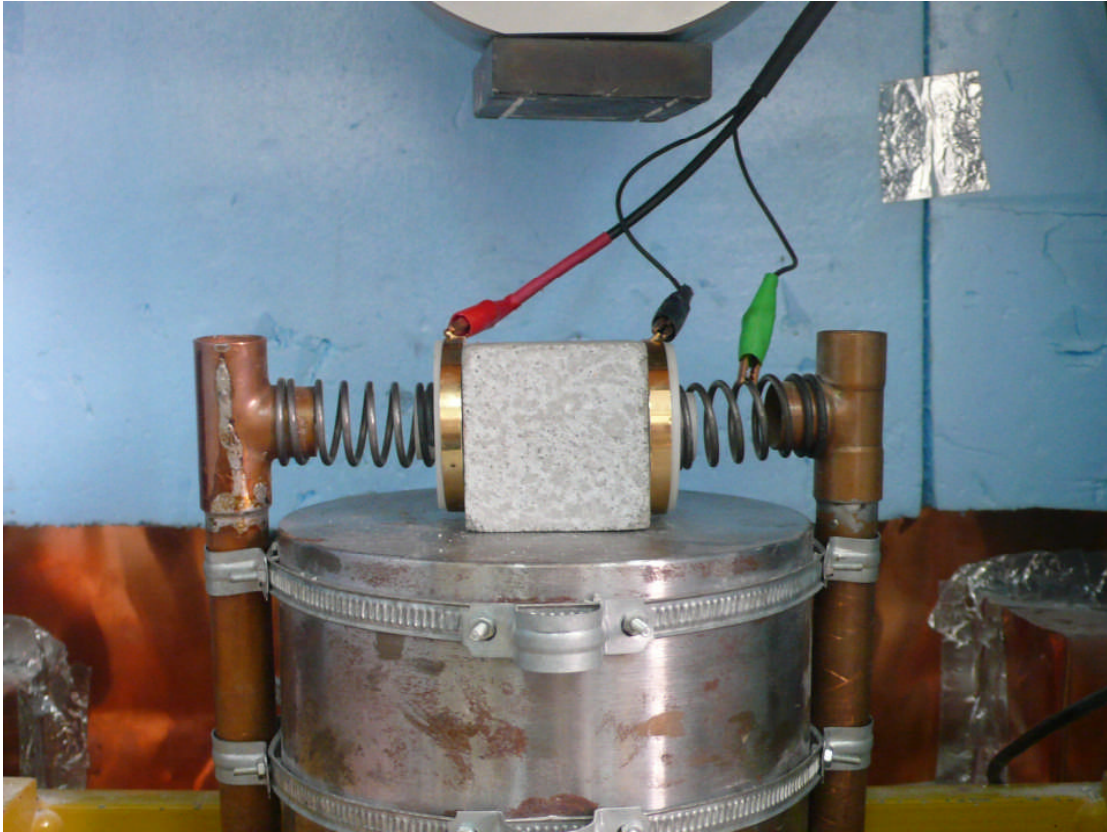

Photo 1

Installation of the cement based material sample without the Teflon interface and the corresponding electrometer wiring in order to conduct PSC measurements. The red and black leads connect the gold plated electrodes that collect the electric current emissions to the programmable sensitive electrometer.

Photo 2

A general view of the Faraday shield protected system to conduct the electric measurements. It includes the stressing cylinder, the base-plate and the sample mounting configuration with the springs that hold the gold plated electrodes attached on the sample. It also includes the load cell that is used to measure the applied load. As can be seen the Faraday shield that is formed by copper sheets and aluminum is protected by the isolation material to avoid mechanical damaging of the shield due to the extracted pieces of the samples under test during fracture.
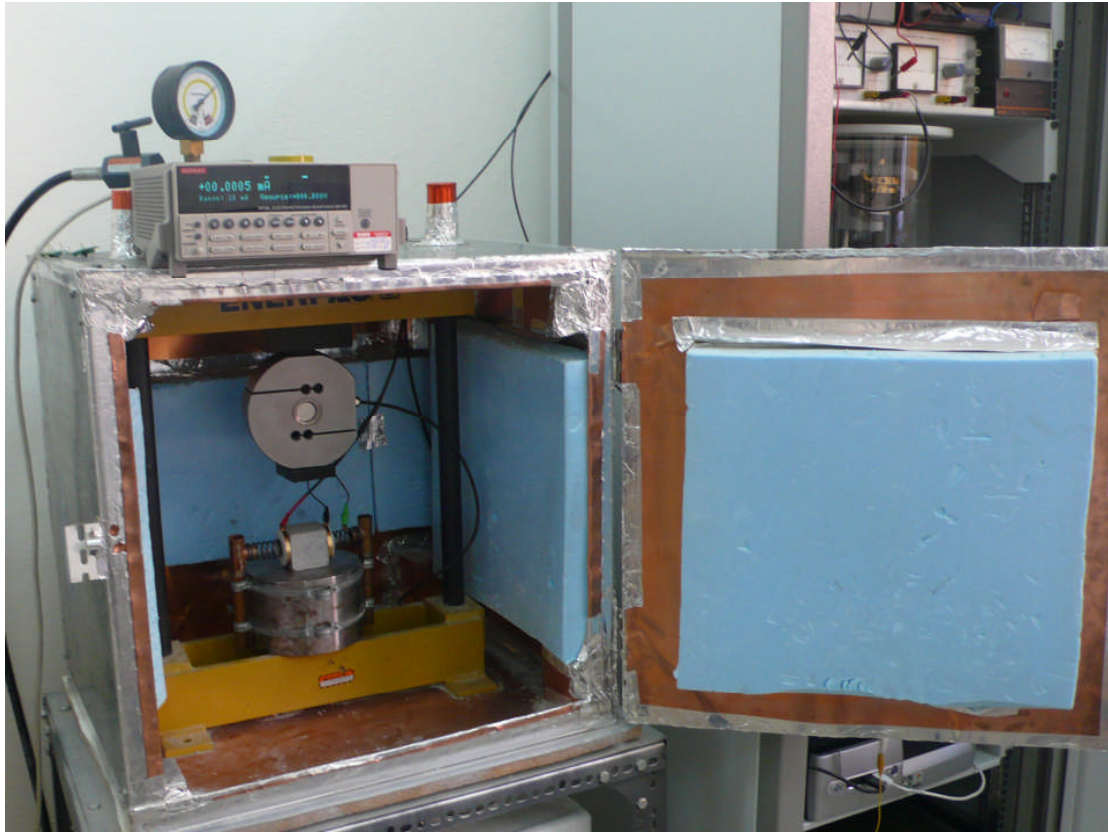
Photo 3

The outer view of the Faraday shield that includes an electrometer as can be seen at the top of the shield. The electrometer is the sensitive programmable instrument used to conduct the electric current emissions. The manometer that can be seen at the top of the photo is used to measure the pressure in the hoses and the hydraulic vales (see left top of the photo) in order to avoid possible damages or harming of the operator of the system.

Photo 4

At the top of the photo the two sensitive programmable electrometers used to conduct the BSC measurements on cement based material beams are presented. The right lower corner shows the amplifier that interprets the microvoltage of the load cell into the range of the voltage level that can be used by the Analogue to Digital Converter used to record the applied loading.

Photo 5

This photo shows the PC that is used to synchronize and configure all the used instrumentation as well as a capture of the program that is used to collect the recordings of the electrometers, the load cell and the strain gages bridge.
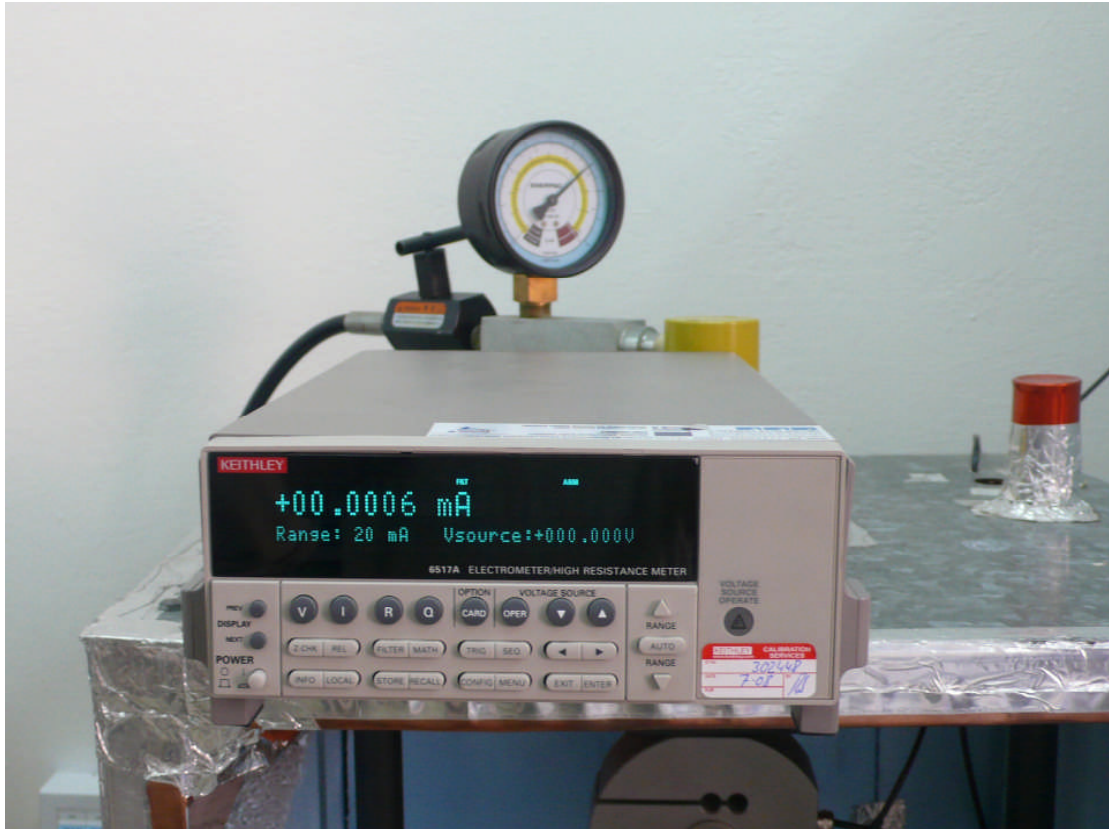
Photo 6

This photo shows one of the used programmable electrometers that were used to conduct the electric current measurements.
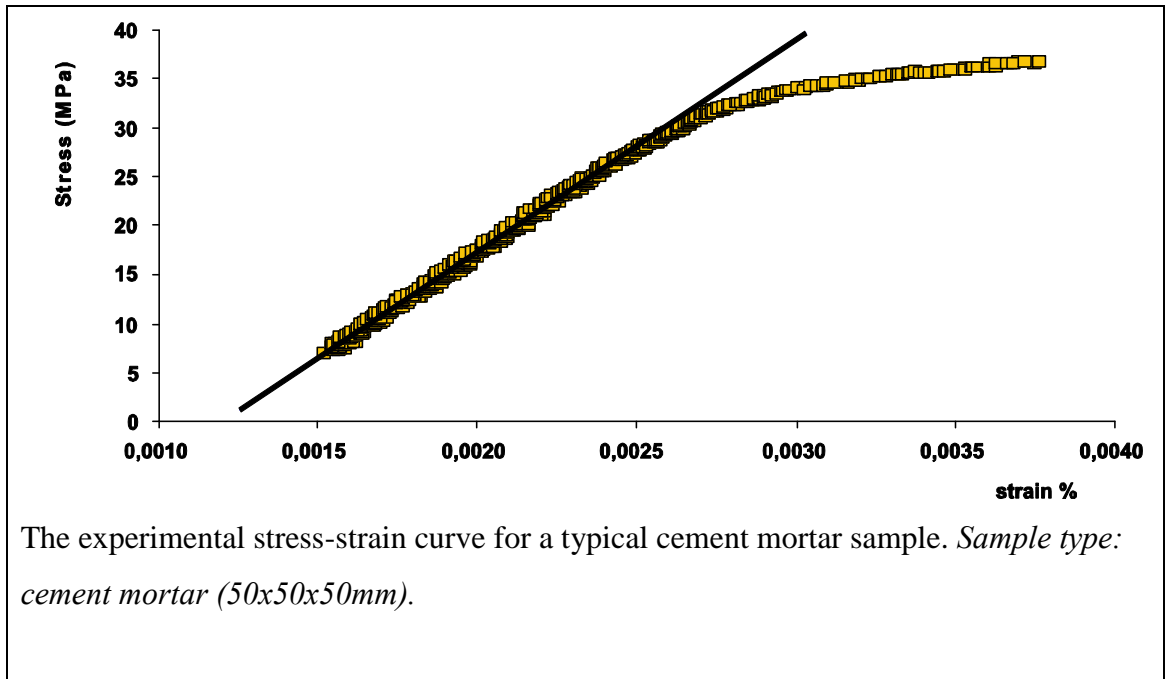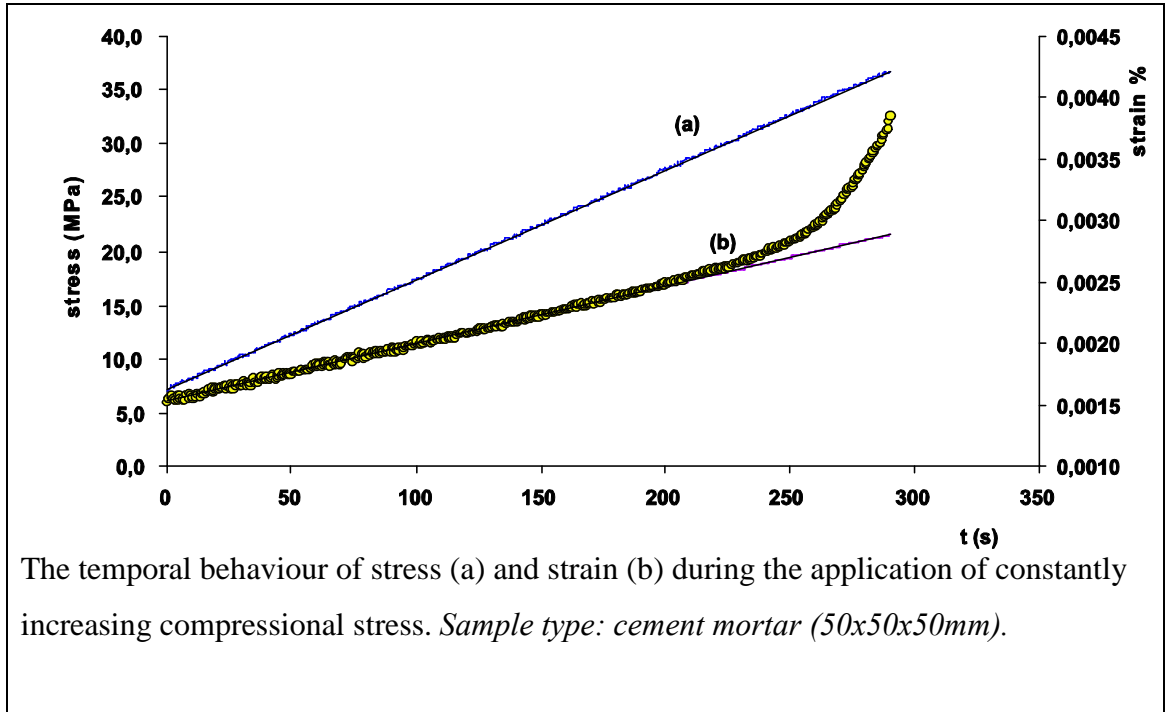
Photo 7

A general view of the mechanical part of the stressing system including the electric pump used to apply and handle the loading. At the left side the photo shows the Acoustic Emissions recordings system. At the top of the photo the Agilent VEE software that was used to build the control and measure environment can be found.
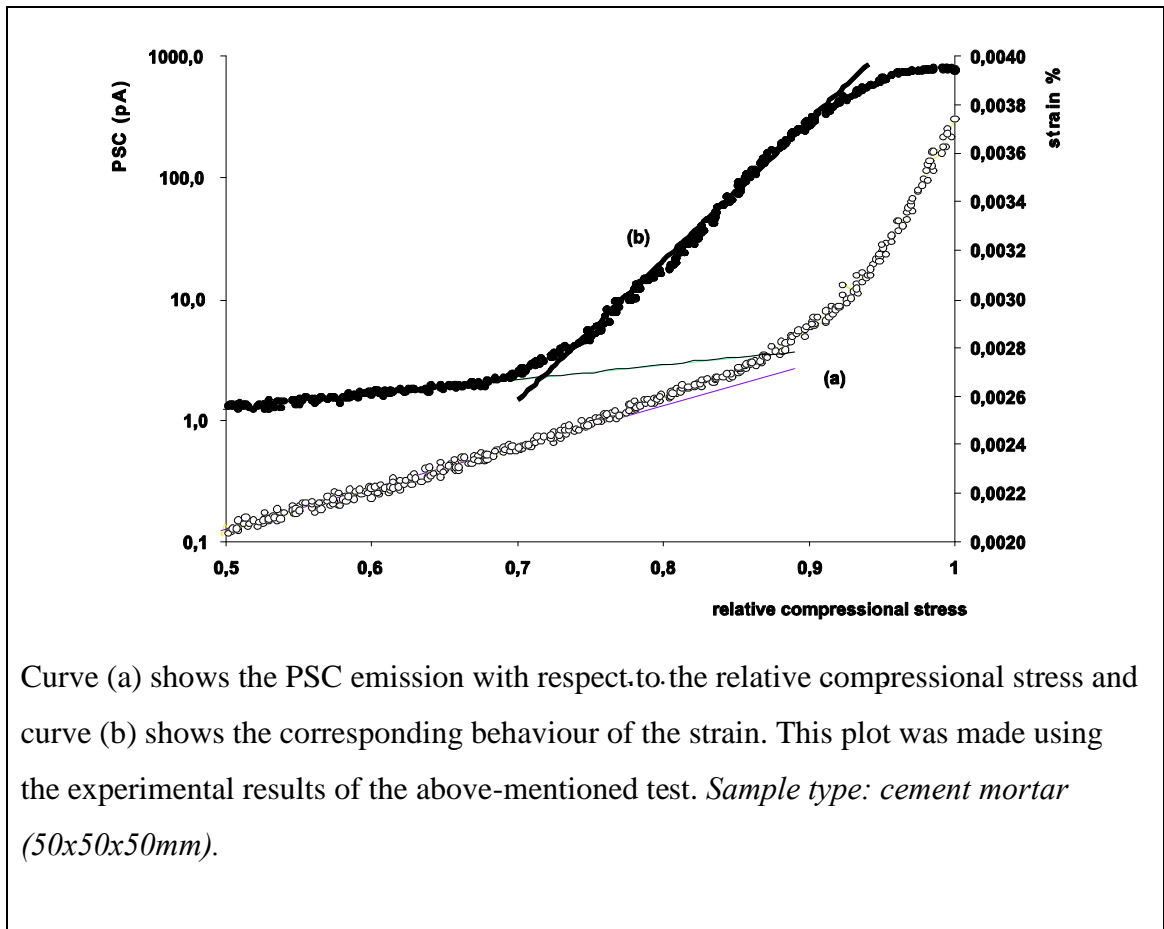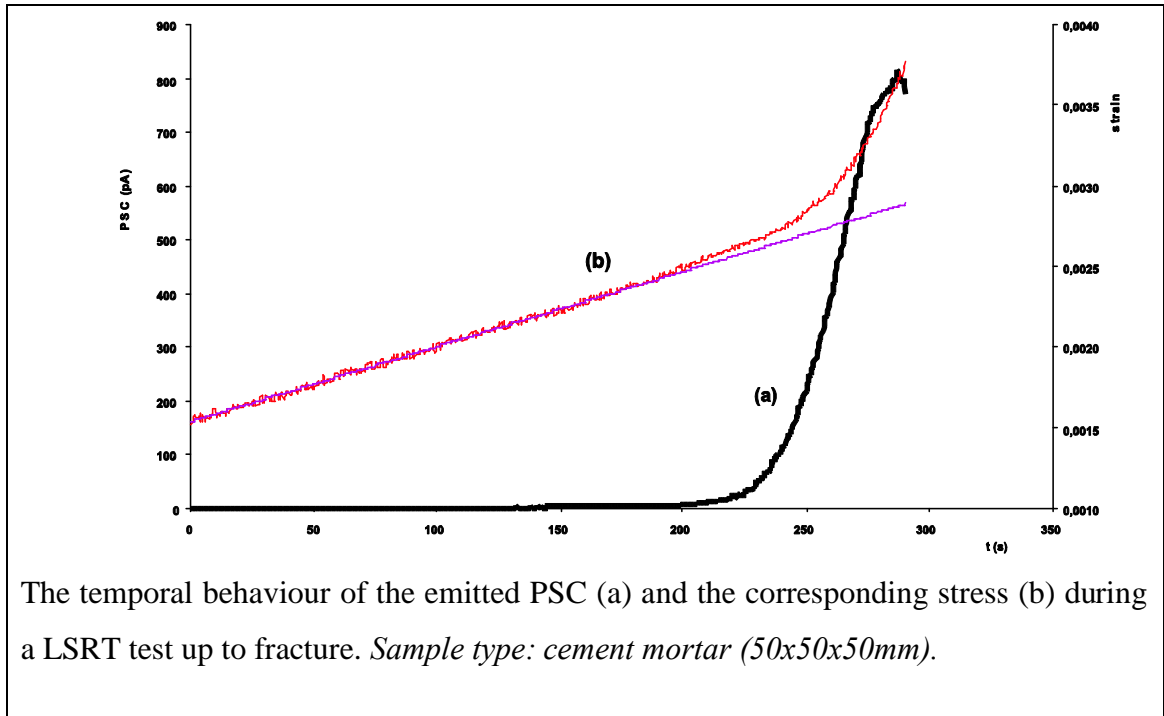
APPENDIX B

Additional experimental measurements conducted on cement based materials during this work.

A1. Stress –Strain tests on various cement based materials.

The temporal behaviour of stress (a) and strain (b) during the application of constantly increasing compressional stress. *Sample type: cement mortar (50x50x50mm).*

The experimental stress-strain curve for a typical cement mortar sample. *Sample type: cement mortar (50x50x50mm).*

A2. Electric current emission (PSC) recordings applying the LSR Technique. (Experiment A)

The temporal behaviour of the emitted PSC (a) and the corresponding stress (b) during a LSRT test up to fracture. *Sample type: cement mortar (50x50x50mm).*

Curve (a) shows the PSC emission with respect to the relative compressional stress and curve (b) shows the corresponding behaviour of the strain. This plot was made using the experimental results of the above-mentioned test. *Sample type: cement mortar (50x50x50mm).*

A3. Electric current emission (PSC) recordings applying the LSR Technique. (study of the "a" exponent at high stress values, Experiment B)

PSC recordings with respect to the normalized stress when applying the LSR Technique. Five similar experiments were conducted in order to study the behavior of the electric current at high stress values. The recorded electric current is plotted on log axis. *Sample type: cement mortar (50x50x50mm).*
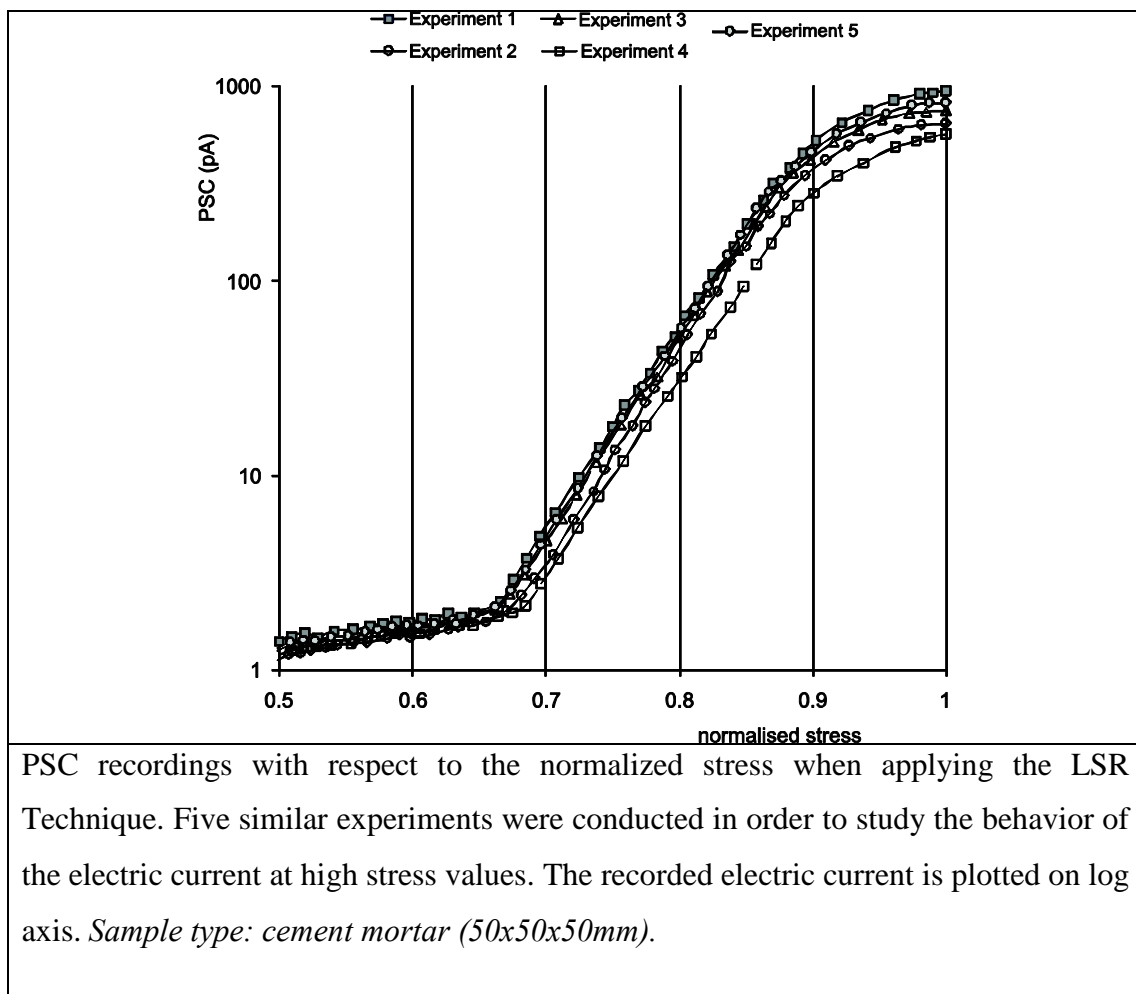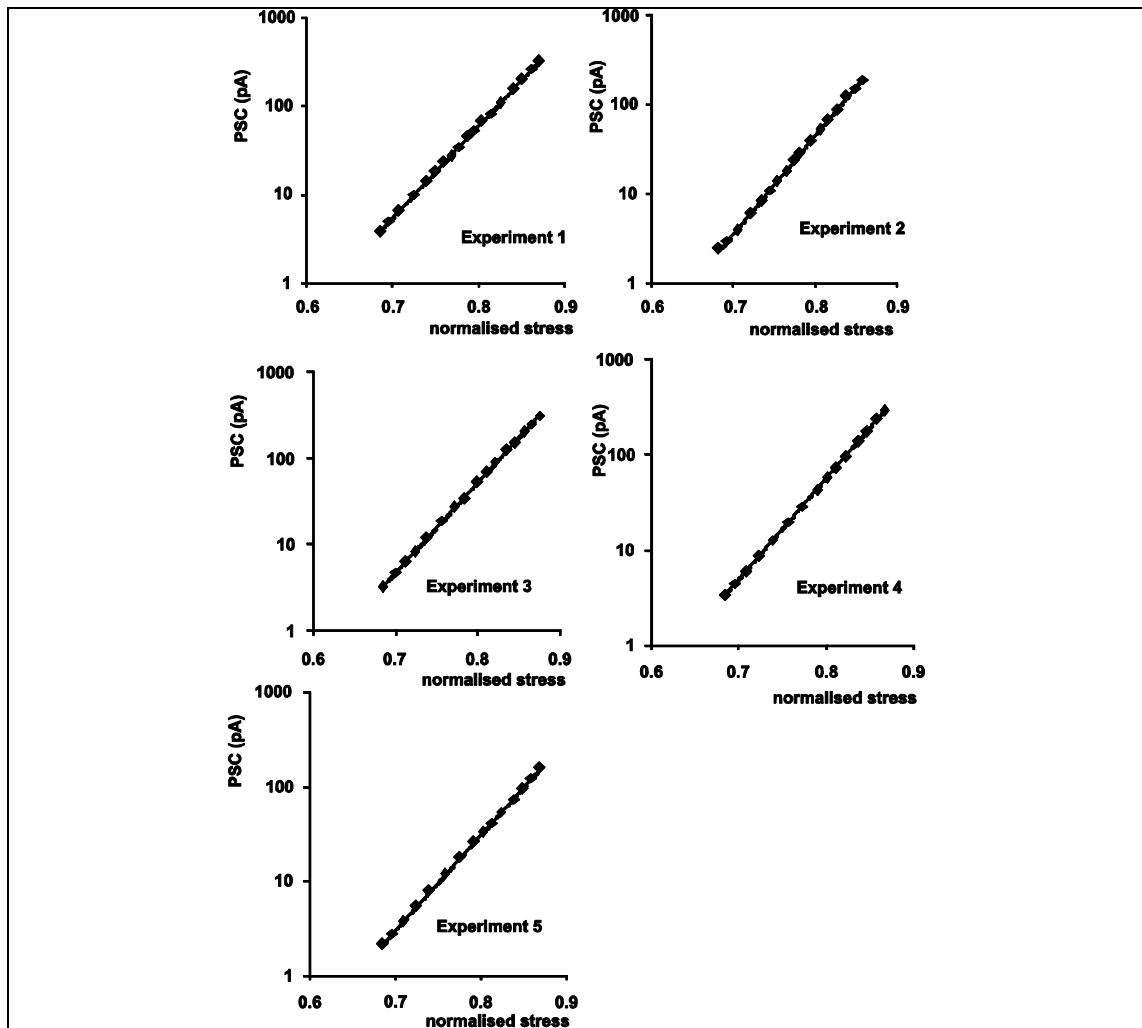
It is clear that in the range $0.7 > \hat{\sigma} > 0.9$ the exponential law is valid. Fitting of the curve PSC vs normalized stress is applied in order to calculate the exponent factor a, for five Experiments with the LSR Technique. *Sample type: cement mortar (50x50x50mm).*

The values of the exponent a calculated with the least squares fitting technique for the five experiments described above.

Experiment No	Value of the Exponent a
1	23.8
2	25.2
3	24.1
4	24.5
5	23.2

A4. Electric current emission (PSC) recordings applying the LSR Technique. (Experiment C)

This experiment is conducted three days after the preparation of the sample. The behaviour of the stress-strain curve and and the value of the Young's modulus are characteristics. For this experiment the Young's modulus is calculated to be around 6.46GPa.
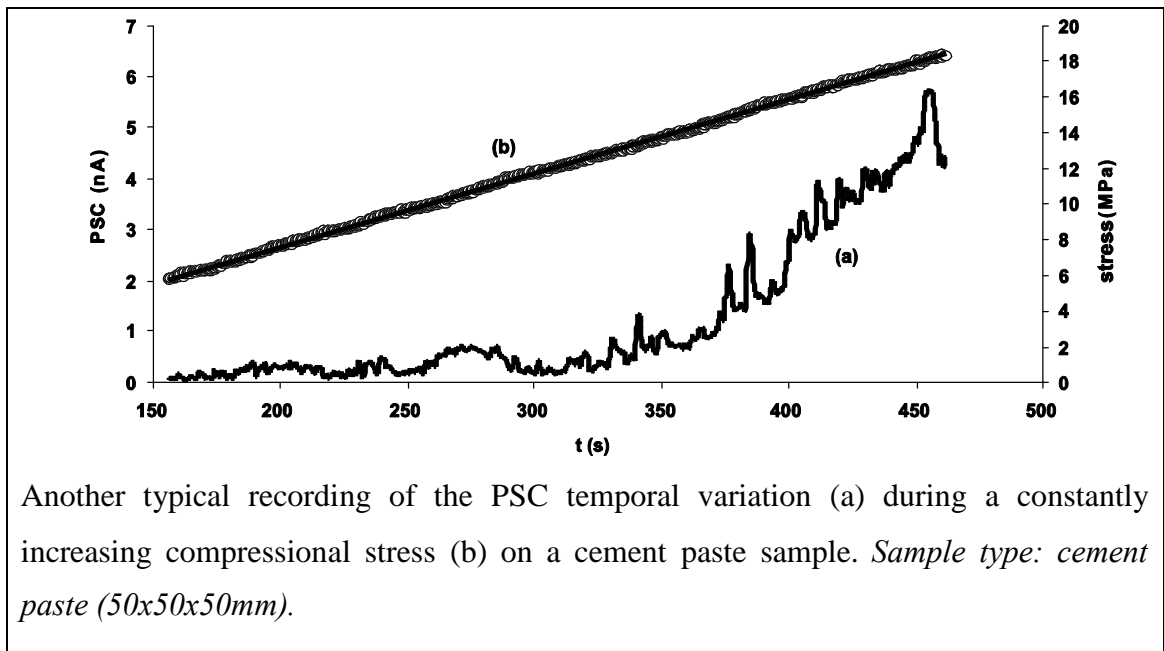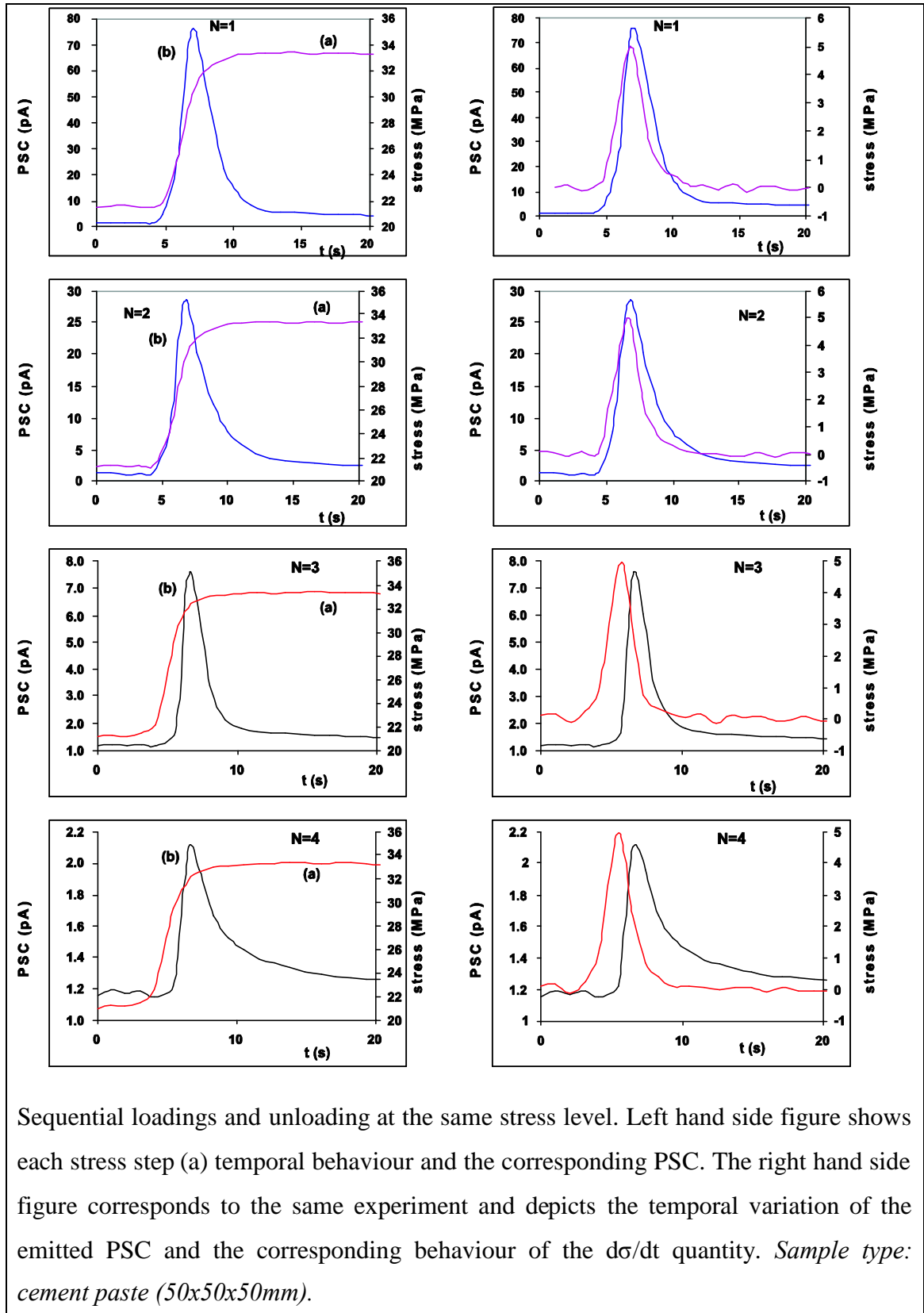

Another typical recording of the PSC temporal variation (a) during a constantly increasing compressional stress (b) on a cement paste sample. *Sample type: cement paste (50x50x50mm).*
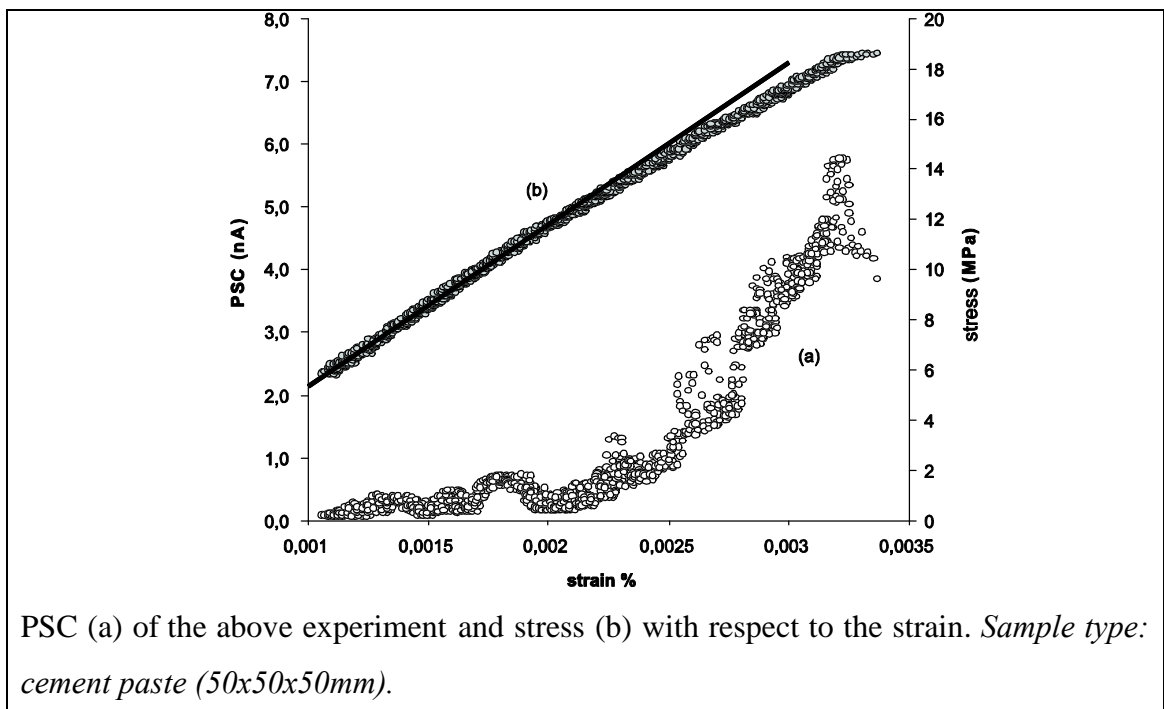
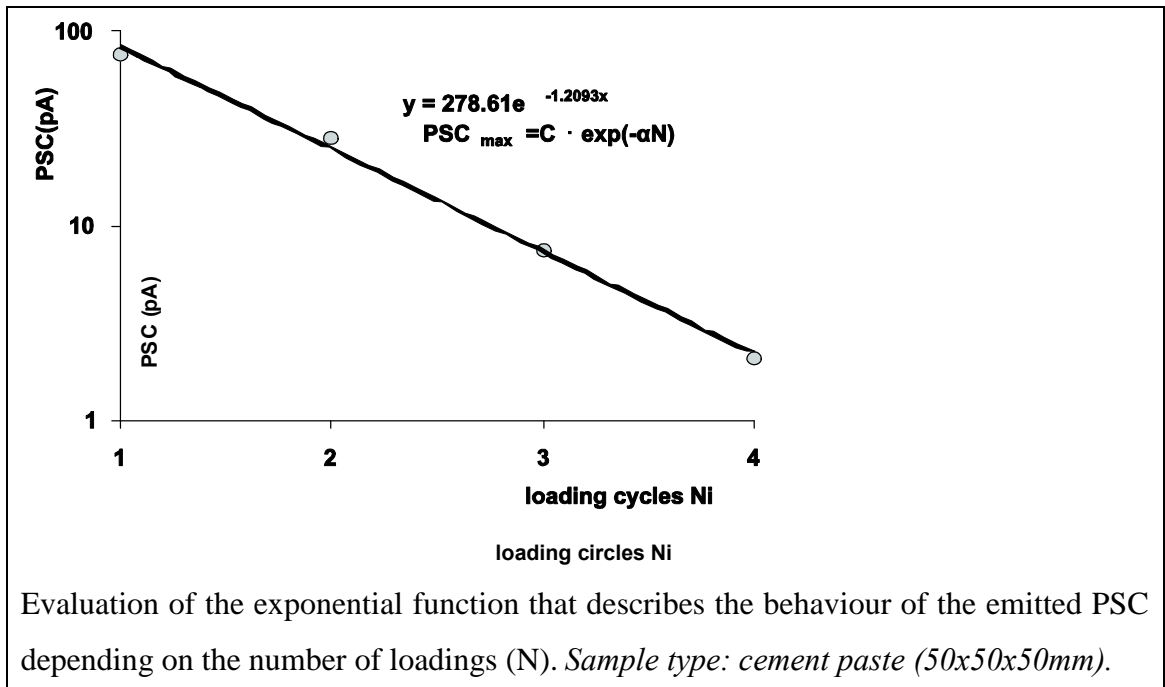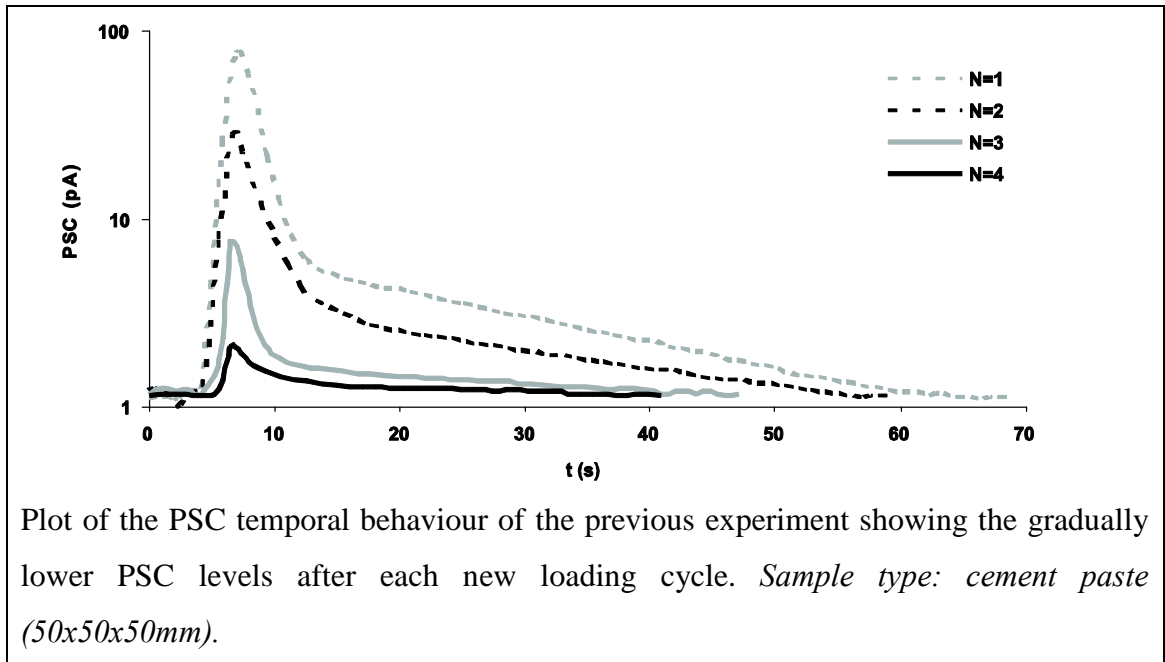PSC (a) of the above experiment and stress (b) with respect to the strain. *Sample type: cement paste (50x50x50mm).*

Calculation of the Young's Modulus using linear fitting on the stress-strain curve on a cement paste sample. *Sample type: cement paste (50x50x50mm).*
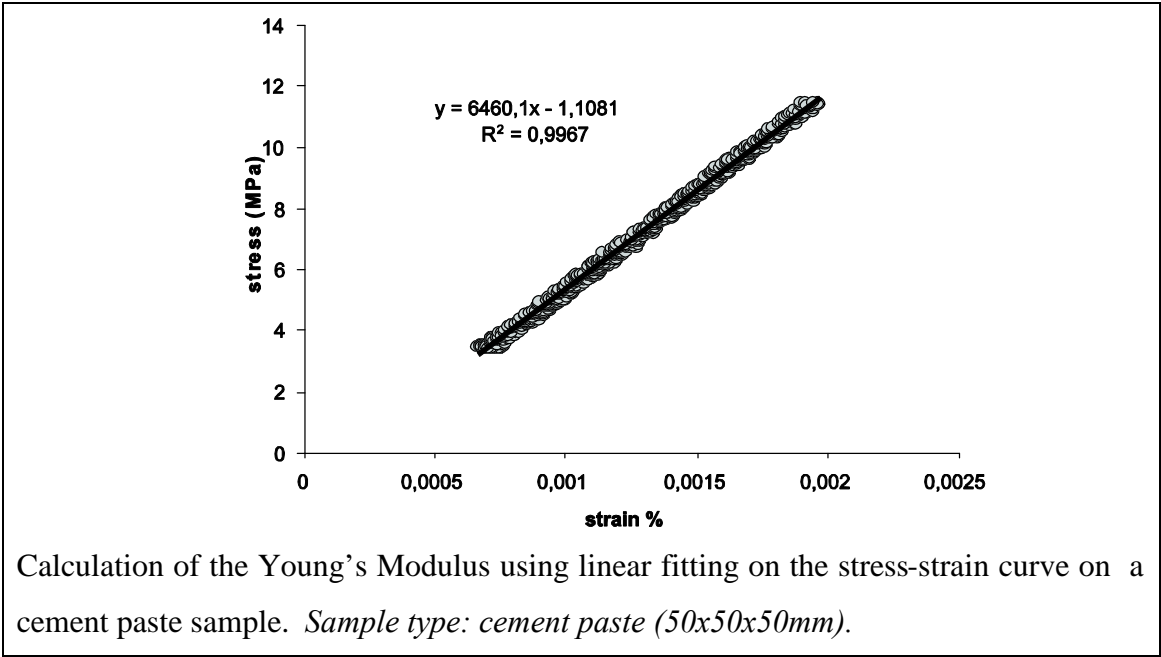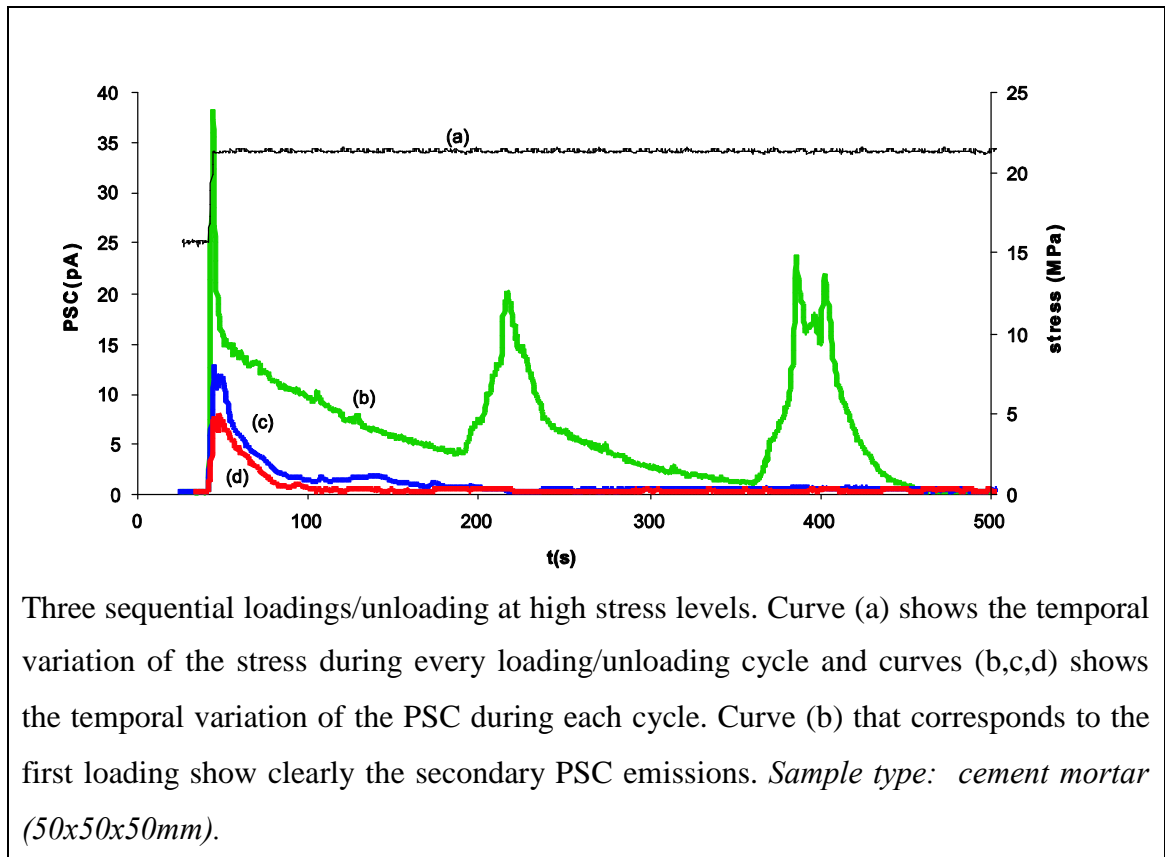
A5. Sequential loadings and unloadings at high stress levels and the corresponding electric current emissions (PSC). Their correlation to the stress rate. (Experiment A)

Sequential loadings and unloading at the same stress level. Left hand side figure shows each stress step (a) temporal behaviour and the corresponding PSC. The right hand side figure corresponds to the same experiment and depicts the temporal variation of the emitted PSC and the corresponding behaviour of the dσ/dt quantity. *Sample type: cement paste (50x50x50mm).*

Plot of the PSC temporal behaviour of the previous experiment showing the gradually lower PSC levels after each new loading cycle. *Sample type: cement paste (50x50x50mm).*

Evaluation of the exponential function that describes the behaviour of the emitted PSC depending on the number of loadings (N). *Sample type: cement paste (50x50x50mm).*

A6. Sequential loadings and unloadings at high stress levels and the corresponding electric current emissions (PSC). Primary and secondary electric current emissions. (Experiment B)


Three sequential loadings/unloading at high stress levels. Curve (a) shows the temporal variation of the stress during every loading/unloading cycle and curves (b,c,d) shows the temporal variation of the PSC during each cycle. Curve (b) that corresponds to the first loading show clearly the secondary PSC emissions. *Sample type: cement mortar (50x50x50mm).*
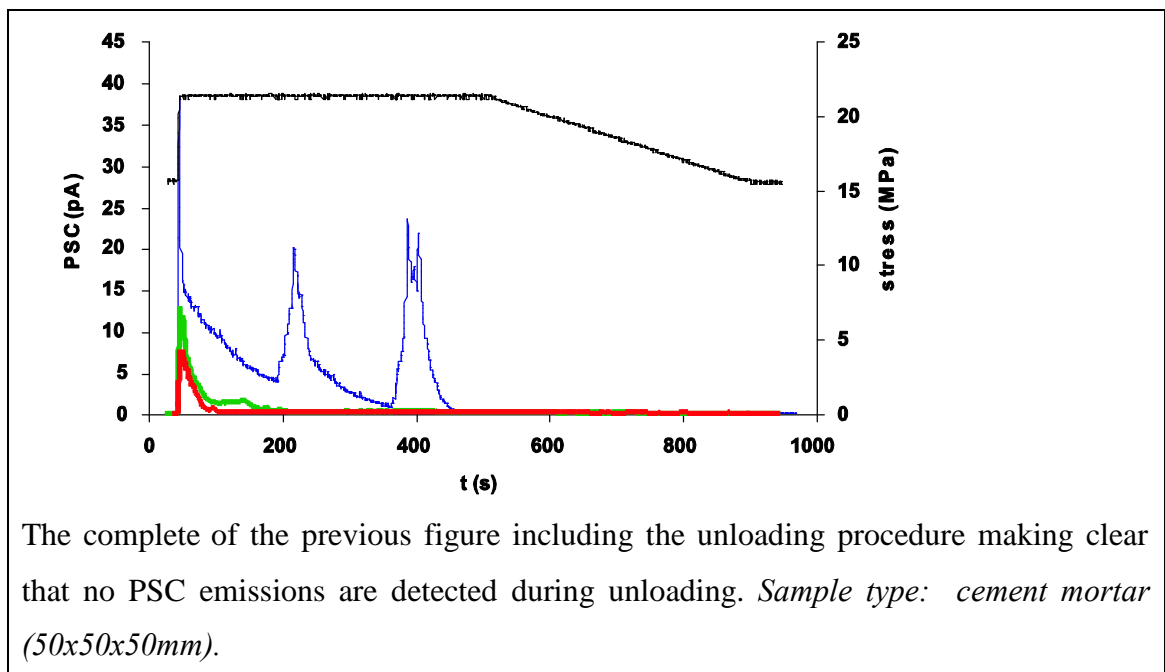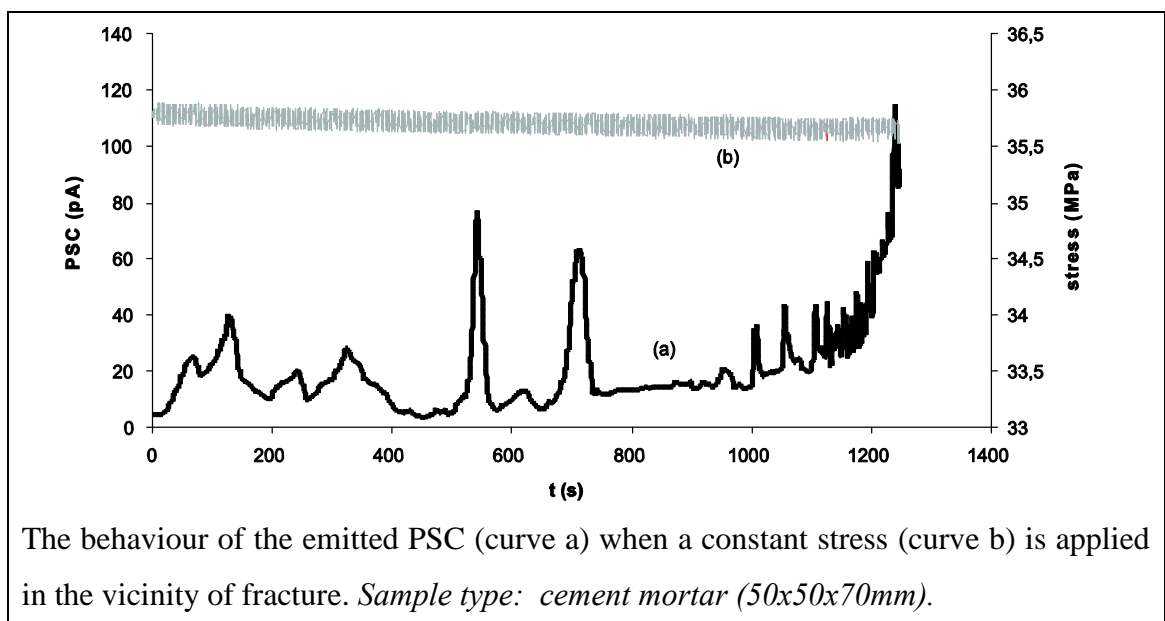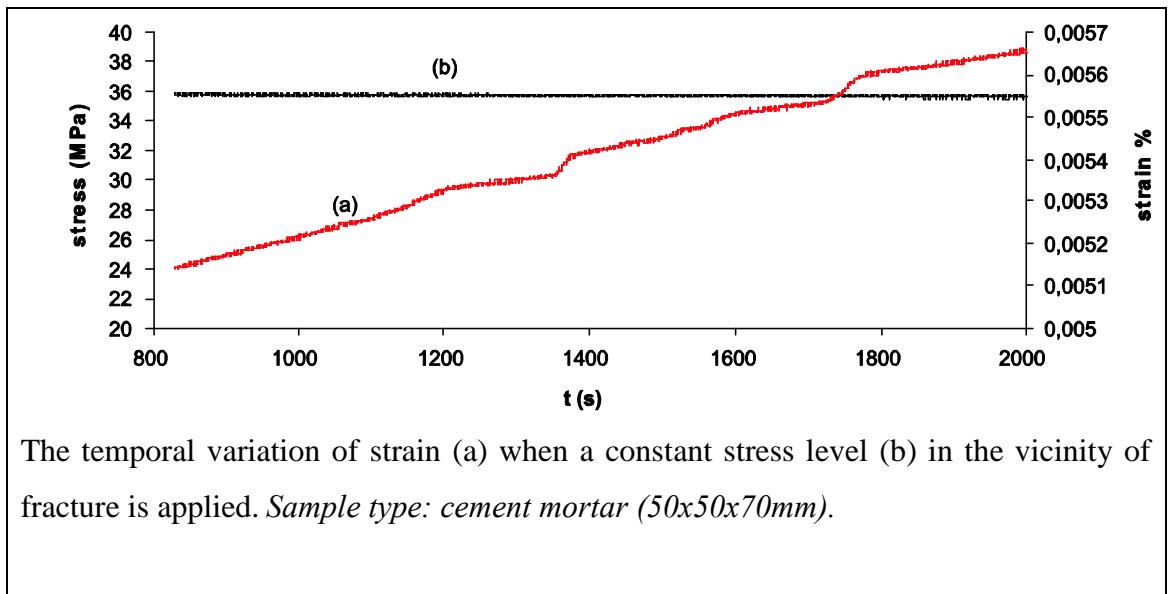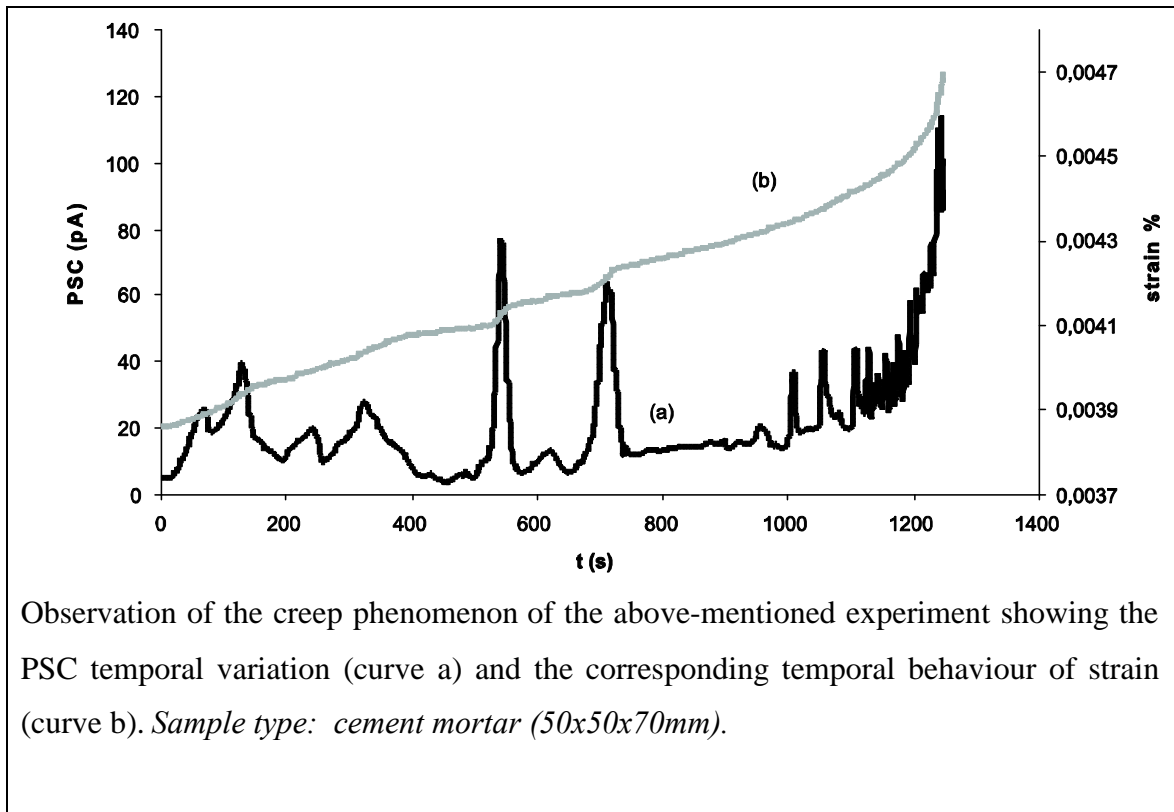

The complete of the previous figure including the unloading procedure making clear that no PSC emissions are detected during unloading. *Sample type: cement mortar (50x50x50mm).*

A7. Electric current emission (PSC) recordings during stress application up to the vicinity of fracture.

The PSC temporal variation during LSRT technique applying the stress at very low rate. *Sample type: cement mortar (50x50x70mm).*
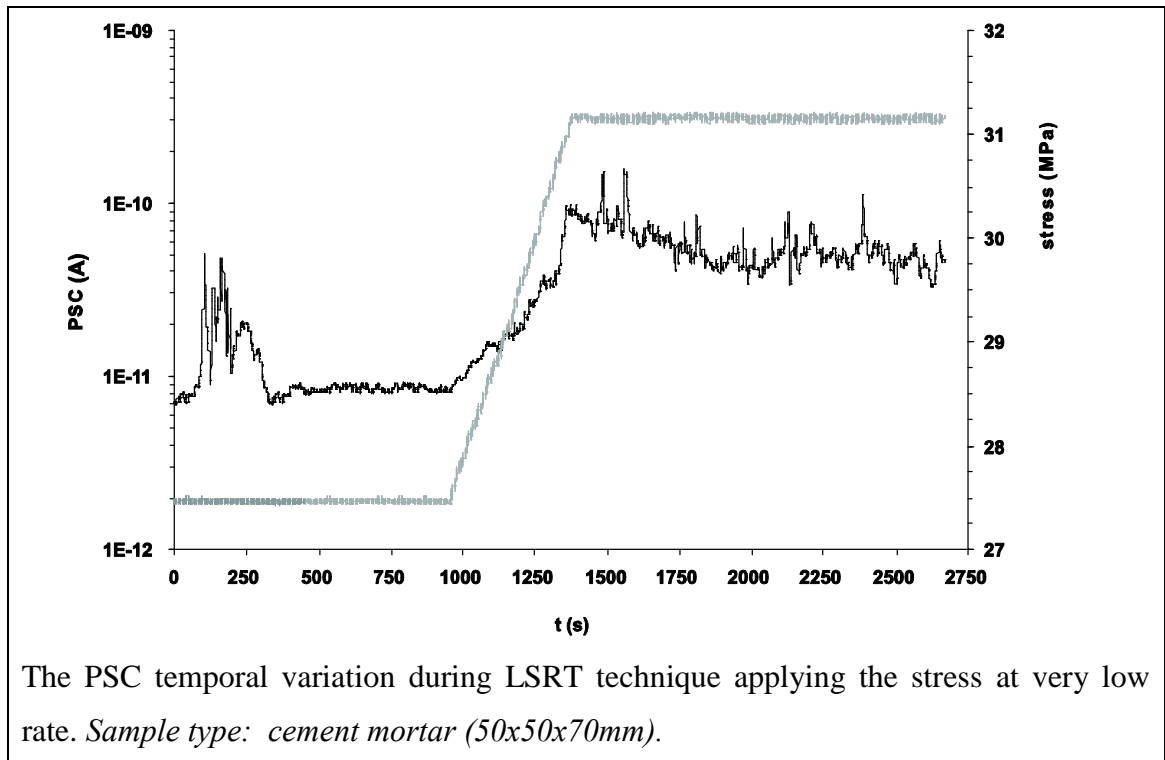
A8. Electric current emission (PSC) recordings when a cement mortar sample suffers constant stress in the vicinity of fracture.

The behaviour of the emitted PSC (curve a) when a constant stress (curve b) is applied in the vicinity of fracture. *Sample type: cement mortar (50x50x70mm).*

Observation of the creep phenomenon of the above-mentioned experiment showing the PSC temporal variation (curve a) and the corresponding temporal behaviour of strain (curve b). *Sample type: cement mortar (50x50x70mm).*

The temporal variation of strain (a) when a constant stress level (b) in the vicinity of fracture is applied. *Sample type: cement mortar (50x50x70mm).*

The corresponding behaviour of the emitted PSC (a) during the above described experiment and the strain variation (b). *Sample type: cement mortar (50x50x70mm)*

The evaluation of the estimated linear relation between the PSC peak max with respect to the corresponding strain rate. *Sample type: cement mortar (50x50x70mm)*

A9. Primary and secondary electric current (PSC) emissions during and after a stress step application in the vicinity of fracture. (Experiment A)

The temporal behaviour of the emitted PSC (a) when the sample suffers uniaxial compressional stress (b) in the vicinity of fracture. The plot makes clear the primary and the secondary PSC emissions. *Sample type: cement paste: (50x50x50mm)*
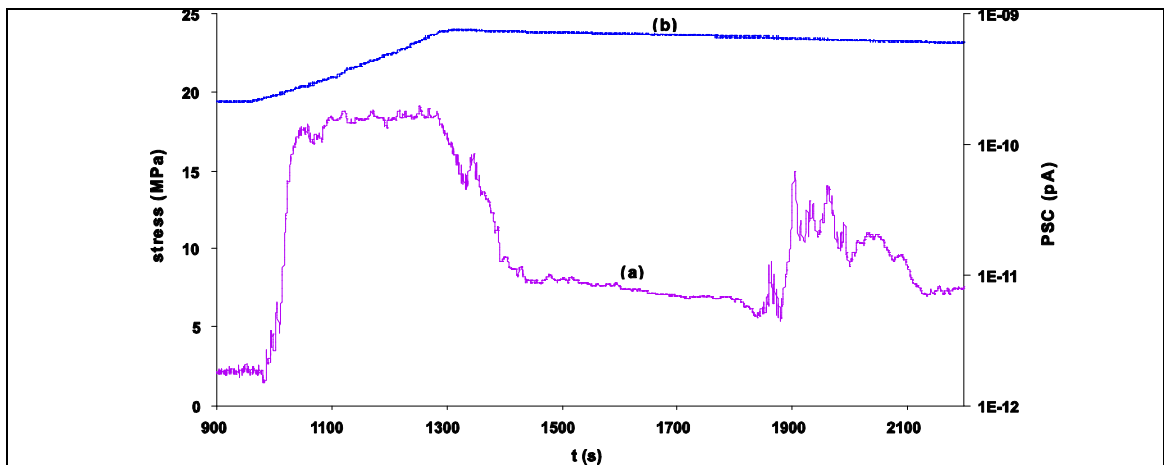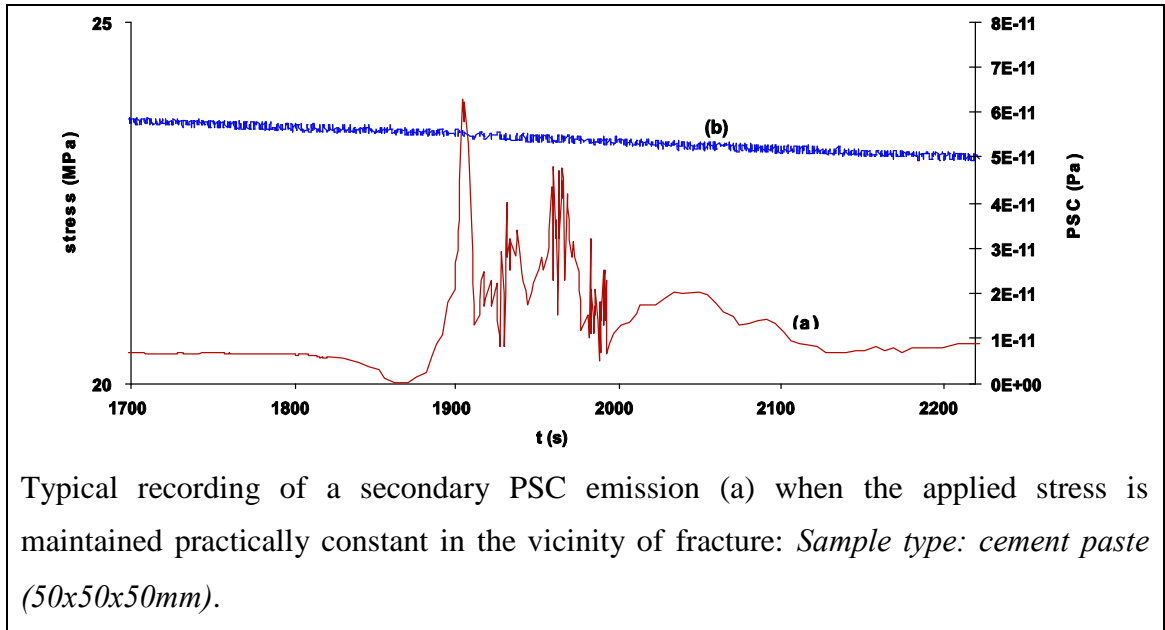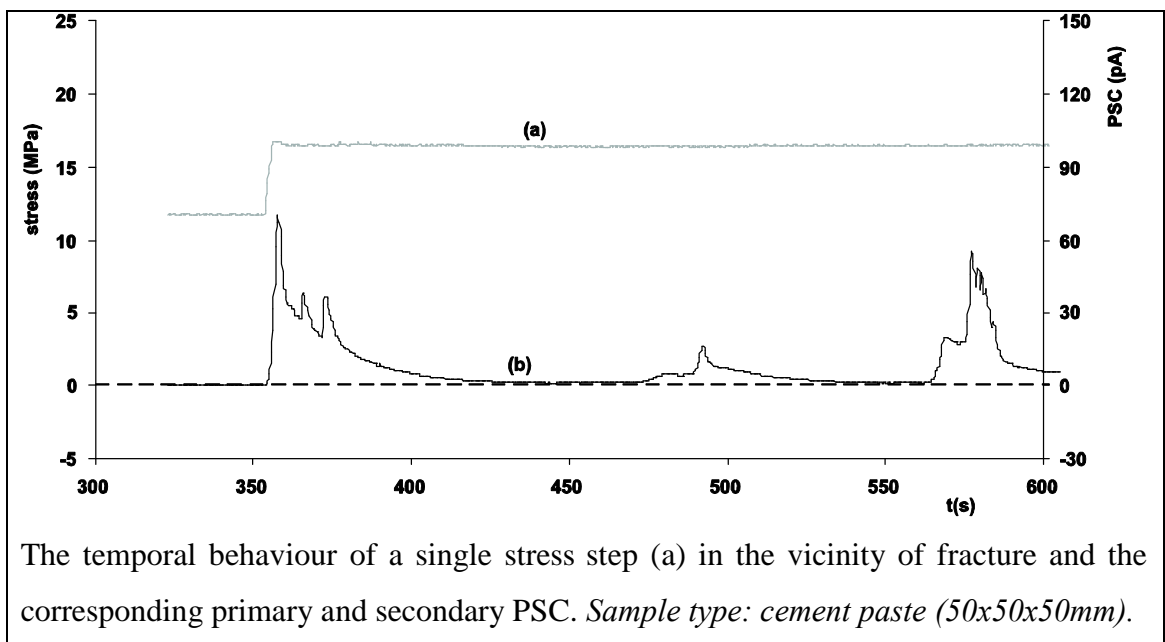
A10. Primary and secondary electric current (PSC) emissions during and after a stress step application in the vicinity of fracture. (Experiment B)

The temporal variation of the PSC emission (a) when a cement paste sample suffers a uniaxially compressional stress-step (b) in the vicinity of fracture: it becomes obvious that two PSC emissions are recorded, one concurrently to the applied stress step (primary PSC emission) and a second PSC emission that is recorded when the applied stress is maintained at high levels close to fracture (secondary PSC emission). *Sample type: cement paste (50x50x50mm).*

Typical recording of a secondary PSC emission (a) when the applied stress is maintained practically constant in the vicinity of fracture: *Sample type: cement paste (50x50x50mm)*.

A11. Primary and secondary electric current (PSC) emissions during and after a stress step application in the vicinity of fracture. (Experiment C).
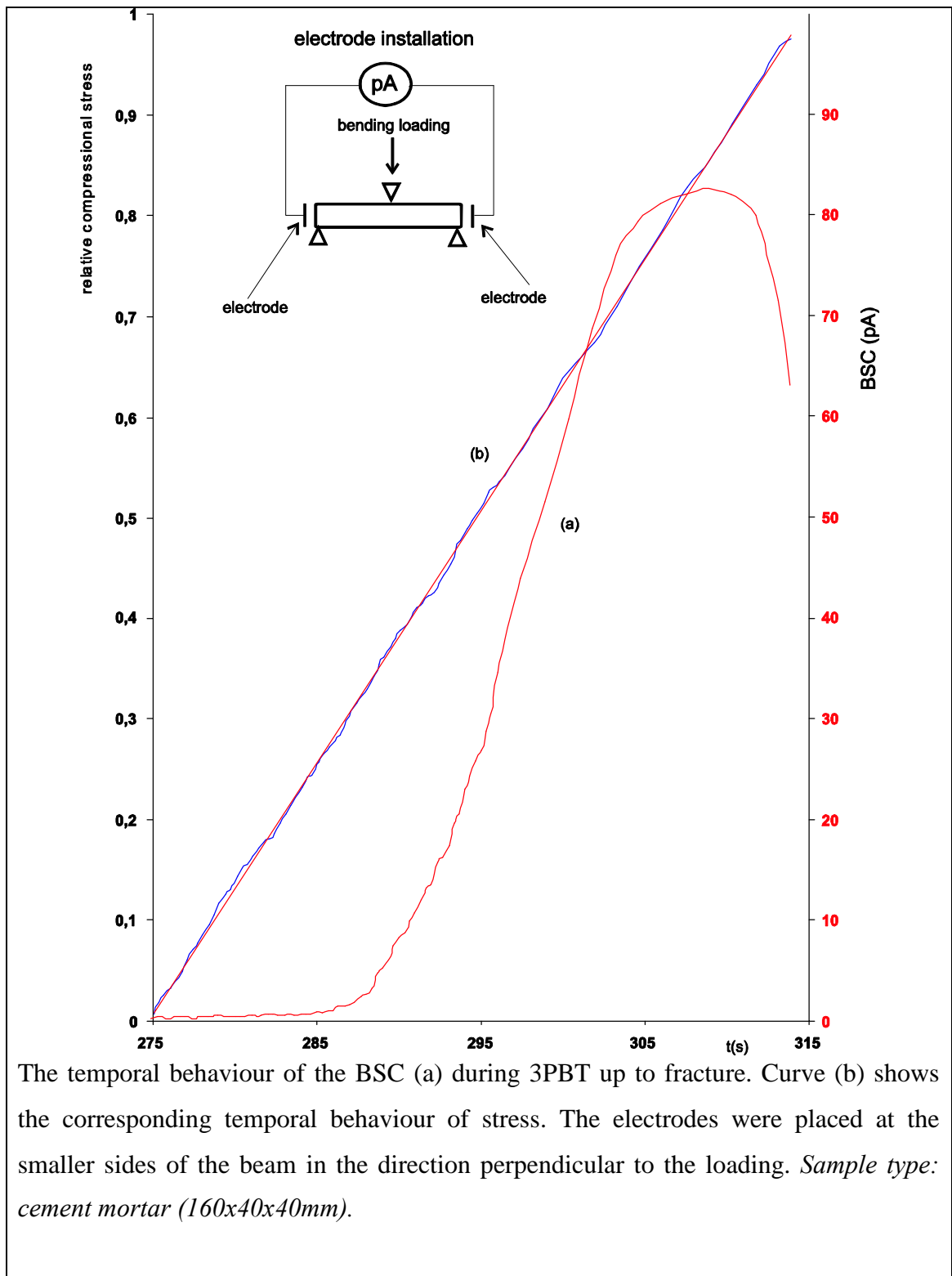

The temporal behaviour of a single stress step (a) in the vicinity of fracture and the corresponding primary and secondary PSC. *Sample type: cement paste (50x50x50mm)*.

A12. Electric current emission (BSC) recordings during three point bending tests on a cement mortar beam. The electrodes are attached to the sides of the sample perpendicularly to the applied stress. (Experiment A)

The temporal behaviour of the BSC (a) during 3PBT up to fracture. Curve (b) shows the corresponding temporal behaviour of stress. The electrodes were placed at the smaller sides of the beam in the direction perpendicular to the loading. *Sample type: cement mortar (160x40x40mm).*
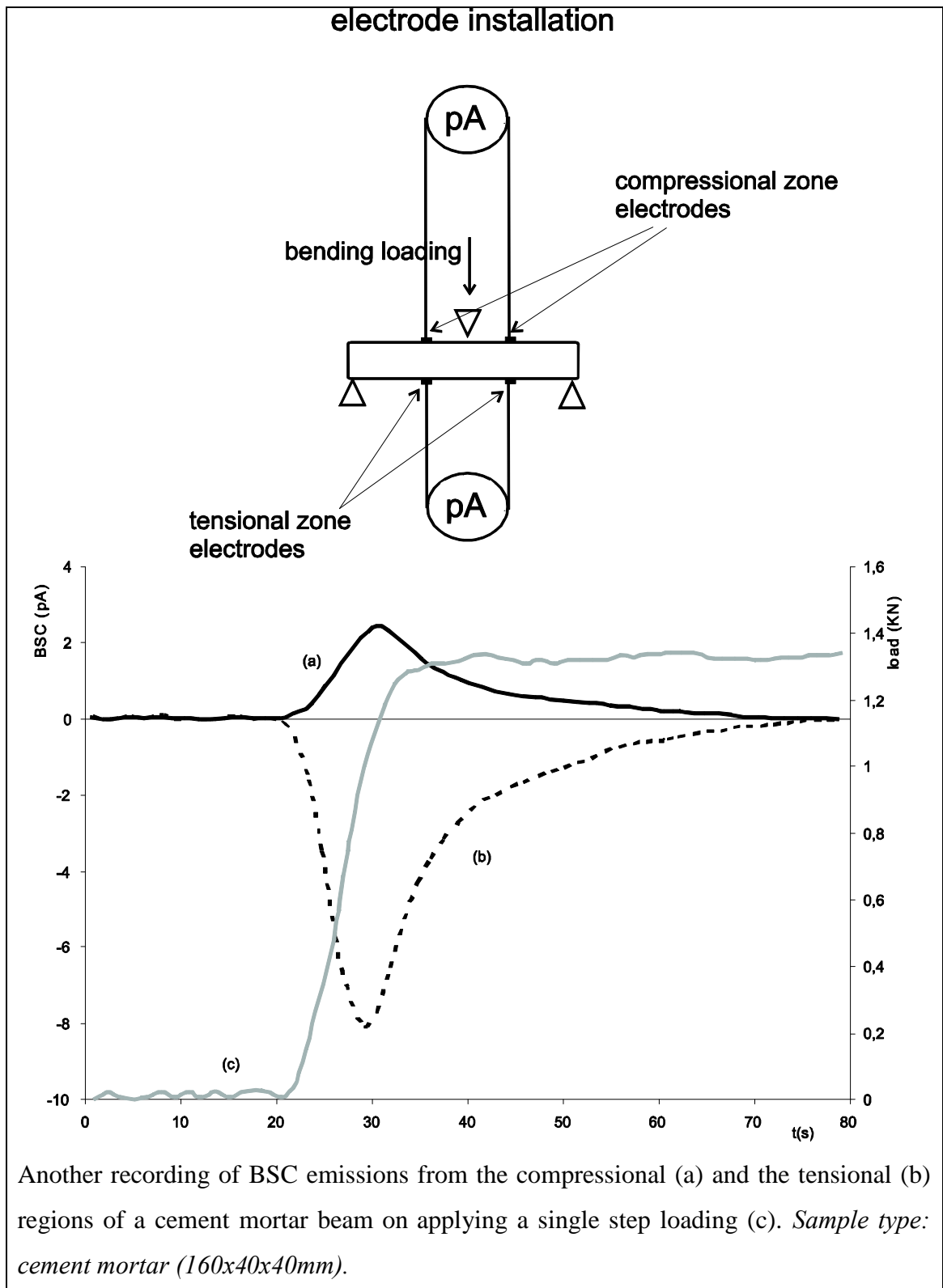
A13. Electric current emission (BSC) recordings during three point bending tests on a cement paste beam. The electrodes are attached to the sides of the sample perpendicularly to the applied stress. (Experiment B)
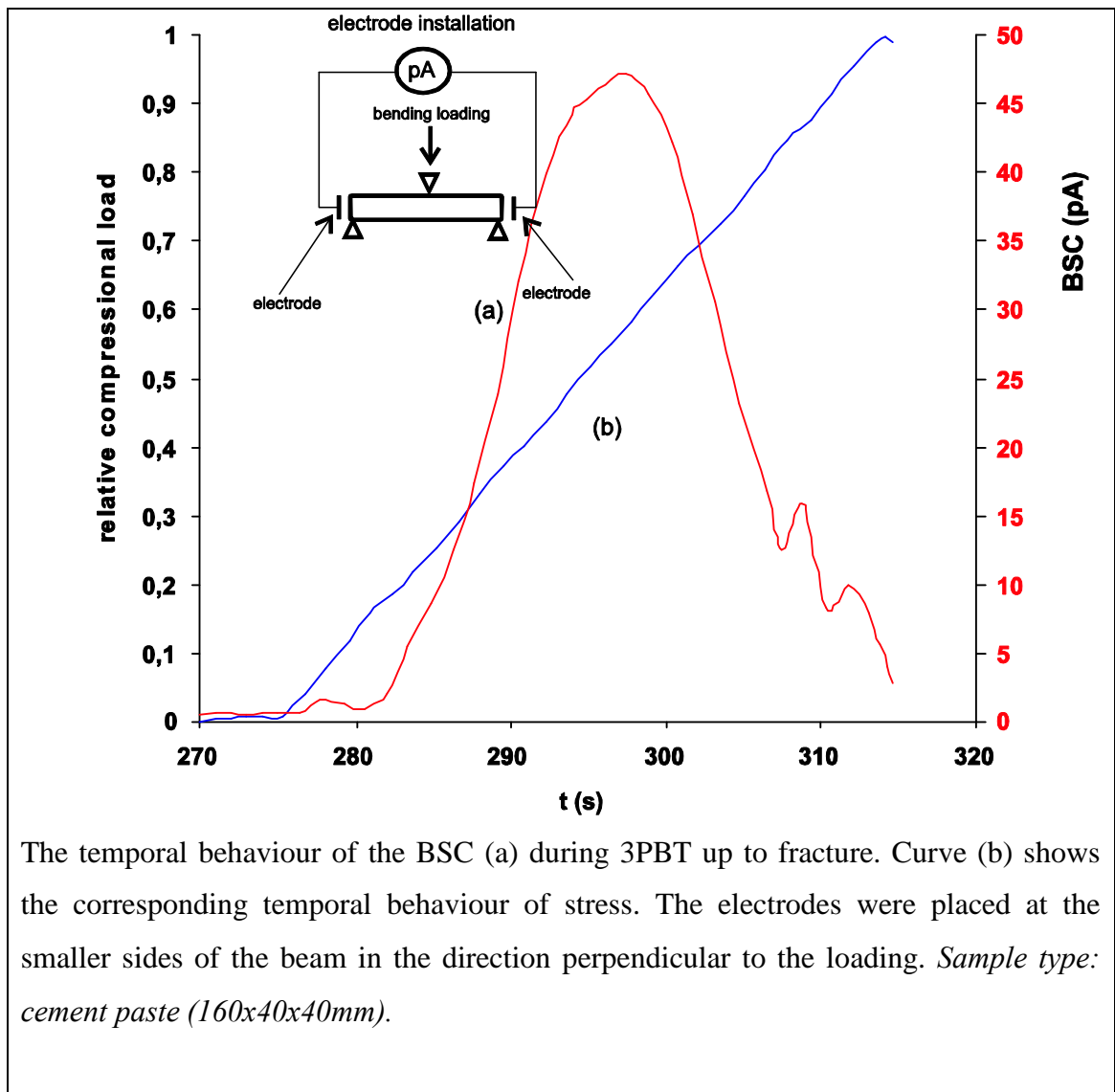

The temporal behaviour of the BSC (a) during 3PBT up to fracture. Curve (b) shows the corresponding temporal behaviour of stress. The electrodes were placed at the smaller sides of the beam in the direction perpendicular to the loading. *Sample type: cement paste (160x40x40mm).*

A14. Electric current emission (BSC) recordings during three point bending tests on a cement mortar beam. The electrodes are attached to the compressional and the tensional sides of the sample. (Experiment B)

Another recording of BSC emissions from the compressional (a) and the tensional (b) regions of a cement mortar beam on applying a single step loading (c). *Sample type: cement mortar (160x40x40mm).*

A15. Electric current emission (BSC) recordings during three point bending tests on a cement mortar beam. The electrodes are attached to the compressional and the tensional sides of the sample. (Experiment A)
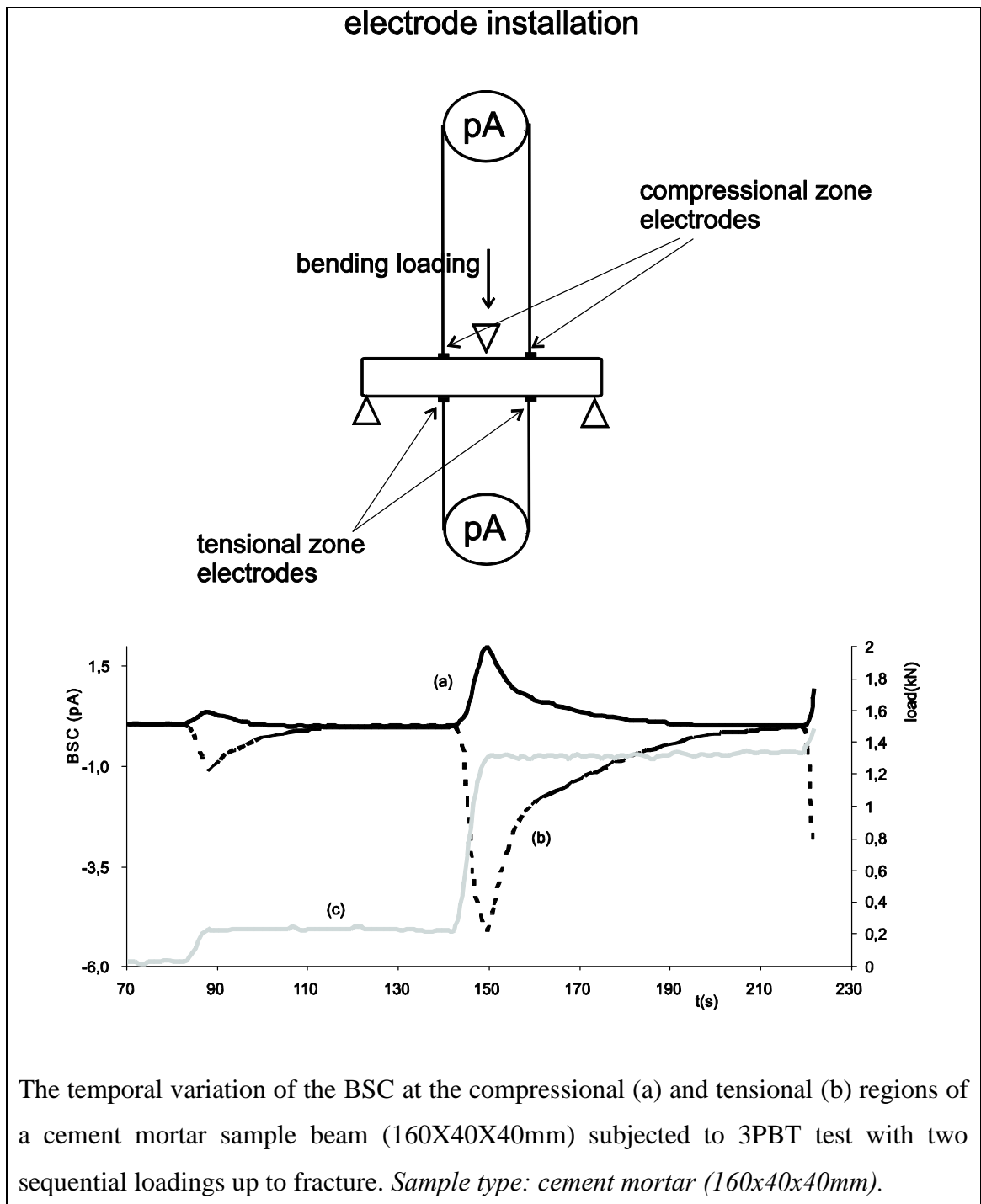
The temporal variation of the BSC at the compressional (a) and tensional (b) regions of a cement mortar sample beam (160X40X40mm) subjected to 3PBT test with two sequential loadings up to fracture. *Sample type: cement mortar (160x40x40mm).*

APPENDIX C

Published work in International Journals and Conferences

Publications (in Journals)

1. **A. Kyriazopoulos** , I. Stavrakas, K.Ninos, C. Anastasiadis, D.Triantis "Pressure Stimulated Current emissions on cement paste samples under repetitive stepwise compressional loading" **International Journal of Microstructure and Materials Properties, (2008 in press).**

2. **A. Kyriazopoulos** , I. Stavrakas, C. Anastasiadis, D.Triantis "Study of weak electric current emission on cement mortar under uniaxial compressional mechanical stress up to the vicinity of fracture" **International Journal of Microstructure and Materials Properties**, **(2008 in press).**

3. D. Triantis, I. I. Stavrakas C. Anastasiadis, **A. Kyriazopoulos** and F. Vallianatos: "An analysis of Pressure Stimulated Currents (PSC), in marble samples under mechanical stress", **Physics and Chemistry of the Earth**, **Parts A/B/C, Volume 31, Issues 4-9, 2006, Pages 234-239.**

4. C. Anastasiadis, D. Triantis, I. I. Stavrakas , **A. Kyriazopoulos**, F. Vallianatos: "Ac conductivity measurements of rock samples after the application of stress up to fracture. Correlation with the damage variable", **WSEAS Transactions on Systems**, Iss. 3, Vol. 4, 2005, pp. 185-190.

Conference Proceedings

1. **A. Kyriazopoulos**, C. Anastasiadis, D. Triantis and I. Stavrakas: «Experimental Pressure Stimulated Currents (PSC) recordings on cement mortar under mechanical stress», **2nd International fib congress, Naples, Italy**, 5-8 June 2006.

2 **A. Kyriazopoulos**, I. Stavrakas, C. Anastasiadis, D. Triantis: "Pressure Stimulated Current (PSC) recordings on cement mortar and marble." **4 WSEAS International Conference on Application of Electric Engineering (AEE 05), Prague,Czech Republic, 13-15 March 2005,pp.12-15.**

3.**A. Kyriazopoulos,** I. Stavrakas, C. Anastasiadis, D. Triantis, F. Vallianatos and Z. Agioutantis: "Pressure stimulated current (PSC) recordings on cement mortar: Preliminary results". **7 National Congress on Mechanics, Chania, Crete, 24- 26 June 2004.**

4. D. Triantis, C. Anastasiadis, **A. Kyriazopoulos** and I. Stavrakas: "The ascertainment of the presence of damage processes using the Pressure Stimulated Current (PSC) technique on marble and cement samples", **ECNDT 2006, Berlin, 25 – 29 September 2006.**

5. D. Triantis, C. Anastasiadis, **A. Kyriazopoulos** P.Kyriazis and N.Alexis: "Electric current emissions during bending of FRP samples up to fracture" Proceedings of the 2th International Conference "**Advances in Mineral Resources Management and Enviromental Geotechnology", 25-27 September,2006-Hania Crete Greece,pp.425-430.**

6. C. Anastasiadis, D. Triantis, **A. Kyriazopoulos**, and I. Stavrakas: « Pressure Stimulated Currents (PSC) recordings on cement mortar under mechanical stress in cement mortar under abrupt stepwise uniaxial stress», **Proceedings of the 15th National Conference of the Hellenic Society for Non-Destructive Testing, Athens, Greece, November 18-19, 2005, pp. 5.14-5.23.**

7. C. Anastasiadis, D. Triantis, I. Stavrakas, **A. Kyriazopoulos**: «Investigation of porous silicates contamination with crude oil using Dielectric spectroscopy», **Proceedings of the International Workshop in Geoenvironment and Geotechnics (GEOENV 2005), Milos Island, Greece, 12–14 September 2005, pp. 201-206.**

8. C. Anastasiadis, I. Stavrakas, **A. Kyriazopoulos**, D. Ninos and D. Triantis: «Non destructive damage estimation on rocks with laboratory measurements of dielectric loss (tanδ)», **Proceedings of the 8th International Conference of the Slovenian Society for Non-Destructive Testing, Portorož, Slovenia, 1-3 September 2005, pp. 401-407. Conference on Applications of Electrical Engineering, AEE 05, Prague, Czech Republic, 13-15 March 2005**

Conference abstracts

1. D. Triantis, C.Anastasiadis, **A. Kyriazopoulos**, P. Kyriazis and I. Stavrakas: "Correlation of the Pressure Stimulated Current (PSC) with the applied uniaxial stress on marble rock samples and Portland type cement–OPC, from low stress levels up to fracture", **Geophysical Research Abstracts, Vol. 8, 03458, EGU, General Assembly Vienna, Austria, 2-7 April 2006.**